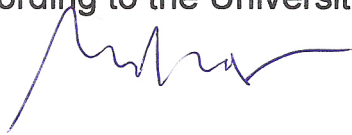


**The University of Jordan
Authorization Form**

I, Maher Khader Matar, authorize the University of Jordan to supply copies of my Thesis/ Dissertation to libraries or establishments or individuals on request, according to the University of Jordan regulations.

Signature:



Date:

21/11/2010

نموذج رقم (١٨)
اقرار والتزام بقوانين الجامعة الأردنية وأنظمتها
وتعليماتها لطلبة الماجستير والدكتوراة

أنا الطالب: عاصم محمد أحمد الرقم الجامعي: ٨.٨.٧٥٩
التخصص: ميكانيكا الكلية: الهندسة

عنوان الرسالة / الأطروحة

Experimental investigation and numerical simulation
for the coefficient of discharge for small opening
orifice at low Reynolds number in a pilot
operated relief valve

أعلن بأنني قد التزمت بقوانين الجامعة الأردنية وأنظمتها وتعليماتها وقراراتها السارية المفعول المتعلقة باعداد رسائل الماجستير والدكتوراة عندما قمت شخصيا" باعداد رسالتي / اطروحتي ، وذلك بما ينسجم مع الأمانة العلمية المتعارف عليها في كتابة الرسائل والأطاريح العلمية. كما أنني أعلن بأن رسالتي /اطروحتي هذه غير منقولة أو مستلة من رسائل أو أطاريح أو كتب أو أبحاث أو أي منشورات علمية تم نشرها أو تخزينها في أي وسيلة اعلامية، وتأسيسا" على ما تقدم فبأنني أتحمل المسؤولية بأنواعها كافة فيما لو تبين غير ذلك بما فيه حق مجلس العمداء في الجامعة الأردنية بالغاء قرار منحي الدرجة العلمية التي حصلت عليها وسحب شهادة التخرج مني بعد صدورها دون أن يكون لي أي حق في التظلم أو الاعتراض أو الطعن بأي صورة كانت في القرار الصادر عن مجلس العمداء بهذا الصدد.

التاريخ: ٢٠١٤ / ١١ / ٢٠

توقيع الطالب: عاصم محمد أحمد

تعتمد كلية الدراسات العليا
هذه النسخة من الرسالة
التوقيع: عاصم محمد أحمد التاريخ: ٢٠١٤ / ١١ / ٢٠

**EXPERIMENTAL INVESTIGATION AND NUMERICAL
SIMULATION FOR THE COEFFICIENT OF DISCHARGE FOR
SMALL OPENING ORIFICE AT LOW REYNOLDS NUMBER IN A
PILOT OPERATED RELIEF VALVE**

By
Maher Khader Matar

Supervisor
Dr. Ahmed S. Al-Salaymeh

**This Thesis was Submitted in Partial Fulfillment of the Requirements for the
Master's Degree of Science in Mechanical Engineering**

**Faculty of Graduate Studies
The University of Jordan**

Nov, 2010

تعتمد كلية الدراسات العليا
هذه النسخة من الرسالة
التوقيع: ١٠/١١/٢٠١٠
١٠/١١/٢٠١٠

COMMITTEE DECISION

This thesis/dissertation (Experimental investigation and numerical simulation for the coefficient of discharge for small opening orifice at low Reynolds number in a pilot operated relief valve) was successfully defended and approved on 26/10/2010

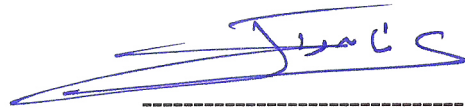
Examination Committee

Signature

Dr. Ahmed S. Al-Salaymeh, (Supervisor)
Assoc. Prof. of Mechanical Engineering



Dr. Adnan Jaradat, (Member)
Assoc. Prof. of Mechanical Engineering



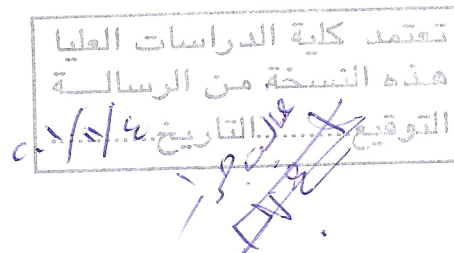
Dr. Ali Badran (Member)
Prof. of Mechanical Engineering



Dr. Omar Badran (Member)
External Examiner
Prof. of Mechanical Engineering
Al-Balqa' Applied University



تعتمد كلية الدراسات العليا
هذه النسخة من الرسالة
التوقيع: 26/10/2010



Dedication

To my friend Mohammad Milhim, for his brave heart.

Acknowledgment

The author wishes to express his sincere thanks to Dr. Ahmed Al-Salaymeh for patient guidance offered throughout this work, and Dr. Malik Amayreh for helpful advices during this study. The author also wishes to say his thanks to all staff members, and to all engineers in the department of mechanical engineering, and would like to thank specially engineers Rasha, Yazan, Yusuf, and Mr. Aref.

The author wishes to thank his family for their encouragement and support.

The author is grateful to Alnida Hydraulics, Al-Fida industries and the technical center for the support in building the setup, and also grateful for the Laboratory supervisors for their help in carrying out the experimental work.

TABLE OF CONTENTS

Subject	Page
Committee Decision	ii
Dedication	iii
Acknowledgement	iv
Table of contents	v
List of tables	vii
List of figures.....	viii
Nomenclatures	x
List of Appendices	xi
Abstract	xii
Chapter One: Introduction	1
1.1 Study importance	1
1.2 Study objectives	2
1.3 Research methodology	3
1.3.1 Experimental setup and measuring devices	3
1.3.2 Experimental procedure	3
1.4 Basic theory of orifice	3
1.5 Thesis layout	6
Chapter Two: Literature review	8
Chapter Three: Relief valve	17
3.1 Pressure relief devices	17
3.2 Reclosing-type pressure relief devices	17
3.3 Pressure relief valves	18
3.4 Safety valves	19
3.5 Relief valves	21
3.6 Conventional pressure relief valves operation	22
3.7 Pilot-operated pressure relief valves	26
3.8 Symbols of different types of hydraulic relief valves	35
3.9 This study pressure relief valve	36
Chapter Four: Computational fluid dynamics	40
4.1 Numerical simulation and computational fluid dynamics	40
4.2 The need for CFD	40
4.3 Applications of CFD	41
4.4 ANSYS Fluent software package	41
4.5 Fluent	42
4.6 Gambit	43

Chapter Five: Experimental setup	45
5.1 The hydraulic circuit	45
5.1.1 The hydraulic circuit description	46
5.1.2 Preparation and modification of the pilot operated relief vale	47
5.2 Pressure Transducers	47
5.3 The positive displacement flow meter	49
5.4 The electronic operational Amplifier	50
5.5 Data acquisition system	52
5.6 Experimental procedure	53
Chapter Six: Experimental and simulation results and discussion	57
6.1 Experimental results	57
6.2 Formula modeling by curve fitting	62
6.3 Simulation results	65
6.4 Experimental and Simulation results comparison	75
6.5 The final shape of the flow equation	79
6.6 Uncertainty analysis	80
6.6.1 Measurement devices uncertainty	82
6.6.2 Setup uncertainty	84
Chapter Seven: Conclusions and Recommendations	87
References.....	89
Appendices	90
Abstract (in Arabic).....	133

LIST OF TABLES

Number	Table caption	Page
Table 3.1	Relief valves hydraulic symbols	36
Table 3.2	Our study relief valve main specifications	37
Table 5.1	Pressure transducer specifications	48
Table 5.2	Flow meter specifications	49
Table 6.1	Sample of data, first 5runs of set 3	57
Table 6.2	Sample of calculate results, first 5runs of set 3	58
Table 6.3	Experimental work, different sets conditions	60
Table 6.4	The result parameters according to fit of equation $C_d = C_{dm} (1 + a_1 e^{(-\Delta_1 \sqrt{Re})})$	64
Table 6.5	Differences between two trials of simulation	72

LIST OF FIGURES

Number	Figure caption	Page
Figure 1.1	Orifice plate and locations of various pressure tapes	4
Figure 2.1	One of the simple empirical models was an exponential function between the C_d and square root of Re . Wu et al, (2002)	9
Figure 2.2	Actual flow rate compared with the Predicted flow rate for spool valve.	10
Figure 2.3	The clearance between the spool and the sleeve	10
Figure 2.4	Comparison between empirical and measured areas	11
Figure 2.5	Formula of area compared with measured area	11
Figure 2.6	Comparison between Calculated flow gain and measured one	13
Figure 2.7	Comparison between Calculated Pressure sensitivity and measured one	13
Figure 2.8	The flow in the domain	14
Figure 3.1	Main types of pressure relief devices	17
Figure 3.2	Types of reclosing relief devices	18
Figure 3.3	Pressure relief valve	19
Figure 3.4	Safety valve	20
Figure 3.5	Electronic relief valve	22
Figure 3.6	Conventional pressure relief valves	23
Figure 3.7	Pilot-operated pressure relief valve	27
Figure 3.8	Piston type pilot-operated pressure relief valve	30
Figure 3.9	Diaphragm-type pilot-operated pressure relief valve	31
Figure 3.10	Pop action pilot-operated pressure relief valve	32
Figure 3.11	Typical relationship between lift of disk and vessel pressure in a pop-action pilot-operated pressure relief valve	32
Figure 3.12	Typical relationship between lift of disk and vessel pressure in a Modulating -action pilot-operated pressure relief valve	33
Figure 3.13	Modulating-flowing-type pilot-operated pressure relief valve	34
Figure 3.14	Pop-action nonflowing-type pilot-operated pressure relief valve	35
Figure 3.15	Cross sectional view of pilot operated relief valve, REXROTH	38
Figure 5.1	Experiment setup schematic diagram	46
Figure 5.2	Pressure transducer	48
Figure 5.3	Piston type flow meter	50
Figure 5.4	Flow chart from the devices to the result	53
Figure 5.5	Levels of data, every 30reading averaged to one run, group of runs make a set and draw a curve, each set generates an empirical formula	55
Figure 5.6	Setup components together, labeled	56
Figure 5.7	Relief valve and pressure sensors mounting	56
Figure 6.1	Plot for C_d vs. \sqrt{Re} for 1st set of data and results	59
Figure 6.2	Scatter plot for all sets, C_d vs. \sqrt{Re}	61
Figure 6.3	Curve fitting C_d vs. \sqrt{Re} sample, 1st set	63

Figure 6.4	Comparison between empirical formula for needle valve (Wu 2002) and our experimental work	65
Figure 6.5	This study orifice 1st generated mesh	66
Figure 6.6	Velocity vector field in orifice by simulation	67
Figure 6.7	Pressure contours in orifice by simulation	68
Figure 6.8	Simulation result for C_d v. \sqrt{Re} , first trial	69
Figure 6.9	Refinement for mesh grid, see crowded cells at orifice edge	70
Figure 6.10	Example of run when residual does not change with iterations	71
Figure 6.11	Number of iterations change with different run conditions	73
Figure 6.12	Comparison between C_d vs. \sqrt{Re} for two simulations, x-marker for fine mesh, o-marker for coarse mesh	74
Figure 6.13	Mesh with modification of cross section	75
Figure 6.14	Simulation results with modification of cross section	75
Figure 6.15	Comparison between Experimental result of set no. 1 and numerical simulation with fixed inlet pressure	76
Figure 6.16	Comparison between Experimental result of set no. 4 and numerical simulation with refined mesh and variable inlet and outlet pressures	77
Figure 6.17	Comparison between Experimental result of set no. 4 and numerical simulation after modification of cross section	78
Figure 6.18	Sources of uncertainty in results	81
Figure 6.19	Temperature-pressure relation of viscosity	86

NOMENCLATURE:

Symbol	Description	Unit
A	Orifice cross-sectional area	m ²
a1	Coefficient in empirical formula	-
C _d	Coefficient of discharge	-
C _{dm}	Maximum value of coefficient of discharge	-
C _{d∞}	Coefficient of discharge value at high Reynolds number	-
d	Orifice diameter	m
K _C	Pressure sensitivity	-
P	Pressure	Pa
P1	Upstream pressure of the orifice	Pa
P2	Downstream pressure of the orifice	Pa
Q	Volumetric flow rate	Lit./min.
Re	Reynolds number	-
t	Time	sec
u	Arbitrary variable, to illustrate an equation	-
V	Velocity vector	m/s
δ ₁	Attenuation coefficient of empirical formula	-
v	Kinematic viscosity	m ² /sec
ρ	Density	Kg/m ³
τ _{ij}	The momentum transport per unit area and unit time	Pa

LIST OF APPENDICES

Appendix	Caption	Page
Appendix A	Matlab M-file for averaging experimental reading data	90
Appendix B	Experimental results	92
Appendix C1	Simulation data and results, first mesh	103
Appendix C2	Simulation data and results, refined mesh	104
Appendix C3	Simulation data and results, modified cross section	105
Appendix D1	Experimental setup electronic circuit for flow meter, signal conditioner	106
Appendix D2	readings of current to voltage convertor	107
Appendix D3	fitting of readings of current to voltage convertor	109
Appendix E	Experimental setup photos	110
Appendix F	Hydraulic oil specification	115
Appendix G	LabVIEW front panel and control panel	118
Appendix H1	Pressure Transducers	120
Appendix H2	Positive displacement piston type flow meter	122
Appendix H3	National Instrument Data acquisition Card	126
Appendix I	Study orifice geometry	131

**EXPERIMENTAL INVESTIGATION AND NUMERICAL
SIMULATION FOR THE COEFFICIENT OF DISCHARGE FOR
SMALL OPENING ORIFICE AT LOW REYNOLDS NUMBER IN A
PILOT OPERATED RELIEF VALVE**

**By
Maher Khader Matar**

**Supervisor
Dr. Ahmed S. Al-Salaymeh**

ABSTRACT

The flow rate through an orifice is usually considered to be linearly proportional to the square root of the pressure difference upstream and downstream of the orifice. This proportionality constant is known as discharge coefficient. But thorough investigations by previous researchers showed that it varies as it is widely affected by several conditions, one of them is the Reynolds number in the orifice. An orifice is used to crack the pressure in the pilot stage in a pilot operated pressure relief valve. More accurate description of the relation between the flow rate and the pressure difference guides the designer of the valve to achieve highly stable performance in hydraulic circuit. The designer often requires a set of correlations which can be used to check out preliminary designs and converge on a solution prior to attempting detailed and expensive analysis.

This study aims to produce a formula that relates the coefficient of discharge to Reynolds number, and to make the prediction of the flow rate in an orifice for given pressures easier and faster.

The experimental work was carried out in the range of Reynolds number of about 16 to 700 for different conditions of viscosity and pressure settings.

In this study numerical simulation for the flow through the orifice was modeled using computational fluid dynamics, using the known software Fluent, the case was generated on the Gambit, then it was imported to Fluent, boundary conditions were applied, software let to solve the problem.

It was found that the coefficient of discharge varies with Reynolds number in small openings, at low Reynolds number values, for viscous flow. The value of the coefficient of discharge range found to be 0.21 to 0.97 for various conditions. The shape of the relation between the coefficient of discharge and the square root of Reynolds number was exponential.

Chapter One: Introduction

To estimate the volumetric flow rate through an orifice, it is common to use the known equation that relates the volumetric flow rate as it is proportional to the area of the orifice and the square root of the pressure difference upstream and downstream through the orifice, i.e. by the proportionality constant coefficient of discharge (C_d). But in practice this was not found exactly true. This is due to coefficient of discharge (C_d) dependency not only on the geometry of the orifice but also on Reynolds number (Re), which depends on the velocity of the flow in the orifice and that is related to the flow rate again, which is the subject of the equation (the required to be calculated). The sequence leads to inappropriate iterative solution. “for very small orifice openings, C_d varies significantly and can result in substantial error if assumed constant” (Wu et al. 2002).

1.1 Study Importance

This study will be performed on a pilot operated relief valve due to its dependency on pressure-flow control restrictions, which could be considered as orifices, and due to the variation of coefficient of discharge with Re in such small openings.

Previous researchers studied laboratory orifices made for special experiments, which were too perfect to be true in practical operations. But some of them studied practically used orifices in hydraulic components, such as directional control spool type valve, and pressure compensated flow control valve.

This study aims to introduce a better description of the relation of the coefficient of discharge with Reynolds number relation in small orifice opening at low Reynolds number

(less than 400). In addition, it aims to fit a formula between C_d and Re from experimental results, and to have clearer idea about the relation between the flow rate and the pressure difference, in a practically used orifice in some industrial device (hydraulic pilot operated relief valve). This could lead to dynamically customized design for hydraulic system, and to maintain high performance and stability for all working conditions, to minimize maintenance cost and to minimize power loss due to leakages and unnecessary high by-pass flows in hydraulic systems, to keep these systems stable and with high response.

A high performance pilot relief valve is the valve that governs the pressure at the setting point without high over shooting, and without early cracking pressure or leakage. This can be achieved by governing the relations of the cracking pressure and the flow rate through the valve, which depends on the relation between the coefficient of discharge and Reynolds number in the control orifices in an indirect way.

1.2 Study Objectives

A pilot operated relief valve will be investigated experimentally to study the relation between C_d and Re in the small opening orifices, and relation to be fitted from experimental data to describe the relation between the flow rate and the pressure drop across the orifices. Numerical simulation using computational fluid dynamics (CFD) software will be carried out and the output results will be compared with the experimental data.

The form of discharge coefficient as a function of Reynolds number makes it possible to mathematically manipulate the orifice flow rate equation, such as differentiating the flow rate to obtain the analytical expression of the pressure sensitivity, K_c . This is extremely

important in determining stability criterion using small signal analysis of hydraulic systems at small orifice openings.

1.3 Research methodology

1.3.1 Experimental setup and measuring devices

An experimental setup is built and data recorded from instrument readings, then results are extracted from this data. A computer simulation is done for the same orifice and flow conditions, and comparison is carried out to verify and judge the match of two results and methods.

1.3.2 Experimental procedure

During the experiment, the upstream and downstream pressures of the orifices and flow rate were measured. Flow rate for each sample is calculated. Then, the data were plotted and a model for the relation between the discharge coefficient and the flow rate was formulated. After that, the calculations and results were generated, to define the coefficient of discharge for the tested valve orifices.

Numerical simulation were carried out using a CFD software .The input were the conservation equations (as required), and the pressure difference across the orifice. The output was the mass flow rate and the flow velocity. The numerical results are plotted in graphs to clarify equations.

1.4 Basic theory of orifice

The layout of a typical orifice plate is shown in Figure (1.1) where D is the inside diameter of the pipe and D_o is the diameter of the orifice. The pressure taps may be placed in several locations as shown above, but the location of the pressure tap will influence the empirically

determined flow coefficient. The values of the flow coefficient must be consistent with the location of the pressure taps.

The base flow may be described by using the laws of conservation of mass and momentum. From the conservation of mass one can get that the mass flow through the pipe will equal the mass flow through the orifice:

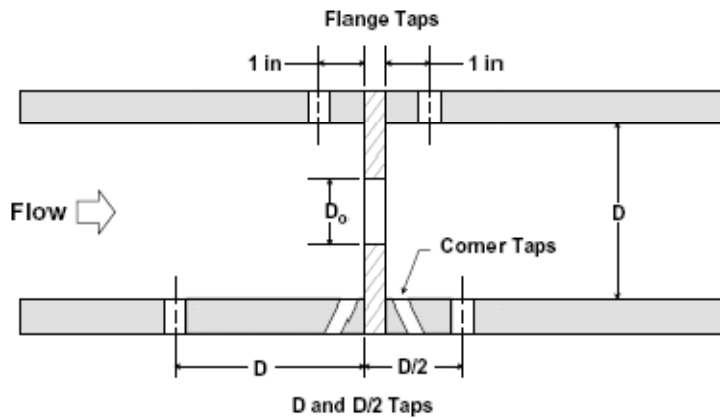


Figure 1.1 Orifice plate and locations of various pressure taps

$$\rho V A = \rho_0 V_0 A_0 \dots \dots \dots (1.1)$$

where ρ is the fluid density, V is the average velocity at a particular location, A is the cross-sectional area, and the subscript O denotes parameters at the orifice. The conservation of momentum may be reduced using a number of assumptions to the Bernoulli equation:

$$P + \frac{1}{2} \rho V^2 = P_0 + \frac{1}{2} \rho_0 V_0^2 \dots \dots \dots (1.2)$$

The density of the fluid is assumed to change very little. This assumption that the density of liquids is constant is valid here. In order to express the pressure drop across the orifice

in terms of the velocity and fluid density, the conservation of momentum equation (1.2) is rearranged.

$$P - P_0 = \frac{\rho}{2} (V_0^2 - V^2) = \frac{\rho V_0^2}{2} \left[1 - \left(\frac{V}{V_0} \right)^2 \right] \dots \dots \dots (1.3)$$

From conservation of mass, equation (1.1), the ratio of the velocities is inversely proportional to the cross-sectional area ratio,

$$\frac{V}{V_0} = \frac{A_0}{A} \dots \dots \dots (1.4)$$

Substituting equation (1.4) into equation (1.3) and solving for the velocity results in the following expression:

$$V_0 = \sqrt{\frac{2(P - P_0)}{\rho \left[1 - \left(\frac{A_0}{A} \right)^2 \right]}} \dots \dots \dots (1.5)$$

The volumetric flow rate is then,

$$Q = A \frac{1}{\sqrt{\left[1 - \left(\frac{A_0}{A} \right)^2 \right]}} \sqrt{\frac{2(P - P_0)}{\rho}} \dots \dots \dots (1.6)$$

Equation (1.6) is the theoretical flow rate for an incompressible fluid without any viscous losses. Flow through an orifice plate has significant flow losses. The nature of these losses must be accounted for in order to accurately measure the mass flow rate using the pressure drop across an orifice.

Let C be a constant that relates the actual mass flow rate with ideal one, and considering constant density fluid,

$$C \equiv \frac{\text{actual mass flow rate}}{\text{ideal mass flow rate}} \dots \dots \dots (1.7)$$

Therefore, the actual flow rate can be expressed as

$$Q = C A \frac{1}{\sqrt{\left[1 - \left(\frac{A_0}{A}\right)^2\right]}} \sqrt{\frac{2(P - P_0)}{\rho}} \dots \dots (1.8)$$

And for a specific area ratio the one over square root of area ratio could be merged in the constant to generate new one C_d , coefficient of discharge,

$$Q = C_d A \sqrt{\frac{2(P - P_0)}{\rho}} \dots \dots (1.9)$$

This is the main equation that the study investigate, specially the C_d , the coefficient of discharge, which has been considered to be constant for each orifice shape, which was found to be not accurate at all. This was the motivation for the previous researchers to find out the effective factors and parameters in this value in addition to the geometry of the orifice, and that was the motivation of this study also to investigate the relation between this value C_d and Reynolds number.

1.5 Thesis Layout

This thesis is composed of 6 chapters. The overall conclusions and recommendations were set in the results chapter.

- Chapter 1, Introduction:

In this chapter basics of orifice theory was presented, and the problem of current assumptions used was described, the motivation of this study was also a key element to show importance of the study. The main procedure steps mentioned as research methodology, and experimental setup components listed briefly.

- **Chapter 2, Literature Survey**

In this chapter previous studies were mentioned with a little bit about the result of each study, in a historical order.

- **Chapter 3, Relief valve**

In this chapter types of relief devices were discussed with the application of each type, the principle of different kinds were also mentioned, and finally this study relief valve was illustrated.

- **Chapter 4, Computational fluid dynamics (CFD)**

In this chapter the principle of numerical simulation for CFD software was shown, started by the need of CFD codes, and internal equations and steps were described, the key benefits of using Fluent and Gambit were mentioned.

- **Chapter 5, Experimental setup**

In this chapter the experimental setup containing the valve to be tested, the measurement devices and the hydraulic circuit were described. The specifications of each component were listed, and the combination of these devices was drawn in one figure.

- **Chapter 6, Results**

In this chapter the results of the experimental work and numerical simulation were discussed, starting from data listing to figures generating then to extract conclusions. Experimental and simulation results were compared to show the validation of using CFD in solving the problem of orifice flow equation.

Chapter Two: Literature review

Studies have been held to represent the C_d versus Re graphically to formulate a relation between them. Various types of orifices were used and modeled. Some practical devices were tested such as hydraulic valves to achieve higher performance.

Previous researchers studied laboratory orifices made for special experiments, which were too perfect to be true in practical operations. But some of them studied practically used orifices in hydraulic components, such as directional control spool type valve, and pressure compensated flow control valve.

Wu et al (2002) performed Experiments on valves to show that C_d changes with Reynolds number for small opening and data was plotted. Curves were fitted to have a model of C_d function with Re for three different types of orifices.

Their results showed that the curve generally had the shape as shown in Fig.(2.1) that represents the relation between C_d and \sqrt{Re} . Most experiments showed that the variation of C_d with Re was in the low Re range (from 0 to 400), then the C_d continues to be constant with higher Re .

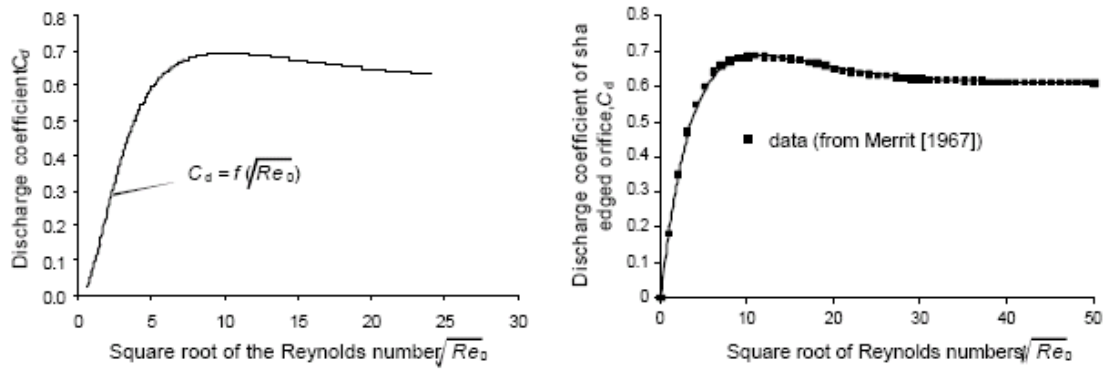


Figure 2.1 One of the simple empirical models was an exponential function between the C_d and square root of Re . Wu et al, (2002)

One of the simple empirical models was an exponential function

$$C_d = C_{\infty} \left(1 - e^{-\frac{\delta}{C_{\infty}} \sqrt{Re}} \right) \dots\dots\dots (2.1)$$

Where δ is called the laminar discharge coefficient, $C_d = \delta \sqrt{Re}$, for very small Reynolds number or mathematically $\left. \frac{\partial C_d}{\partial \sqrt{Re}} \right|_{\sqrt{Re}=0} = \delta C_{d\infty}$, is C_d at high Re where C_d is independent of Re .

All rest formulas were in same shape differs in number of terms and in constant definition.

Wu et al (2003) investigated coefficient of discharge with Reynolds number relation for small opening in a practical application (spool valve). The flow equation involved two modifications, first cross sectional area of orifice or spool valve opening modification due to clearances and chamfers of edges as a result of machining limitation, second coefficient of discharge modification due to varying with orifice geometry and Reynolds number.

The following Fig. (2.2) shows the actual flow and the theoretically predicted flow through pilot stage spool valve with respect to spool opening (displacement).

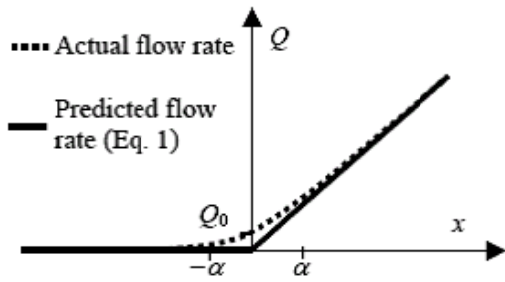


Figure 2.2 Actual flow rate compared with the Predicted flow rate for spool valve.

The difference between the actual flow rate and the predicted flow rate could be assumed as leakage, due to clearances and chamfer resulted by machining limitations in the valve. This small gaps could be considered as orifices as shown in Fig. (2.3).

The study assume the opening of the spool valve as rectangular, where (w) is the width, represents the average of the perimeter of the spool and the sleeve, and (d) is the height of the rectangle which depends on the displacement of the spool (x). the area is given by:

$$A(x) = \begin{cases} w(\sqrt{(2r+c)^2 + (2r+x)^2} - 2r) & x > -2r \\ w d_o & x = 0 \\ w c & x < -2r \end{cases} \dots\dots (2.2)$$

Where r, d_o, c and x are shown in fig. 3

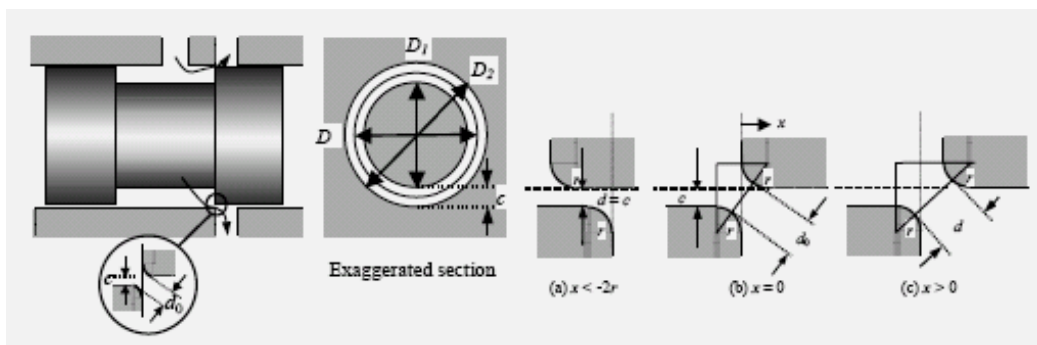


Figure 2.3 The clearance between the spool and the sleeve

After modeling the area the modification equation compared with the indirectly measured area in Fig. (2.4)

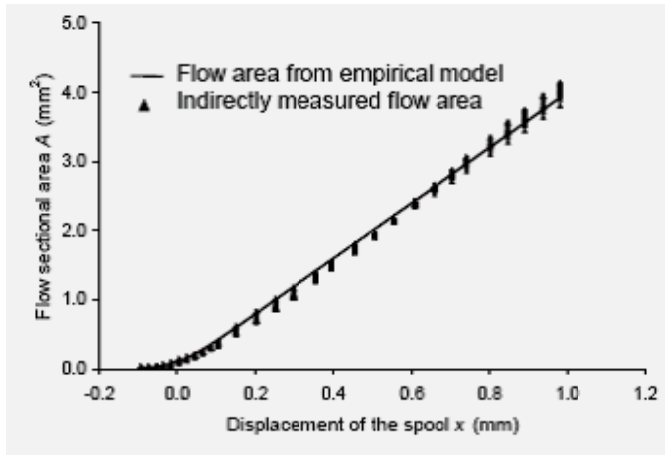


Figure 2.4 Comparison between empirical and measured areas

An empirical model is proposed $A(x) = \frac{wx}{1-e^{-ax}}$ and Fig. (2.5) shows the formula of area compared with measured area.

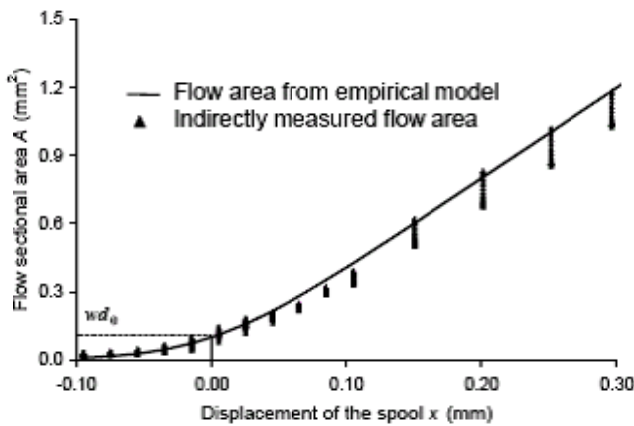


Figure 2.5 formula of area compared with measured area

Flow was modeled as the following equation

$$Q = C_{d\infty} \left(1 + a e^{\frac{\delta_1}{C_{d\infty}} \sqrt{Re}} + b e^{\frac{\delta_2}{C_{d\infty}} \sqrt{Re}} \right) \frac{w x}{1 - e^{-x}} \sqrt{\frac{2}{\rho} \Delta P} \dots \dots (2.3)$$

Where Q is volumetric flow rate, ΔP is pressure difference across the orifice, X=x/d_o and

$$\delta_1 = \frac{\delta e^{\frac{\delta_2}{C_{d\infty}}\sqrt{Re_m}}}{\frac{C_{dm}}{C_{d\infty}} - 1 + e^{-\frac{\delta_2}{C_{d\infty}}\sqrt{Re_m}}} \quad \delta_2 = \frac{\delta e^{\frac{\delta_1}{C_{d\infty}}\sqrt{Re_m}}}{\frac{C_{dm}}{C_{d\infty}} - 1 + e^{-\frac{\delta_1}{C_{d\infty}}\sqrt{Re_m}}} \dots \dots \dots (2.4)$$

Where C_{dm} is the maximum value of C_d and Re_m is Re at C_{dm} . This equation combines the modification of the C_d with the modification of area.

The flow gain K_q and the pressure sensitivity K_c can then derived as :

$$K_q = \frac{\partial Q}{\partial x} = \frac{C_d w}{1 - \varepsilon} \frac{(1 - (1 + X)e^{-X})}{(1 - e^{-X})^2} \sqrt{\frac{2}{\rho} \Delta P} \dots \dots \dots (2.5)$$

$$K_c = \frac{\partial Q}{\partial \Delta P} = \frac{C_d w X}{(1 - \varepsilon)(1 - e^{-X})\sqrt{2\rho\Delta P}} \dots \dots \dots (2.6)$$

Where $\varepsilon = \frac{\left(-a e^{\frac{\delta_1}{C_{d\infty}}\sqrt{Re}} - b e^{\frac{\delta_2}{C_{d\infty}}\sqrt{Re}}\right)\sqrt{Re}}{2C_d}$

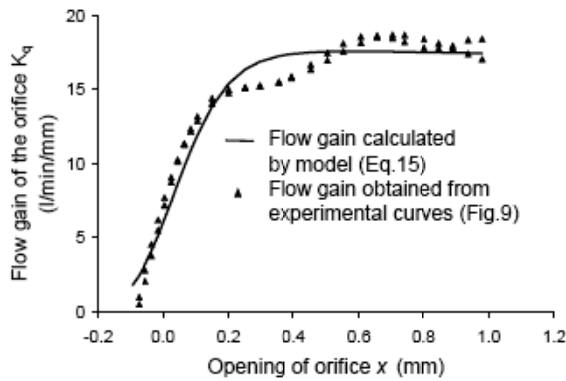


Figure 2.6 Comparison between Calculated flow gain and measured one

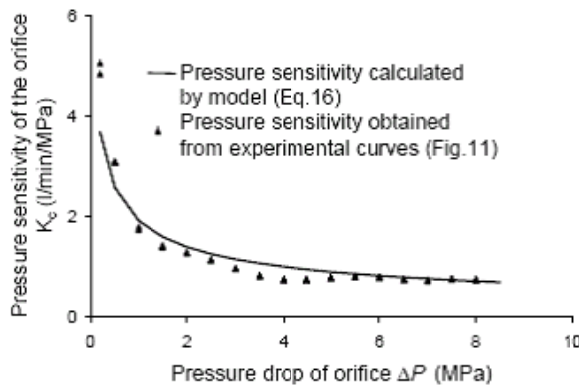


Figure 2.7 Comparison between Calculated Pressure sensitivity and measured one

Wu et al (2007) studied a pressure-compensated valve (PC valve). This is a type of flow control device that is a combination of a control orifice and a compensator (often called a hydrostat). The compensator orifice modulates its opening to maintain a constant pressure drop across the control orifice. In other words, the PC valve is designed such that the flow rate through the valve is governed only by the opening of the control orifice and is independent of the total pressure drop across the valve. The effect of the nonlinearities on the performance of the PC valve is investigated.

A generic nonlinear model of a PC valve is developed. Using this model, all possible operating conditions can be determined. Then a linearized model is developed and used to analyze the dynamic behavior of the PC valve.

Bulut et al (2004) studied an analytical solution of a steady flow problem of a viscous incompressible fluid through an orifice by using the Adomian's decomposition method. The numerical results show the effectiveness of the method for this type of equations, they show that the present approach is relatively easy and highly accurate.

Greenspan has formulated a problem which contains the basic components of all axi-symmetrical orifice flow problems. Under the assumption of axial symmetry, the problem can be treated as a plane problem as shown in Fig. (2.7). The flow in the domain D whose vertices are A, B, C, D, E, F, G and H; is governed by the Navier–Stokes equations in cylindrical coordinates.

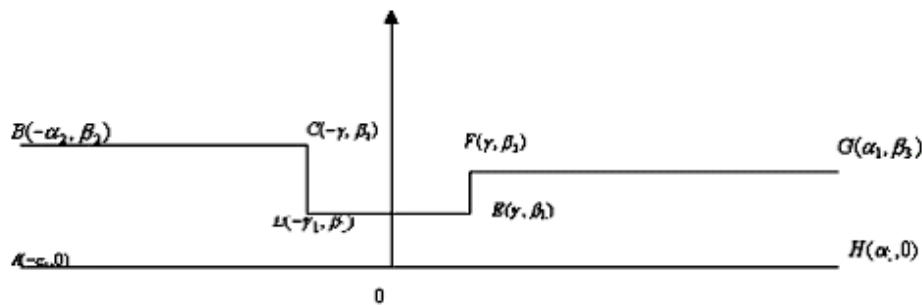


Figure 2.8 The flow in the domain

$$\frac{\partial^2 \psi}{\partial r^2} - \frac{1}{r} \frac{\partial \psi}{\partial r} + \frac{\partial^2 \psi}{\partial x^2} = -r^2 \Omega \dots \dots \dots (2.7)$$

$$r \frac{\partial^2 \Omega}{\partial r^2} + \frac{3}{r} \frac{\partial \Omega}{\partial r} + \frac{\partial^2 \Omega}{\partial x^2} = R \left(\frac{\partial \psi}{\partial r} \frac{\partial \Omega}{\partial x} - \frac{\partial \psi}{\partial x} \frac{\delta \Omega}{\delta r} \right) \dots \dots \dots (2.8)$$

Where ψ is the stream function, Ω is related to the vorticity ξ by $\Omega = \xi / r$, and R is Reynolds number.

The study considers steady, two-dimensional motion of a viscous fluid in a tube. The equations of motion which govern the flow field in the tube are the Navier–Stokes equations in cylindrical coordinates and they are given by

$$\frac{\partial^2 \psi}{\partial r^2} - \frac{1}{r} \frac{\partial \psi}{\partial r} + \frac{\partial^2 \psi}{\partial x^2} = \phi(x, r) \dots \dots \dots (2.9)$$

$$\psi(0, r) = f(x), \quad \psi'(0, r) = g(x) \dots \dots \dots (2.10)$$

Here $\phi(x, r)$ is given function of x and r .

The unknown function $\psi(x, r)$ is computed in terms of the components defined by the decomposition series given as

$$u(x, r) = \sum_{n=0}^{\infty} u_n(x, r) \dots \dots \dots (2.11)$$

As a results, the series solutions is given by

$$\psi(x, r) = \psi_0 - \sum_{n=1}^{\infty} \left\{ L_x^{-1} \frac{1}{r} (\psi_{n-1})_r - L_x^{-1} L_r \psi_{n-1} \right\} \dots \dots \dots (2.12)$$

Where L_x and L_r symbolize $\partial^2/\partial x^2$ and $\partial^2/\partial r^2$ respectively and assuming inverse operator exists;

$$L_x^{-1} = \int_0^x \int_0^x (\cdot) dx dx$$

Reader-Harris et al (1995) stated that the orifice plate is the recognized flow meter for the measurement of natural gas and light hydrocarbon liquids, and the orifice discharge coefficient equation in use in the international standard ISO 5167-1:19911 is based on data collected more than 50 years ago.

The study described the work undertaken to derive an improved orifice plate discharge coefficient equation based on the enlarged EEC/API database including the data collected in 50 and 600 mm

pipes. It consists of several terms, each is based on an understanding of the physics. An earlier version of this equation, based on a smaller database, was accepted at a meeting of EEC and API flow measurement experts in New Orleans in 1988. Emphasis is placed on the two principal changes to the equation: improved tapping terms for low Reynolds number and an additional term for small orifice diameter, and its physical basis in orifice edge roundness given.

Cruz-Maya et al (2006) selected a toroidal Venturi nozzle, operating mainly at critical conditions and shaped according to the recommendation of the ISO Standard 9300. The focus was to provide a new theoretical and numerical correlation for the calculus of the discharge coefficient on turbulent boundary layer conditions for gases at $Pr = 0.7$. The study was performed to investigate the effects of the viscous stresses in the boundary layer, dimensionless wall temperature in the throat nozzle, and the flow field curvature at the nucleus of the nozzle on the discharge coefficient. The determination of this coefficient was based on the turbulent boundary layer theory and a numerical simulation for a two-dimensional flow. The numerical simulation of the flow was carried out by means of the commercial CFD code. The correlation obtained was validated by means of a direct comparison between the experimental correlations of the discharge coefficient of ISO-9300 and the correlations obtained by the Korea Research Institute of Standards and Science (KRISS) with turbulent boundary layer. This validation was performed for throat Reynolds numbers from 1.4 to 2.6×10^6 . The agreement of the theoretical and measured discharge coefficients by these correlations was better than 0.2%.

Chapter Three: Relief valve

3.1 Pressure Relief Devices

A pressure relief device is actuated by inlet static pressure and is designed to open during emergency or abnormal conditions to prevent a rise of internal fluid pressure in excess of a specified value. The device may also be designed to prevent excessive internal vacuum.

Pressure relief devices protect a vessel against overpressure only. These devices do not protect against structural failure when the vessel is exposed to abnormal conditions such as high temperature due to fire. The main types of pressure relief devices are: (1) reclosing-type pressure relief devices, (2) vacuum-type pressure relief devices, and (3) non-reclosing-type pressure relief devices. Figure 3.1 shows the main types of pressure relief devices.

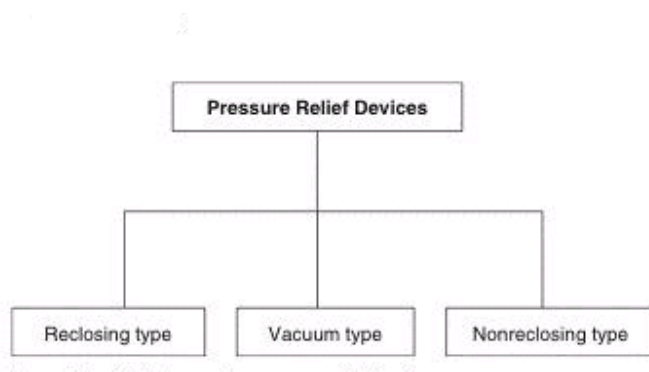


Figure 3.1 Main types of pressure relief devices

3.2 Reclosing-Type Pressure Relief Devices

A reclosing-type pressure relief device is a pressure relief device designed to close after operation. There are many types of reclosing-type pressure relief devices. Figure (3.2) shows types of reclosing-type pressure relief devices.

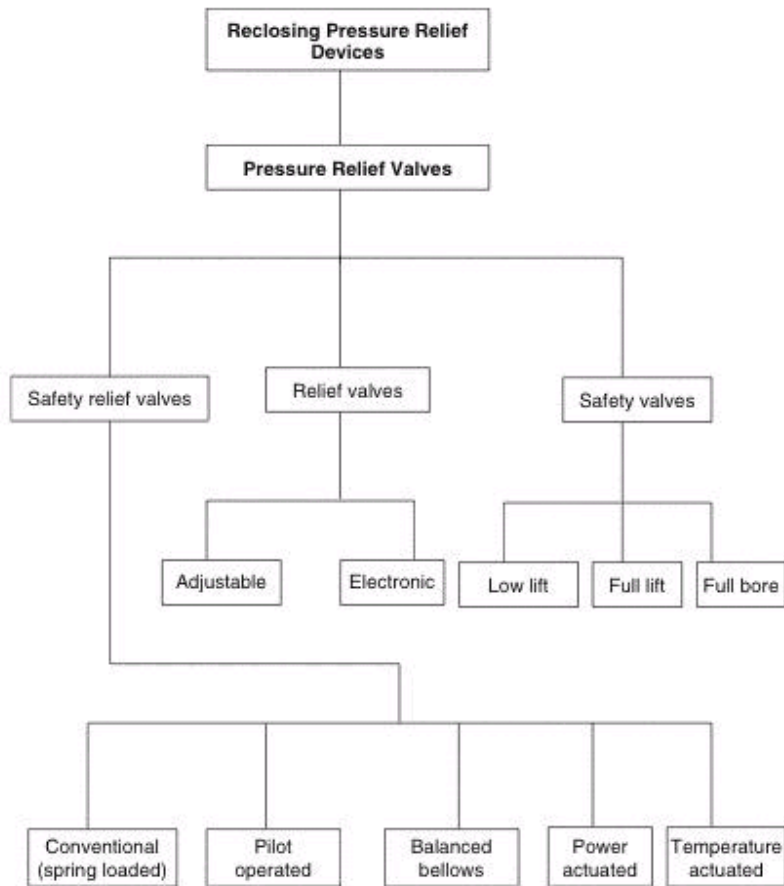


Figure 3.2 Types of reclosing relief devices

3.3 Pressure relief valves

A pressure relief valve is a spring-loaded pressure relief device, which is designed to open to relieve excess pressure and to reclose and prevent further flow of fluid after normal conditions have been restored (Fig. 3.3). It may be used for either compressible or incompressible fluids, depending on design, adjustment, or application. Pressure relief valve is a general term, which includes safety valves, relief valves, and safety relief valves.

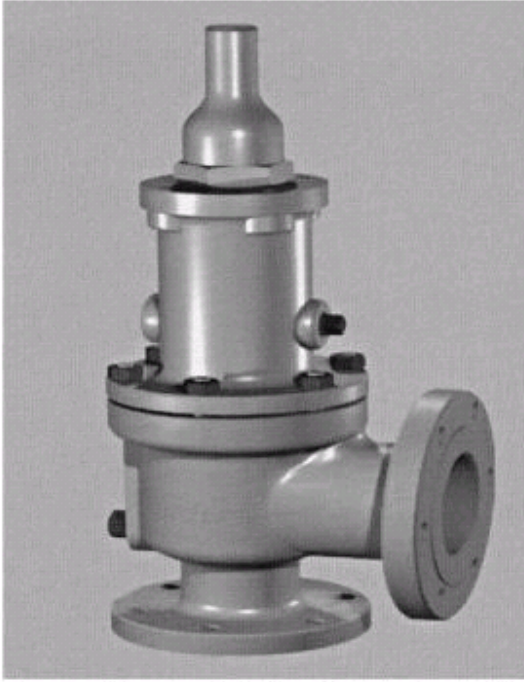


Figure 3.3 Pressure relief valve

3.4 Safety valves

A safety valve is a pressure relief valve actuated by inlet static pressure and characterized by rapid opening or pop action (Fig. 3.4). Safety valves are used primarily with compressible gases and in particular for steam and air.



Figure 3.4 Safety valve

Safety valves are classified according to the lift and bore of the valves. Types of safety valves are low-lift, full-lift, and full-bore safety valves.

- Low-lift safety valve. A low-lift safety valve is a safety valve in which the disk lifts automatically such that the actual discharge area is determined by the position of the disk.
- Full-lift safety valve. A full-lift safety valve is a safety valve in which the disks lift automatically such that the actual discharge area is not determined by the position of the disk.
- Full-bore safety valve. A full-bore safety valve is a safety valve which has no protrusions in the bore and in which the valve disk lifts to an extent sufficient for

the minimum area at any section at or below the seat to become the controlling orifice.

3.5 Relief valves

A relief valve is a pressure relief device actuated by inlet static pressure and having a gradual lift generally proportional to the increase in pressure over opening pressure. It may be provided with enclosed spring housing suitable for closed discharged system applications. Relief valves are commonly used in liquid systems, especially for lower capacities and thermal expansion applications. They can also be used on pump systems as pressure overspill devices.

Adjustable relief valve.

Adjustable relief valves feature convenient adjustment of the pressure setting through the outlet port. These are generally available with pressure ranges up to 508 psi (35 bar), and operating temperature up to 600°F (315°C). Adjustable relief valves are suitable for nonvented or vented inline applications in chemical, petrochemical, and high-purity gas industries.

Electronic relief valve.

An electronic relief valve (ERV) is a pilot-operated relief valve which offers zero leakage. The ERV package combines a zeroleakage isolation valve with electronic controls to monitor and regulate system pressure. These valves provide protection either in a capacity relieving function or simply in an overpressure-protection application. An electronic relief valve system is shown in Fig. (3.5).

The electronic relief valve system consists of:

1. The valve. Generally a metal seated ball valve is used.
2. The actuator. The actuator may be electric, hydraulic, or pneumatic and operated by gears.

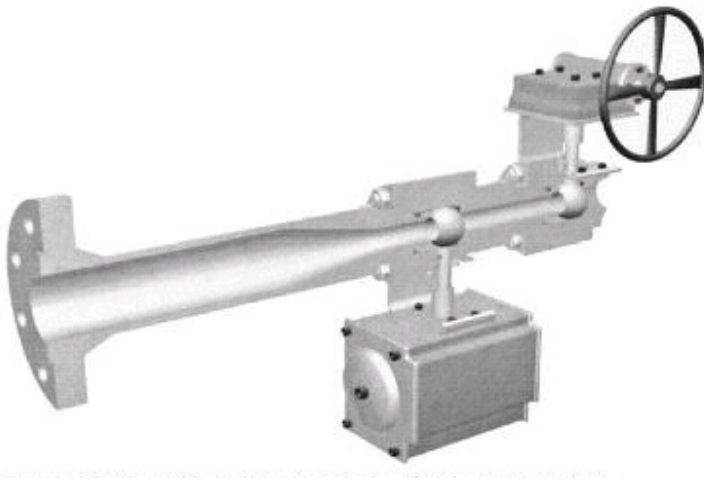


Figure 3.5 Electronic relief valve

3. The control system. The ERV is supplied with or without remote controls and display. Numerous pressure ranges from zero to 5000 psi (34.5 MPa) are available. Accuracy of 1/4% is achieved for 1000to 3000-psi and 0.1% for 5000-psi units. Standard units operate from 115 V ac or V 125 dc and control AC, DC, or pneumatic actuators.

3.6 Conventional pressure relief valves Operation

The conventional pressure relief valve is characterized by a rapid-opening pop action or by opening in a manner generally proportional to the increase in pressure over the opening pressure (Figs. 3.6). The basic elements of a conventional pressure relief valve consist of:

- An inlet nozzle connected to the vessel or system to be protected
- A movable disk which controls flow through the nozzle
- A spring which controls the position of the disk

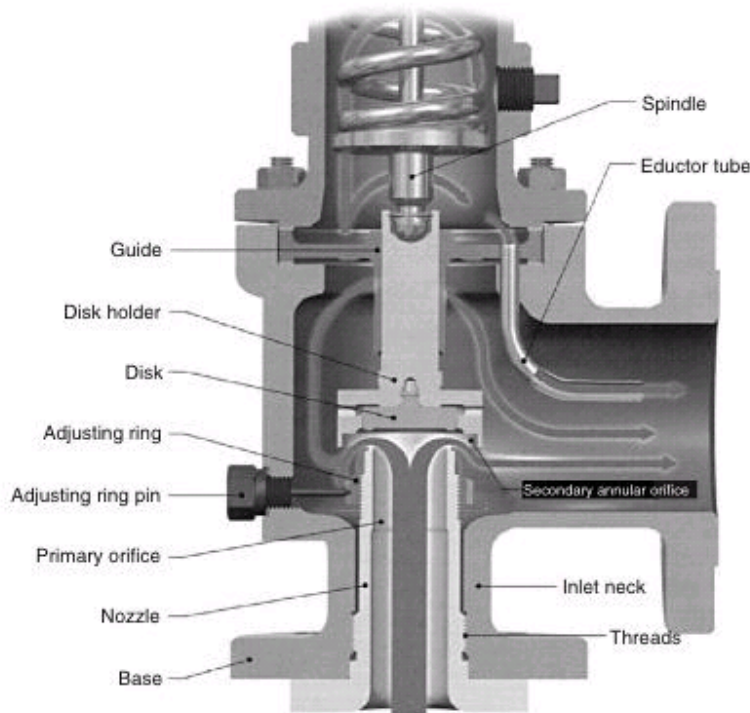


Figure 3.6 Conventional pressure relief valves

Under normal operating conditions, the pressure at the inlet is below the set pressure and the disk is seated on the nozzle, preventing flow through the nozzle. Conventional pressure relief valves are used for applications where excessive variable or built-up back pressure is not present in the system. The operational characteristics are directly affected by changes of the back pressure on the valve.

Working principle.

The working principle of a conventional spring loaded pressure relief valve is based on the balance of force. That means the spring load is preset to equal the force exerted on the closed disk by the inlet fluid when the system pressure is at the set pressure of the valve. The disk remains seated on the nozzle in the closed position when the inlet pressure is below the set pressure. The valve opens when the inlet pressure exceeds set pressure, overcoming the spring force. The valve recloses when the inlet pressure is reduced to a level below the set pressure.

When the pressure relief valve is closed during normal operation, the vessel pressure acting against the disk surface is resisted by the spring force. When the vessel pressure approaches the set pressure, the seating force between the disk and the nozzle approaches zero. When vessel pressure slightly exceeds the set pressure, fluid will move past the seating surfaces into the huddling chamber. During this operation, pressure is built up in the huddling chamber as a result of restricted flow between the disk holder and adjusting ring. The controlled pressure buildup in the huddling chamber will overcome the spring force, causing the disk to lift and the valve to pop open. Additional pressure buildup occurs, causing the disk to lift substantially at pop. This is the result of sudden flow increase and the restriction to flow through another annular orifice formed between the inner edge of the disk holder skirt and the outside diameter of the adjusting ring.

The pressure relief valve closes when the inlet pressure has dropped considerably below the set pressure, allowing the spring force to overcome the summation of forces. The pressure at which the valve reseats is called the closing pressure. The difference between

the set pressure and the closing pressure is called blowdown. During operation, the disk travels as pressure is built-up. The disk travels from the set pressure to the maximum relieving pressure during overpressure, and to the closing pressure during blowdown.

Types of valves.

Seat leakage is an important consideration in the design of a conventional pressure relief valve. Seat leakage may result in continuous loss of system fluid and may cause progressive damage to the valve seating surfaces. Based on the seating material, conventional pressure relief valves are classified as: metal seated valves and soft seated valves.

Conventional metal seated valves.

Metal-to-metal seats, commonly made from stainless steel, are normally used for high temperature such as steam. The following are advantages of conventional metal-seated pressure relief valves:

- Lowest cost (in smaller sizes and lower pressures)
- Wide chemical compatibility
- High temperature capability
- Standard center-to-face dimensions (API 526).
- General acceptance for most applications

The following are disadvantages of conventional metal-seated pressure relief valves:

- Seat leakage, resulting in lost product and unacceptable emissions, causing environmental pollution.

- Simmer and blowdown adjustment is a compromise, which may result in intolerable leakage, and product loss.
- Vulnerable to effects of inlet pressure losses.
- Sensitive to effects of back pressure (set pressure and capacity).
- Generally not able to obtain accurate, in-place set-pressure verification.

Conventional soft seated valves.

As alternative to metal, resilient disks can be fixed to either or both the seating surfaces where tighter shut-off is required, specially for gas or liquid applications. These inserts may be made from a number of different materials, but Viton, nitrile or EPDM are the most common. Soft seal inserts are not recommended for steam use. The conventional soft seated pressure relief valve has the following advantages:

- Good seat tightness before relieving
 - Good reseal tightness after relieving
 - Good cycle life and maintained tightness
 - Low maintenance costs
- The conventional soft seated valve has the following disadvantages:
- Temperature is limited to seat material used.
 - Chemically limited according to soft goods used.
 - Vulnerable to effects of inlet pressure losses.

3.7 Pilot-operated pressure relief valves

A pilot-operated pressure relief valve is a pressure relief valve in which the major relieving device is combined with and is controlled by a self actuated auxiliary pressure relief valve

(Fig. 3.7). The primary difference between a pilot-operated pressure relief valve and a spring-loaded pressure relief valve is that the pilot-operated valve uses process pressure to keep the valve closed instead of a spring. A pilot is used to sense process pressure and to pressurize or vent the dome pressure chamber which controls the valve opening or closing.

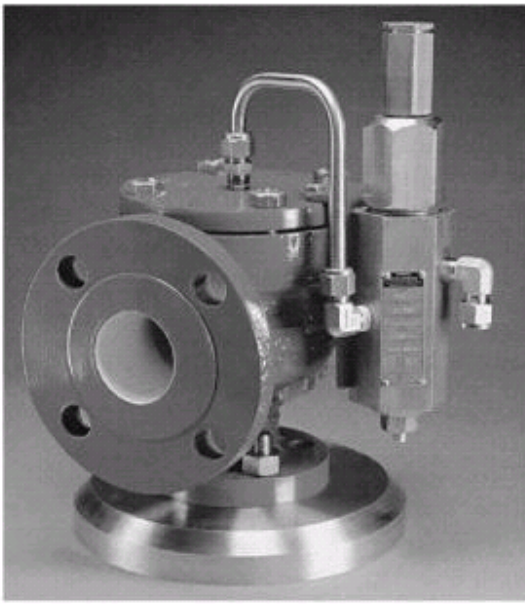


Figure 3.7 Pilot-operated pressure relief valve

A pilot-operated pressure relief valve consists of the main valve, a floating unbalanced piston assembly, and an external pilot. The pilot controls the pressure on the top side of the main-valve unbalanced moving chamber. A resilient seat is normally attached to the lower end of this member.

- At pressures below set, the pressure on opposite sides of the moving members is equal.

- When the set pressure is reached, the pilot opens, depressurizes the cavity on the top side and the unbalanced member moves upward, causing the main valve to relieve.
- When the process pressure decreases to a predetermined pressure, the pilot closes, the cavity above the piston is depressurized, and the main valve closes.

Advantages of the pilot-operated pressure relief valve are as follows:

- The pilot-operated valve's set pressure is not affected (comparing with conventional relief valve) by back pressure. The pilot control valve, isolated from the influence of downstream pressure, controls the main valve's opening and closing.
- The pilot-operated valve operates bubble tight at higher operating pressure-to-set pressure ratios, allowing operators to run very close to the vessel's maximum allowable working pressure.
- As the system pressure increases, the force holding the disk in closed position increases. This allows the system operating pressure to be increased without danger of increased seat leakage in the main valve.
- Reduced cost of the larger size valves. The large spring and associated envelope is replaced by a small pilot, thus reducing the mass and cost of the valve.
- Less susceptible to chatter.
- Pilot-operated pressure relief valves have the following disadvantages:
 - Pilot is susceptible to plugging.
 - Potential for back flow.

Working principle of pilot operated-pressure relief valve.

The working principle can be described for three positions: Closed valve position, relieving cycle, and reclosing cycle.

Closed valve position. As the system approaches set pressure, the pressure pickup transmits the pressure from the inlet of the main valve through the pilot control and into the dome of the main valve. This pressure acts on the top of the piston in the dome, holding the piston firmly against the seat on the nozzle of the main valve.

Relieving cycle. When the inlet pressure overcomes the spring force in the pilot valve, the pilot valve lifts. As the seat assembly in the pilot control begins to lift, it seals off the flow of pressure to both the vent and the main valve dome. At that time, the pressure in the dome is released through the pilot vent. As the pressure in the dome has been released, the system pressure acting on the bottom of the piston lifts the piston and relieves system overpressure.

Reclosing cycle. When the system pressure blows down, the spring force in the pilot valve overcomes the force of the system acting on the pilot control seat assembly. The pilot control redirects system pressure back into the main valve dome, closing the main valve. Of course, blowdown can be adjusted by raising and lowering the blowdown adjuster position in the pilot valve.

Types of valves.

There are two general types of pilot-operated pressure relief valves: piston and diaphragm.

Piston-type pilot-operated pressure relief valve.

This type of valve (Fig. 3.8) uses a piston for the unbalanced moving member. A sliding O-ring or spring-loaded plastic seal is used to obtain a pressure seal for the dome activity. The piston-type valve is used for pressures from 5 to 10,000 psig, and occasionally for even higher pressures.

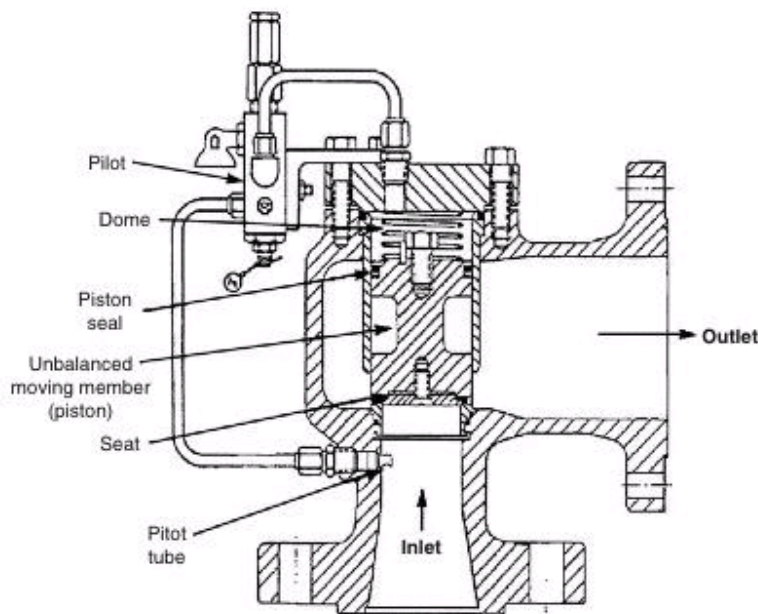


Figure 3.8 Piston type pilot-operated pressure relief valve

Diaphragm-type pilot-operated pressure relief valve.

This type of valve (Fig. 3.9) is similar to the piston type except that a flexible diaphragm is used to obtain a pressure seal for the dome volume instead of a piston and sliding piston seal. This is done to eliminate sliding friction and permit valve operation at much lower pressures than would be possible with a sliding seal. The diaphragm-type valve can be used for pressures from 3-in water column (0.108 psig) to 50 psig.

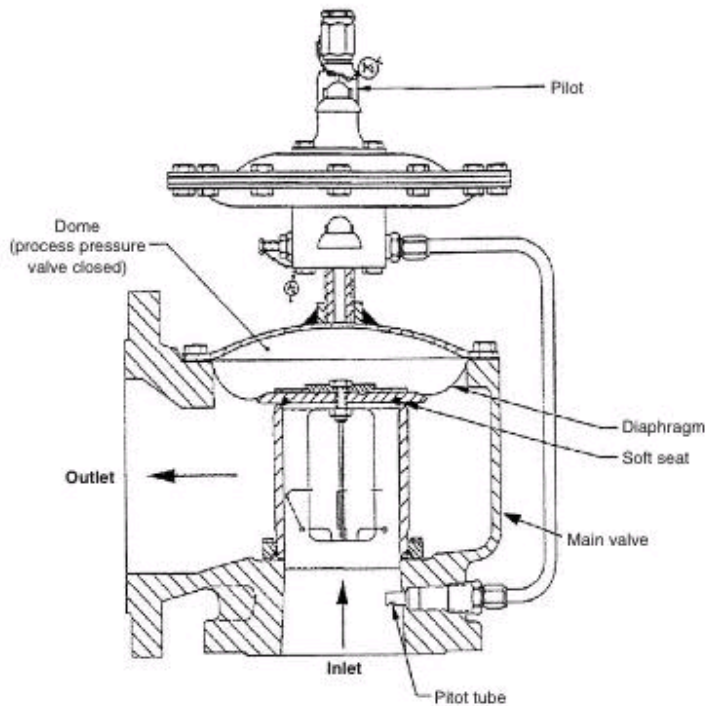


Figure 3.9 Diaphragm-type pilot-operated pressure relief valve

Types of pilots.

The pilot that operates the main valve can be classified based on (1) action and (2) flow.

Based on action.

Based on action, the pilot may be classified as a popaction or a modulating-action pilot.

Pop-action pilot. The pop-action pilot (Fig. 3.10) causes the main valve to lift fully at set pressure without overpressure. Typical relationship between lift of disk or piston and vessel pressure in a pop-action pilot operated pressure relief valve is shown in Fig. (3.11).

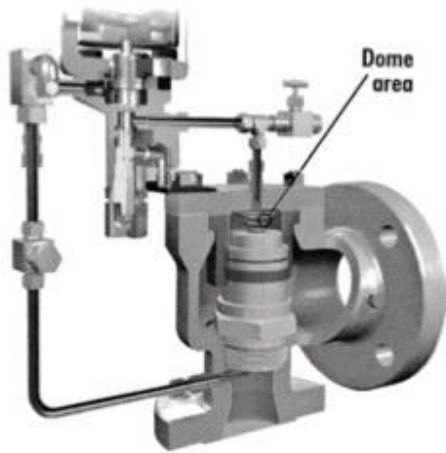


Figure 3.10 Pop action pilot-operated pressure relief valve

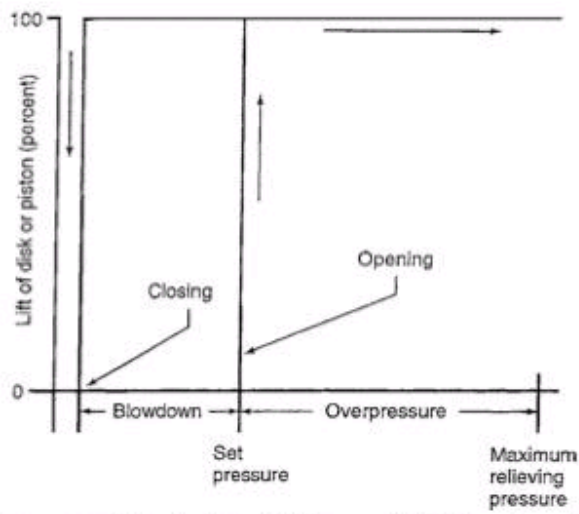


Figure 3.11 Typical relationship between lift of disk and vessel pressure in a pop-action pilot-operated pressure relief valve

Modulating-action pilot valve.

The modulating pilot opens the main valve only enough to satisfy the required relieving capacity. Typical relationship between lift disk or piston and vessel pressure in modulating-action pilot-operated pressure relief valve is shown in Fig. (3.12).

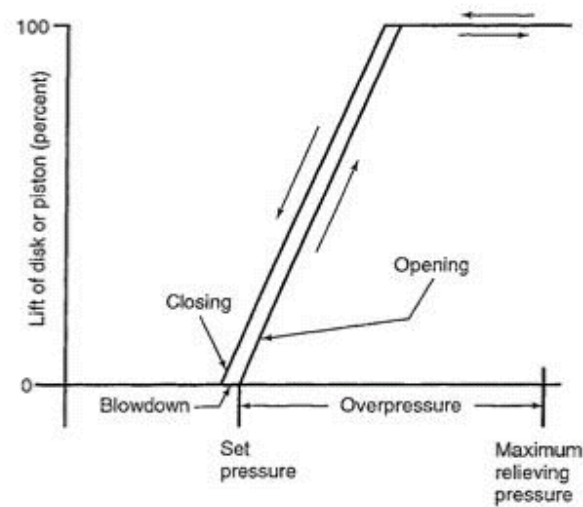


Figure 3.12 Typical relationship between lift of disk and vessel pressure in a Modulating -action pilot-operated pressure relief valve

Based on flow.

Based on flow, the pilot may be classified as flowing or nonflowing type.

Flowing-type pilot.

The flowing type allows process fluid to flow continuously through the pilot when the main valve is open (Fig. 3.13).

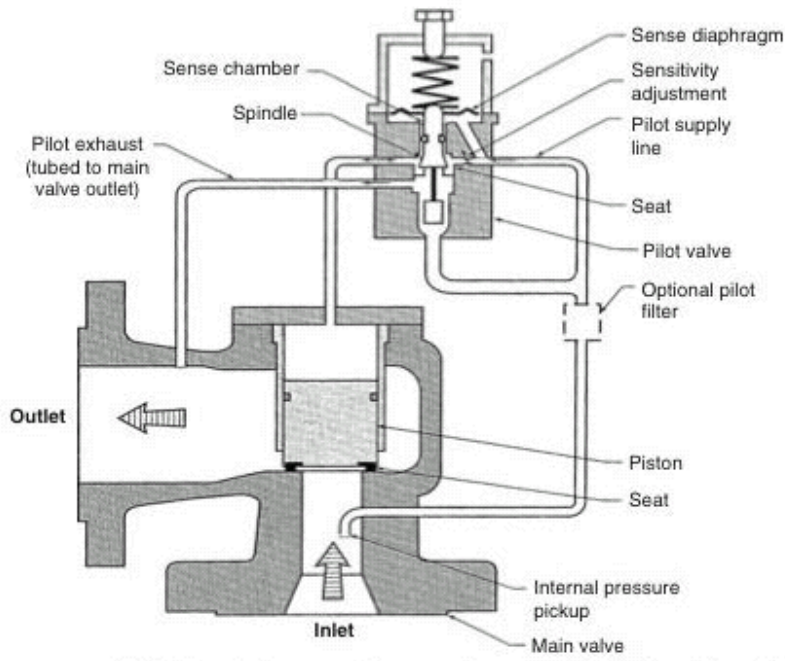


Figure 3.13 Modulating-flowing-type pilot-operated pressure relief valve

Nonflowing-type pilot.

The nonflowing-type pilot does not allow process fluid to flow continuously when the main valve is open (Fig. 3.14). This type of pilot is generally recommended for services to reduce the possibility of hydrate formation (icing) or solids in the landing fluid affecting the pilot's performance.

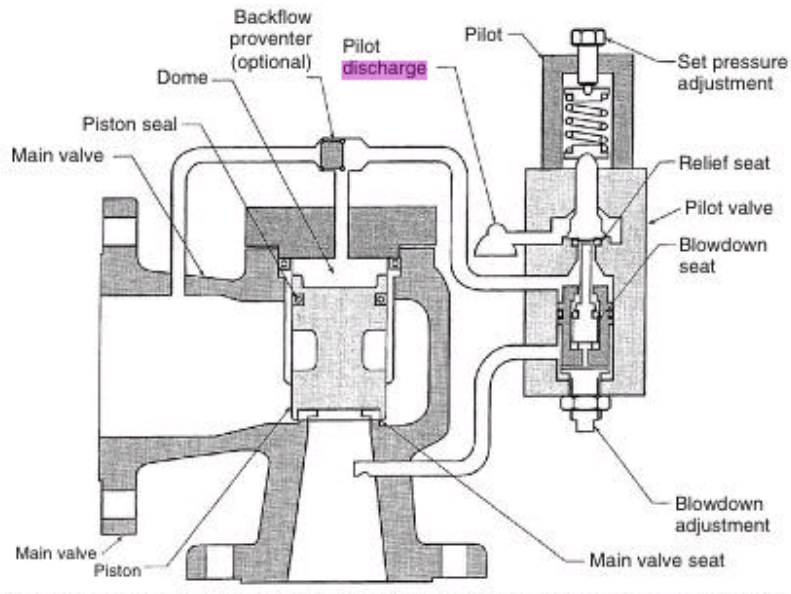
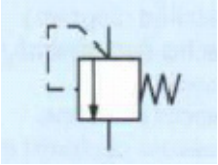
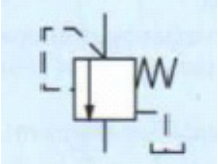
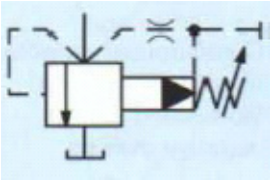
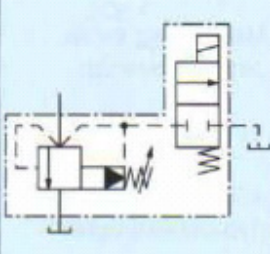


Figure 3.14 Pop-action nonflowing-type pilot-operated pressure relief valve

3.8 Symbols of different types of hydraulic relief valves:

Here is a table of hydraulic symbols for different types of relief valves according to DIN ISO 1219.

Table 3.1 Relief valves hydraulic symbols

Symbol	Description
	Pressure relief valve Direct operated Internal pilot oil feed
	Pressure relief valve Direct operated External pilot oil feed
	Pressure relief valve Pilot operated Internal pilot oil feed and return
	Pressure relief valve Pilot operated Electrically operated relief Internal pilot oil feed External pilot oil return

3.9 This study of pressure relief valve

The study investigates a hydraulic pilot operated relief valve, due to the dependency of controlling pilot pressure on orifices, and the aim of this study is to describe the relation

between C_d and \sqrt{Re} , which could be used by designer of hydraulic components to understand the relation between the flow and the pressure drop through the orifice better.

A relief valve from Rexroth Bosch group has been chosen with the following specification:

Table 3.2 This study relief valve main specifications

Series	DB
Nominal size	20
Pressure setting	315bar
Mounting	subplated

This valve has the options of simple blocking of unnecessary pilot control lines, easy to insert porting plate between the main stage and the pilot stage, changeable orifice so one can dismantle the orifice and make dimension measurement.

The work principle of the pilot operated relief valve which is shown in Fig. (3.15) can be explained as below:

The pressure present in port (A) acts on the main poppet (3). At the same time pressure is applied via the control line (6), which is fitted with orifices (4) and (5), on the spring loaded side of the main poppet (3) and at the ball (8) in the pilot control stage. If the pressure in port (11) exceeds the value set at the spring (9), the ball (8) opens against the spring (9). The signal for this comes internally via the control lines (6) from port (A). The pressure fluid on the spring loaded side of the main poppet (3) now flows via the control line, and ball (8) into the spring (9) chamber. It flows internally via the control line (13) to

tank. Due to the orifices (4) and (5) a pressure drop occurs at the main poppet (3), the connection from port (A) to tank port is open, now the pressure fluid flows from port (A) to tank whilst maintaining the set operating pressure. (Rexroth Bosch Group).

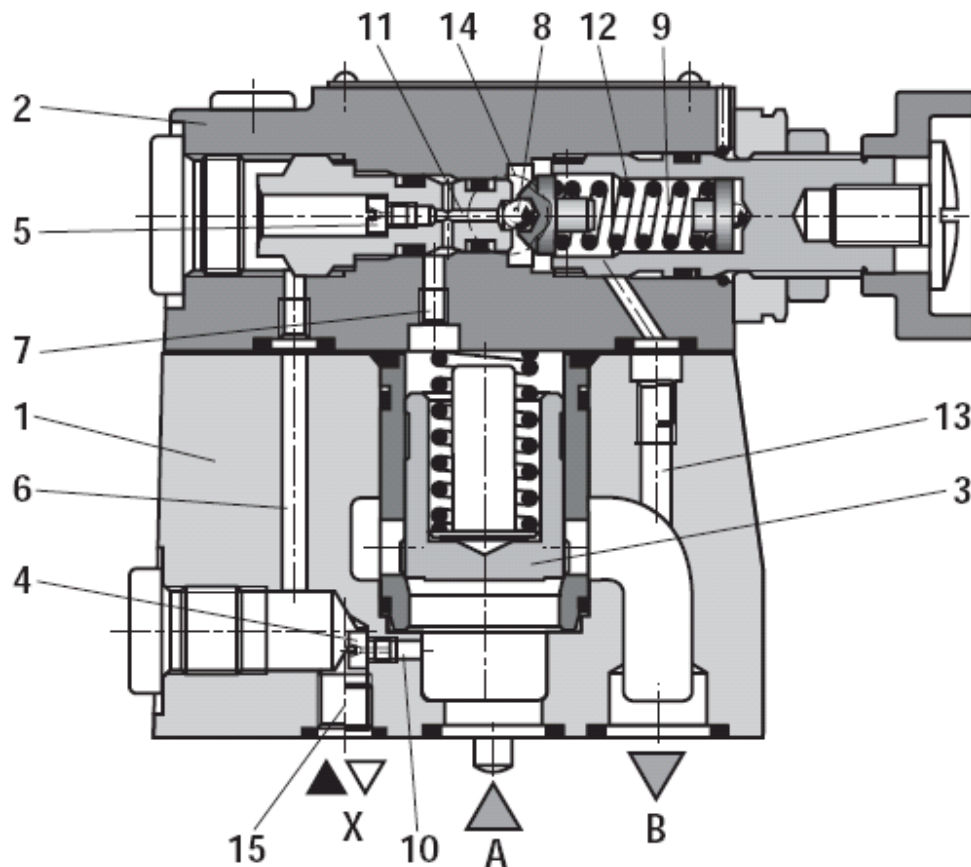


Figure 3.15 Cross sectional view of pilot operated relief valve, REXROTH

The aim of putting the orifice in the pilot stage is to crack the pressure to have control pilot pressure -which is a fraction of the main pressure- to support the spring forces -poppet closing forces- to hold the poppet closed acting opposite of the force of main pressure that tries to open the poppet. So the pilot pressure and spring forces hold the poppet close till the main pressure exceeds the set point, in that case the main pressure pushes the poppet

and forces it to move upward, allowing the fluid to pass to tank line, which is the relief action.

The opening of the poppet (the circumferences area between the edge of poppet and the housing cavity of the valve) depends directly on the flow rate that is required to be passed to the tank line to maintain the pressure at the set point, so higher flow rate to be discharged higher area to be created, which leads to longer stroke the poppet has to travel, and knowing that the spring force depends directly on the compression stroke, this means that higher flow rate to be discharged higher stroke poppet has to travel and higher spring force leads directly to rise the main pressure under the poppet higher than the set point, which could be considered as disadvantage of the nonlinearity of the relief valve, that the relief valve starts to open in the set point pressure, then it overshoots the pressure setting to a higher pressure if the valve has to pass higher flow rate, in other word the pressure setting is no more independent of flow rate, which puts the designer in two bad option; to have early crack pressure for the relief valve , or to have high overshoot for the system pressure. This makes the following sentence totally right in both direction –for the flow or for the pressure- : *“Because of the high nonlinearities associated with this type of valve (pressure flow control valves), it is impossible, in practice, to design such a valve where the flow rate is completely unaffected by the pressure drop across the valve.”*, (Wu , et al. , 2007). This generates the recommendation of carrying out thorough investigations on the pressure-flow control devices, including orifices.

Chapter Four: Computational Fluid dynamics

Computational fluid dynamics (CFD) is an engineering method in which flow fields and other physics are calculated in detail for an application of interest. The CFD, or fluid simulation, results can be used as part of a simulation driven product development process to illustrate how a product or process operates, to troubleshoot problems, to optimize performance and to design new products.

4.1 Numerical Simulation and Computational Fluid Dynamics

This is a description of the main steps of Computational Fluid Dynamics software that are automatically generated, by ready options and functions, already programmed code and prepared as graphical user interface. Famous software package will be used in this study which is Fluent and Gambit. This chapter is just a demonstration how things happen internally.

4.2 The Need for CFD

Applying the fundamental laws of mechanics to a fluid gives the governing equations for a fluid. The conservation of mass equation is

$$\frac{\partial \rho}{\partial t} + \nabla \cdot (\rho \vec{V}) = 0 \dots \dots \dots (4.1)$$

And the conservation of momentum equation is

$$\rho \frac{\partial \vec{V}}{\partial t} + \rho (\vec{V} \cdot \nabla) \vec{V} = -\nabla p + \rho \vec{g} + \nabla \cdot \tau_{ij} \dots \dots \dots (4.2)$$

These equations along with the conservation of energy equation form a set of coupled, nonlinear partial differential equations. It is not possible to solve these equations analytically for most engineering problems.

However, it is possible to obtain approximate computer-based solutions to the governing equations for a variety of engineering problems. This is the subject matter of Computational Fluid Dynamics (CFD).

4.3 Applications of CFD

CFD is useful in a wide variety of applications and here is a brief to give an idea of its use in industry. The simulations shown below have been performed using the FLUENT software.

The CFD analysis showed the effectiveness of a simpler manifold design without the need for field testing.

CFD is attractive to industry since it is more cost-effective than physical testing. However, one must note that complex flow simulations are challenging and error-prone and it takes a lot of engineering expertise to obtain validated solutions.

4.4 Ansys Fluent Software Package

Fluent fluid flow analysis technology allows for an in-depth analysis of the fluid mechanics in many types of products and processes. Not only does it reduce the need for expensive prototypes, it provides comprehensive data that is not easily obtainable from experimental tests. Fluid simulation can be used to complement physical testing. Some designers use it to analyze new systems before deciding which validation tests, and how many, need to be performed. When troubleshooting, problems are solved faster and more

reliably because fluid dynamics analysis highlights the root cause, not just the effect. When optimizing new equipment designs, many what-if scenarios can be analyzed in a short time. This can result in improved performance, reliability and product consistency.

4.5 Fluent

Fluent software contains the broad physical modeling capabilities of this important engineering design and analysis tool have been successfully applied to industrial applications ranging from flow over an aircraft wing to combustion in a furnace, from bubble columns to glass production, from blood flow to wastewater treatment plants. The ability of the software to model internal combustion engines, aeroacoustics, turbomachinery and multiphase systems has served to broaden its reach.

Fluent software makes it easy for new users to come up to productive speed.

Its adaptive architecture enables users to easily set up anything from standard fluid flow analyses to complex interacting systems with simple drag-and-drop operations. Users can easily assess performance at multiple design points or compare several alternative designs.

Fluent technology is a leader in the number of complex physical models offered for solution on unstructured meshes. Combinations of elements in a variety of shapes are permitted such as quadrilaterals and triangles for 2-D simulations and hexahedra, tetrahedra, polyhedra, prisms and pyramids for 3-D simulations. Meshes can be created using Ansys or Gambit or third-party meshing products and, in the case of polyhedra, via automatic cell agglomeration directly within Fluent software.

Inside Fluent software, sophisticated numeric and robust solvers — including a pressure-based coupled solver, a fully-segregated pressure-based solver and two density-based

solver formulations — help ensure robust and accurate results for a nearly limitless range of flows.

Inside Fluent software, several popular k - ϵ and k - ω models are available, as is the Reynolds stress model (RSM) for highly swirling or anisotropic flows. Advanced computing power is making large eddy simulation (LES) and the eddy simulation (DES) turbulence models very attractive for applications. Innovative models such as those for predicting laminar-to-turbulent transition and the novel scale-resolving Scale-Adaptive Simulation (SAS) model for flows in which steady-state turbulence models are insufficient are also available. Wall functions and enhanced wall treatment options allow for the representation of all wall-bounded flows.

4.6 Gambit

This software is an advanced engineering tool to draw 2D and to model 3D problems, and to generate mesh automatically for CFD problem solvers, e.g. Fluent. It provides the ability to draw by converting the point to line to shape to model, or by direct modeling using top-down approach.

The “top-down” approach means that one will construct the geometry by creating volumes (bricks, cylinders, etc.) and then manipulating them through Boolean operations (unite, subtract, etc.). In this way, one can quickly build complicated shapes without first creating the underlying vertices, edges, and faces. Once one has built a valid geometry model, one can directly and (in many cases) automatically creates the mesh. More complicated geometries may require some manual decomposition before one can create the mesh.

Furthermore, details and options, like; adjusting the distribution of nodes on individual edges of the geometry, setting continuum types (for example, identifying which mesh

zones are fluid and which are solid) and boundary types, can be use to improve the preparations of the mesh.

Chapter Five: Experimental setup

The experiment setup consisted of:

- A hydraulic power pack (a pump, tank, electric motor, safety valve, and an inlet filter),
- Positive displacement flow meter
- Flow control valve
- Pressure transducers
- Pilot operated relief valve which is tested.

5.1 The hydraulic circuit

A hydraulic schematic diagram Fig.(5.1) shows the components in their symbols. The hydraulic unit exists in the hydraulic and pneumatic laboratory at JU was used, to reduce the cost of the required equipment. The hydraulic flow control valve and safety valve also existed and was suitable for this study.

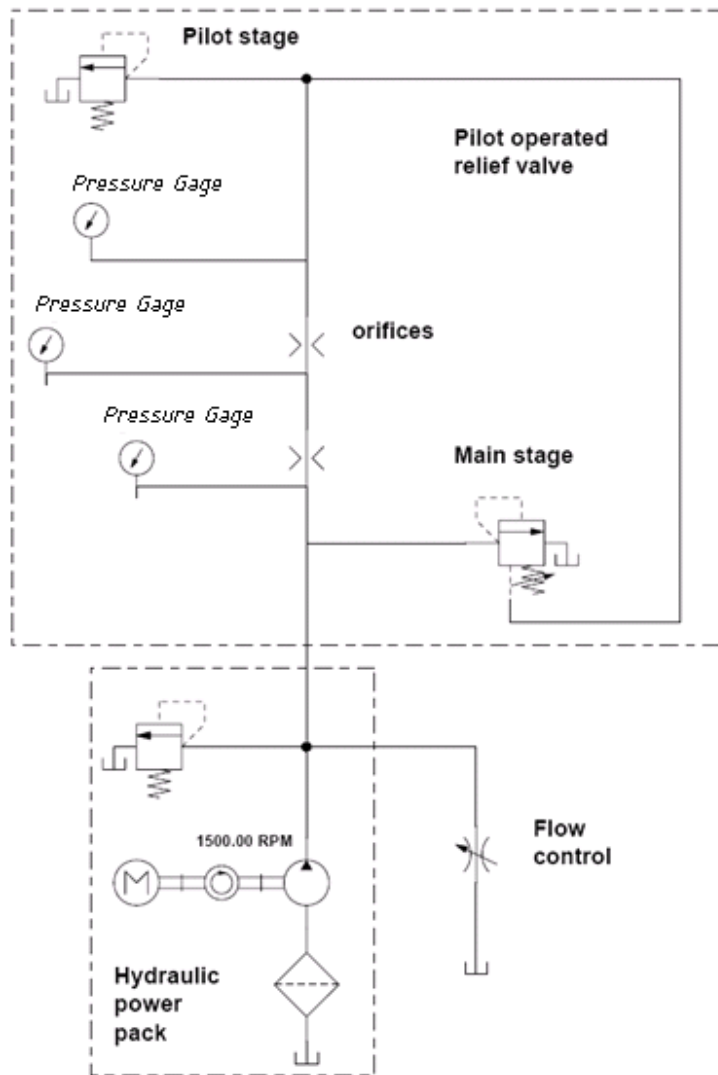


Figure 5.1 : Experiment setup schematic diagram

5.1.1 The hydraulic circuit description

As it is known that each hydraulic component has its function(s), according to the position it exists in. But to understand a hydraulic circuit, one should have the basic knowledge about the interaction between the components' functions, and the details of “know how” inside each component. Side by side of the knowledge of the general function of each

component, the details about the function will be obvious when reader reach the experimental procedure.

5.1.2 Preparation and modification of the pilot operated relief vale

The pilot stage and the main stage of the valve were sub-plate mounted originally by manufacturer design, refer to Fig. (3.27) in the relief vale chapter, the pilot control lines pressures are to be measured in the experiment, so simply a spacing aluminum plate is inserted between the two stages, to extract the pressure from the pilot control lines to sensors ports and to block unnecessary pilot lines in account of this experiment.

Two pressure sensors, see Fig (5.2), and a volumetric flow meter are used to carry out the required measuring. The first pressure transducer was placed upstream of the orifice and the second one was placed downstream of the same orifice.

5.2 Pressure Transducers

Referring to Fig (3.27) in the case of studying flow though the orifice (5), the first pressure transducer is placed on the control line (6) and the second pressure transducer is placed on the control line (7). The range of each pressure transducer was 0-40bar outputs it as 0-5volt scale with nonlinearity of 0.25% as manufacturer specifications, table (5.1) shows full specifications. Simply the measured pressure is calculated as

$$P = \frac{40}{5} \left[\frac{\text{bar}}{\text{volt}} \right] * \text{measured voltage} .$$

Table 5.1 Pressure transducer specifications

Specs.	
Pressure range (Gauge)	40 Bar
Outputs	5V
Pressure Connection	1/4" BSPP
Operating temperature	Ambient - 5 to 40°C (41 to 104°F)
Fluid temperature	-20 to 100°C (-4 to 212°F) Compensated range
Temperature effects	±2% Full scale typical
Accuracy	± 0.25% Full scale
Proof pressure	Minimum 2 times full scale

**Figure 5.2 Pressure transducer**

5.3 The positive displacement flow meter

The positive displacement piston type flow meter shown in Fig (5.3), is placed on the drain (outlet) line of the pilot stage (14), which is the unique outlet of the pilot stage after blocking the unnecessary pilot control lines between the pilot stage and the main stage (7), and after blocking the tank line of the main stage (B) to guarantee no by-pass flow or leakage due to loosely lapping of the poppet (3). The electronic output signal of the flow meter was modified in a signal conditioner to convert it from 0-20mA to 0-10volt scaled to 0-7lit/min., the signal conditioner was built up with an operational amplifier and a ripple smoothing simple filter, refer to appendix C for the amplifier circuit, while the flow meter specifications are shown in table (5.2).

Table 5.2 Flow meter specifications

Specs.	
Measuring Range	6-420 lit/h.
Accuracy	±1.0% of reading
Repeatability	±0.2% of reading
Viscosity Range	5-100 cSt
Process Temp. Range	Max. 80 °C
Ambient Temp.	-10 to +60 °C
Connection	G ¼
Power supply	24 VDC ±20%
Output	0-20 mA, 3-wire
Max. Load	500Ω



Figure 5.3 Piston type flow meter

5.4 The electronic operational Amplifier

There are three facts one should know when designing an operational amplifier; first there is no operational amplifier has 100% linearity (0% non-linearity), second there is no operational amplifier has no bias or initial drift, third there is no operational amplifier that has fixed exactly known value of amplification factor. To solve these problems first let start with easiest one (to me at least); the amplification factor, choosing approximate resistances values for input and output circuits with one or more variable resistance(s), to control the ratio between input and output voltage, and to fix it at desired optimum value. In this study design one position is selected to put the variable resistance, but practically two parallel variable resistances with different ranges were used, to achieve the option of changing the amplification factor in coarse mode (rapid change of factor by a little bit change in a resistance), or fine mode (fine change of factor by a large change in the another resistance), the resistances were calibrated to finally get an operational amplifier converts the range of 0-20mA (which is the output of the flow meter) to 0-10V (which is the suitable input to the data acquisition card), at the most accurate factor could be achieved. The other two problems; bias and nonlinearity, were solved by testing the operational

amplifier using a current source and precise digital multi-meter(s), the procedure was to input some known current at the input circuit and measure the output voltage at the output circuit, and the result data entered to Matlab to perform curve fitting to have a relation between the input current and the output voltage, so reversely in experimental study measured voltage at the output of the operational amplifier represent that some current has entered the operational amplifier according the relation, which represents the flow rate. The reading and curve fitting in mentioned in appendix D3.

$$V [volt] = 0.4969 I [mA] + 0.006586 \dots \dots \dots (5.1)$$

At these values in the equation, one can say that the range of 0-20mA was converted to 0-10volt, meaning that equation (5.1) could be reduced to be $V [volt] = 0.5 I [mA]$ with root mean square error of 0.008. And easily $flow\ rate \left[\frac{lit}{min} \right] = 0.7 * V [volt]$, due to the fact that the flow rate 0-7lit/min. is proportional to the current 0-20mA proportional to the voltage 0-10volt. But if high accuracy is needed –and available for no extra cost– equation (5.1) should be used, the flow rate as manufacturer is,

$$Q \left[\frac{lit}{min} \right] = I [mA] * \frac{7 \left[\frac{lit}{min} \right]}{20 [mA]}$$

Arranging, $I [mA] = Q * \frac{20}{7}$

Substitute in equation (5.1) $V = 0.4969 * \frac{Q*20}{7} + 0.006586$

Rearranging $Q = \frac{V-0.006586}{\left(\frac{0.4969*20}{7} \right)}$

This is how to predict volumetric flow rate from the voltage measured by the data acquisition card, used in the Matlab program code.

5.5 Data acquisition system

The data acquisition system consists of a data acquisition card (DAQ), software and PC. The DAQ card that was used was National Instruments USB-6008, it accepts 8-analogue inputs, and the output is Universal Serial Bus (USB). The software used is LabVIEW; it is a graphical development environment, can quickly create front panel user interface, and specify system function by assembling diagrams for a natural design notation.

The voltage output signals from the pressure transducers and the flow meter (after signal conditioner) are entered to the data acquisition card, the data is then acquired by LabVIEW software, this configuration basically grabs the analogue voltage signals and displays it on a waveform chart on the front panel, shows the flow rate on dial gage, and stores them in an excel sheet, in a batch sample of 30 reading for each run for each signal, in a rate of 30 reading every 3 seconds, storing updates and display updates every batch (every 3 seconds). A Matlab code is written to average the 30 reading of each run for one reading for each signal, then simple calculating generated the coefficient of discharge and square root of Reynolds number for each batch, and a curve fitting tool is opened to formulate the data in a fitting equation, which will be discussed in results part.

The connection of the measuring devices and DAQ is shown in Fig (5.4).

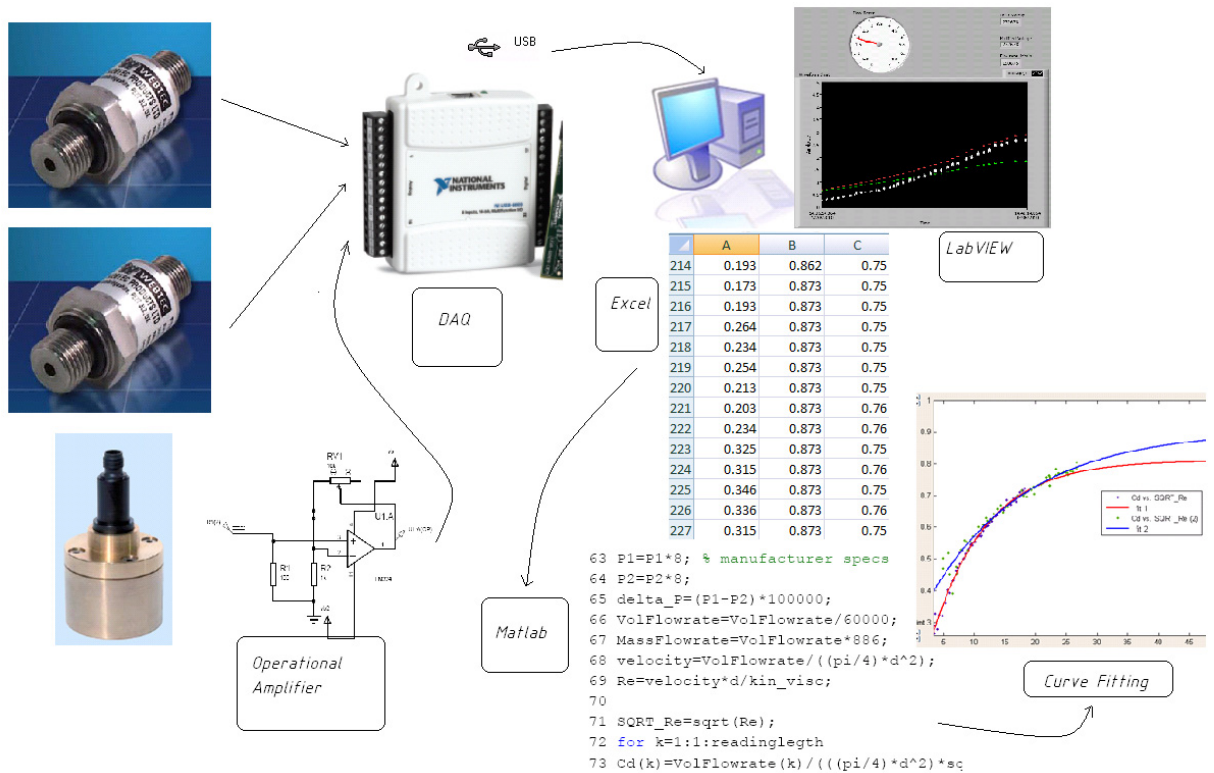


Figure 5.4 Flow chart from the devices to the result

5.6 Experimental procedure

The pump converts the mechanical energy to hydraulic energy, and generates a flow that has “the potential of pressure” if any restriction faces the flow. A main relief valve is mounted to protect the system from over pressure and to guarantee the minimum level of safety, this valve is not this study relief valve, and this valve has –almost- no effect on the circuit while the pressure is within the safety limit of the experiment.

As in the hydraulic schematic diagram Fig (5.1), the flow has two options; to pass through the flow control valve or to flow through the orifices to push the needle and the spring of the pilot stage. Knowing that the main stage outlet is blocked to guarantee that all flow passes the orifices exists from the drain line of the pilot stage to be measured in the flow

meter, if the flow control valve is totally opened, it could handle all the flow rate freely without any noticeable rise of pressure, due to the small value of flow rate that the pump delivers and to the suitable size of the flow control valve.

While carrying out the experiment, the flow control valve is closed -manually- slowly while noticing the rising of main system pressure which in an indirect indicator to the rising of the pilot control line pressure. The pressure reaches a value that is able to open the pilot stage and flow starts in the control line which contains the orifice. At this moment one has an indicator about flowing through the pilot stage, which is the reading of the flow meter on the front panel of the LabVIEW software on the PC.

As much as the flow control valve is closed, the main pressure increases, making the pilot pressure increase –which is originally a crack pressure of the main pressure, and for this reason the orifice is put there- and flow rate through the pilot stage increase. All these data is grabbed by the data acquisition card and recorded by the software to an excel sheet, as mentioned.

Now, the run is started, the software recorded 30 readings in 3 seconds for each parameter; upstream pressure (P1), downstream pressure (P2), volumetric flow rate. All these reading will be averaged to one reading per run, after the software finishes the threes second period, the flow control valve sitting was change, then after waiting a hold for a second, and another single run by software was performed, see Fig (5.5). This holding second is just to make sure everything reached steady state, even all components have a very high response comparing with human reaction, e.g. a hydraulic circuit has pipes and hoses of

totally length in order of few meters has a response in order of milliseconds, and so is the pressure sensor (as manufacturer, and as the common sense of its working principle).

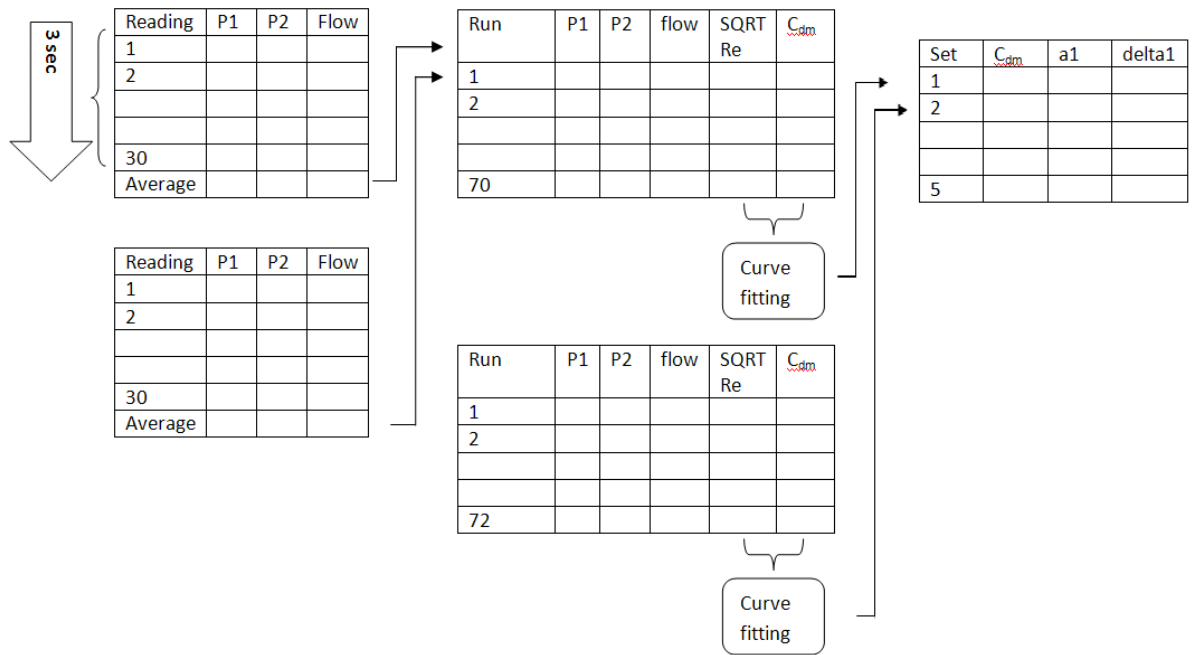


Figure 5.5 Levels of data, every 30reading averaged to one run, group of runs make a set and draw a curve, each set generates an empirical formula

- Note: a rough test has performed to test the response of the flow meter, by carrying out a continuous run for the software, and flow control valve is changed suddenly, all three signals changed at the same position on the wave form history diagram, which means that the flow meter has the same order of response of pressure sensors, that is so fast for human reaction, that makes “holding second(s)” more than enough for the hydraulic circuit and measuring devices to achieve steady state.

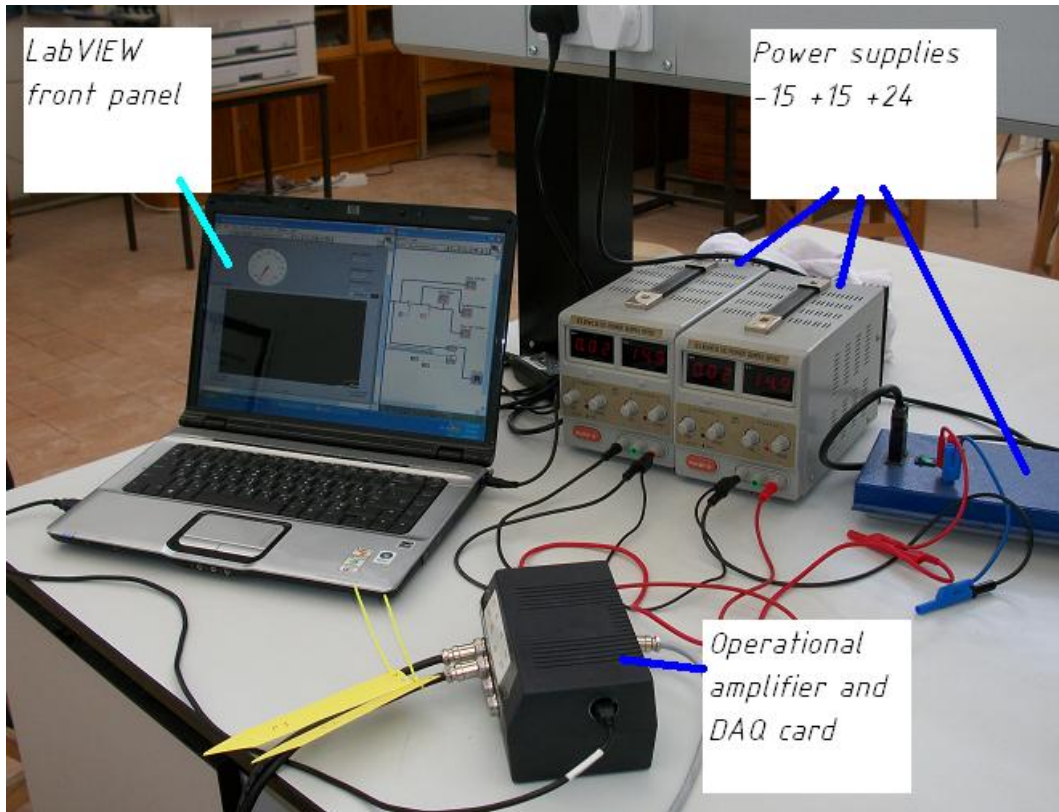


Figure 5.6 Setup components together, labeled

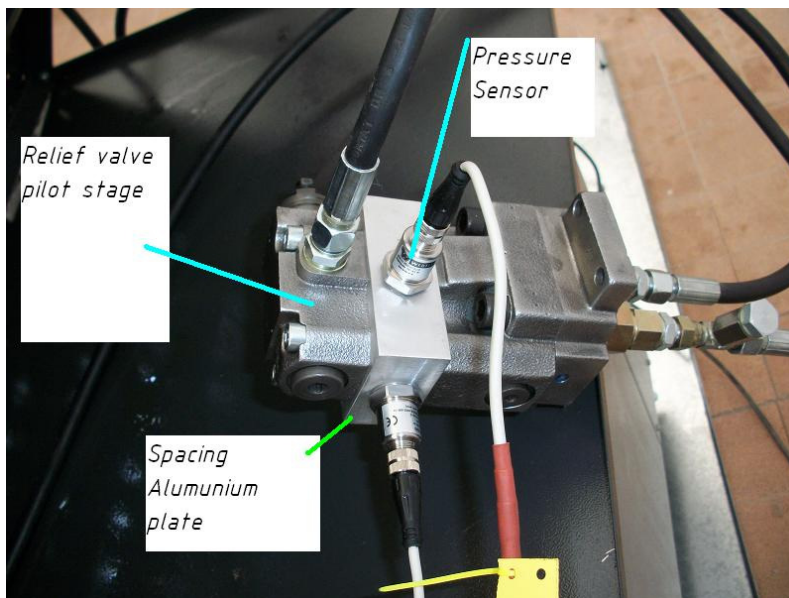


Figure 5.7 Relief valve and pressure sensors mounting

Chapter Six: Experimental and simulation results and discussion

This chapter will show the results of the experimental work and numerical simulation, and discuss each of them, after that compare both results together, to verify the model.

6.1 Experimental results

As experimental setup was described the in the previous chapter, and the experimental procedure also, it is the “harvesting time” now. All data were stored by computer software, and entered into Matlab code to average them. Here are a sample of data for the upstream pressure P1, downstream pressure P2 and volumetric flow rate from the third set, to see full data refer to Appendix B.

Table 6.1 Sample of data, first 5runs of set 3

Run no.	P1 [bar]	P2 [bar]	Vol Flow [lit/min]
1	7.653333	7.404533	0.077279
2	7.814667	7.586667	0.077537
3	7.901333	7.714667	0.077068
4	8.013333	7.864	0.077749
5	8.245333	8.021333	0.104538

A sample of results for set no.3 is shown in table (6.2), the readings data were converted simply to results by entering them in the Matlab code, more details Appendix A, which contains the calculations of the equations, and results then entered to curve fitting tool.

Table 6.2 Sample of calculate results, first 5runs of set 3

Run no.	P1 [bar]	P2 [bar]	Vol Flow [lit/min]	SQRT RE	Cd
1	7.653333	7.404533	0.077279	3.660322	0.210328
2	7.814667	7.586667	0.077537	3.666433	0.220446
3	7.901333	7.714667	0.077068	3.655314	0.242158
4	8.013333	7.864	0.077749	3.671426	0.273133
5	8.245333	8.021333	0.104538	4.257216	0.299854

The result of the first experimental set is shown in Fig (6.1), which proves the variety of C_d with \sqrt{Re} , that is the theory states that “the coefficient of discharge is constant” could really cause a large error in the case of small opening orifice at low Reynolds number. The C_d value changes widely over the range of \sqrt{Re} from 4 to 20.

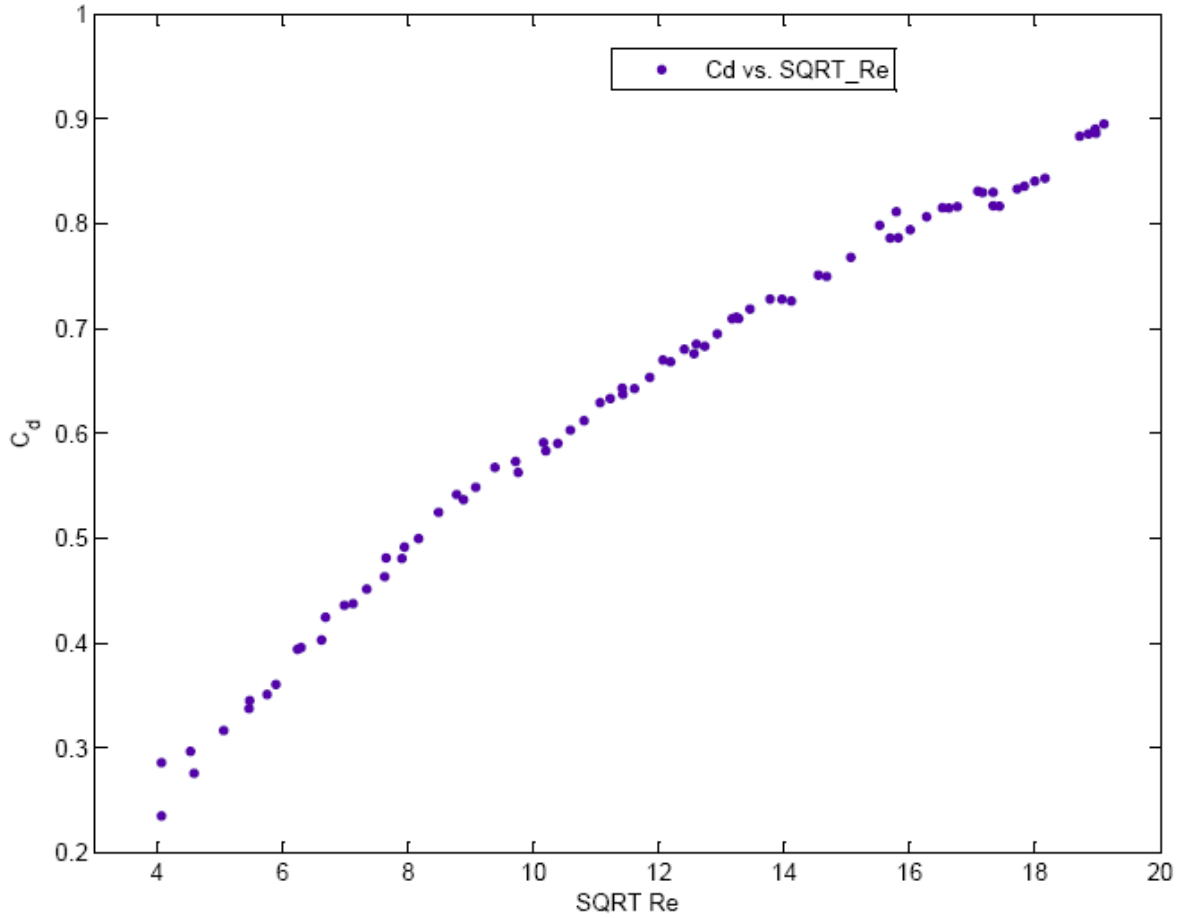


Figure 6.1 Plot for C_d vs. SQRT Re for 1st set of data and results

To make the result more reliable, the experiment was carried out several times, five sets were considered, each set has its own conditions, table (6.3). The downstream pressure of the orifice were controlled, by changing the setting of the pilot stage spring load, this made both pressures –upstream and downstream- to be changed, for example; if 28bar was applied at the inlet of the orifice and 15bar at the outlet, then one can get 13bar pressure difference, and if 20bar was applied at the inlet of the orifice and 7bar at the outlet, then one can get 13bar pressure difference, this should give same results -theoretically- due to the nature of the relation of flow rate, which is related to the square root of pressure difference, and this is obvious from the crowded scattered results in Fig (6.2), even the

pressure ranges were changed widely, but the results showed that the key parameter was the pressure difference.

Table 6.3 Experimental work, different sets conditions

Set no.	P1 range [bar]	P2 range [bar]	Spring load	Temperature °C	Kin Viscosity [m ² /s]
1	3.2304 - 27.7869	2.979733 - 15.26693	medium	27.5	0.000133
2	1.850667 - 19.82747	1.373333 - 6.354933	low	28.5	0.000125
3	7.653333 - 31.19787	7.404533 - 20.40667	high	29.5	0.000120
4	4.0664 - 27.58213	3.917067 - 16.14373	medium	34	0.000092
5	2.117333 - 23.89413	1.954667 - 12.4816	medium	40	0.000068

- Note: The digit accuracy of reading is generated due to averaging the 30 reading of each run, although the real accuracy of the measuring devices does not reach such level.

On the other hand viscosity was changed for each set, by changing the temperature of the oil. The results were comparable in most of the range, but the low viscosity experiment reached high Reynolds number due to the nature of the relation -inversely proportional- between the Reynolds number and viscosity, at the same maximum flow rate that is limited by the hydraulic unit ability (about 2.25lit/min.). Unfortunately, when the experiment were designed and the range of data were selected to carry out the work on at the proposal phase, it was expected that the hydraulic unit could handle the nominal 3lit/min., which is

the specification, so the curve did not show obviously and surely that C_d approaches from a fixed number, even it looks like to tend to rest on some maximum value. But it is recommend that deeper researches to be carried out with higher turn down ratio (ratio between the maximum flow rate and the minimum flow rate), to cover higher range of Reynolds number, specially that in this study investigation reached Reynolds number about 700, and previous researchers got the approach of the C_d from the maximum limit of it before this Reynolds number for some types of orifice, e.g. for needle valve the C_d value reached the maximum at \sqrt{Re} of about 15, (Wu 2002).

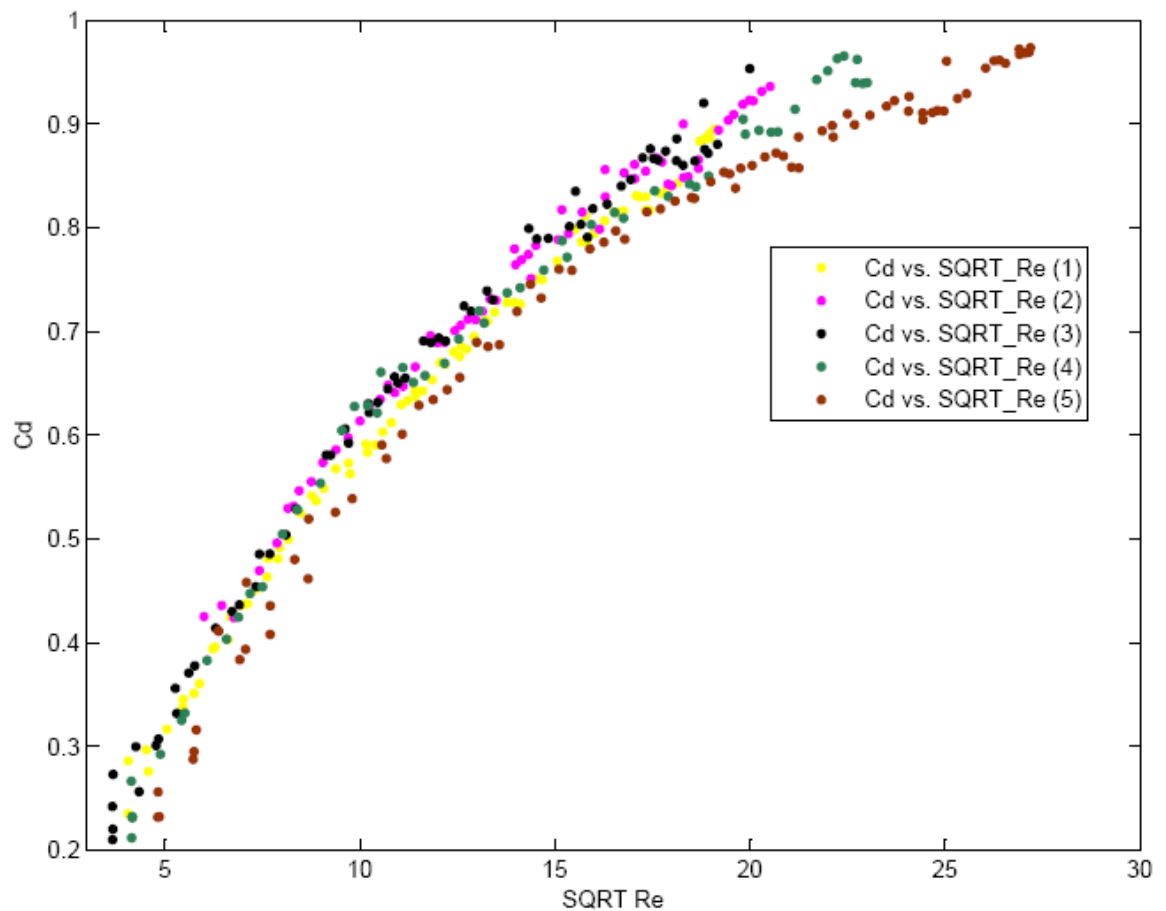


Figure 6.2 Scatter plot for all sets, C_d vs. SQRT Re

The temperature affects the viscosity, and the viscosity is included in the Re already so it is not correct mathematically to consider independent axis for viscosity, and experimentally all sets showed the same curve and all points tend to condense in same region, even for different temperatures.

6.2 Formula modeling by curve fitting

The empirical formula that Wu suggested was an exponential function of one or two terms, the first one was in the shape of $C_d = C_{d\infty} (1 + a e^{-\delta \sqrt{Re}})$, and the second one was $C_d = C_{d\infty} (1 + a_1 e^{-\delta_1 \sqrt{Re}} + a_2 e^{-\delta_2 \sqrt{Re}})$. As noticed from previous studies that the second form is more convenient for the relation between C_d and \sqrt{Re} when there is an overshoot in the shape of function, Fig (2.1), meaning that C_d value reaches a high value C_{dm} in some small value of \sqrt{Re} rapidly then it return to stable at $C_{d\infty}$, which is value that C_d approaches to at \sqrt{Re} approaches ∞ . But in this study the orifice did not result an overshoot, and the value of $C_{d\infty}$ could be considered identical with C_{dm} , and the first model was more appropriate, with one exponential term.

Matlab curve fitting is shown in Fig (6.3), as a sample for set no. 1, and the resultant parameters for all sets are listed in table (6.4) for different data sets.

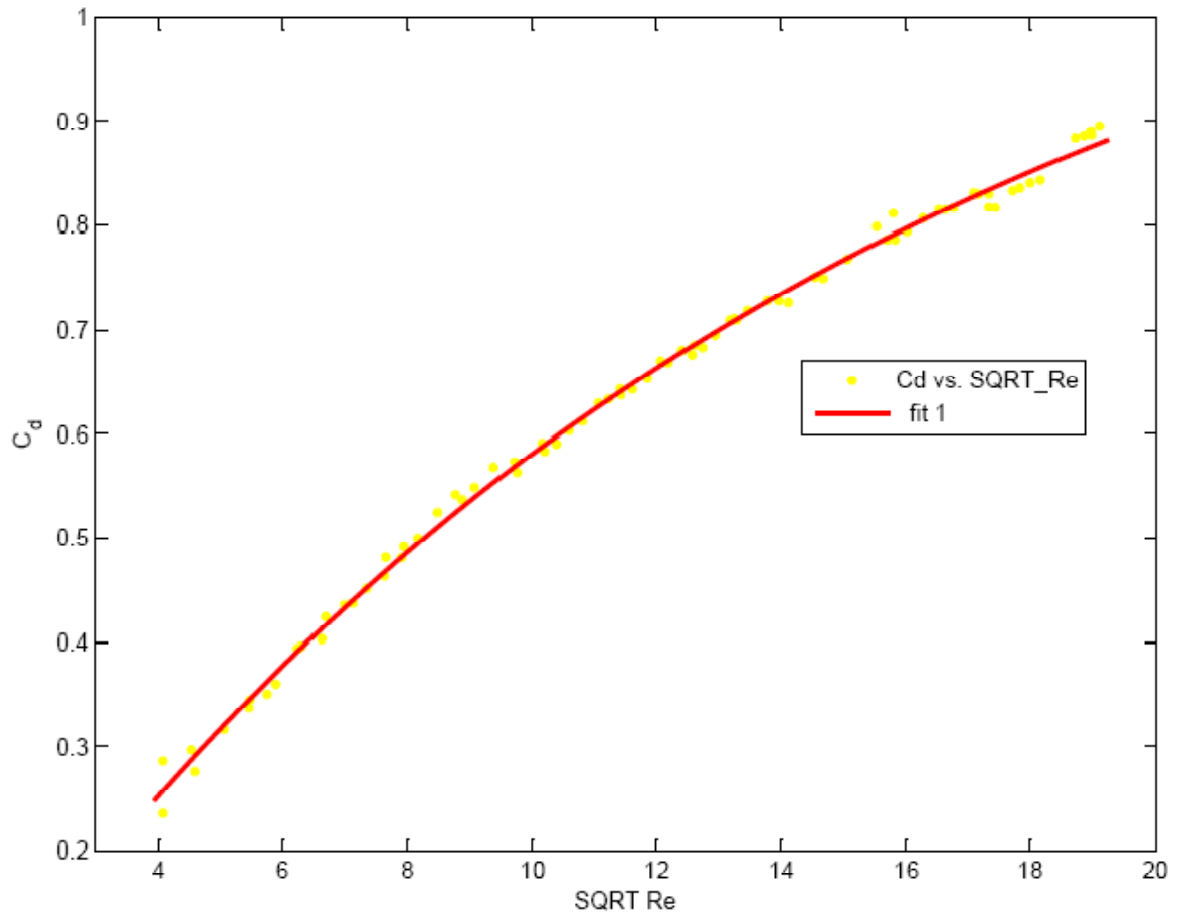


Figure 6.3 Curve fitting C_d vs. $\text{SQRT } Re$ sample, 1st set

The different sets showed the same phenomena, with a very small difference in the higher range of \sqrt{Re} . The maximum value of discharge coefficient achieved were about 0.98, but the predicted value from the empirical formula showed that the value could reach about 1.2 for some sets, if the experiment range extended to higher Re till the C_d approaches a constant value, which seems not to be realistic, even there is some explanations and excuses.

Table 6.4 The result parameters according to fit of equation $C_d = C_{dm} (1 + a_1 * e^{(-\delta a_1 * \sqrt{Re})})$

Set no.	C_{dm}	a_1	δa_1	RMSE
1	1.213	-1.046	0.06975	0.009572
2	1.181	-1.032	0.07557	0.01395
3	1.148	-1.089	0.08413	0.01487
4	1.089	-1.15	0.09327	0.01747
5	1.059	-1.207	0.09387	0.01548

The experiments showed high C_d value for this study orifice comparing with sharp edge shaped orifices in previous researches, this could be resulted because of more than one reason; besides it could be error due a combination of uncertainties, but it could be for a physical reason, which is that the entrance of this study orifice has the shape of convergence, acts like a nozzle which converts hydraulic energy (pressure energy component) to kinetic energy (velocity energy component), due to the smooth pressure gradient at the entrance, in the time that sharp edge shaped orifices result a sudden pressure change and this converts hydraulic energy to heat, but this could be “under studying theory” till investigation prove its correctness, and it still just a point of view. Thorough investigation should be carried out with the help of measuring temperature in each position in the orifice which could be considered a real challenge for measurement setup.

To compare this work with previous researches, a comparison should be made with some works on similar orifice geometry, but due to that this is new field of research and that there is no available data for this orifice, it was found that Wu formulate an empirical formula for a needle valve, the physical behavior is just showed in Fig (6.4), which compares the empirical formula for needle valve

$$C_d = 0.75 - 2.47 e^{-0.22 \sqrt{Re}} + 1.72 e^{-0.28 \sqrt{Re}}$$

with this experimental work set no. 1, it shows the same shape of curve but some shifting due to different type of orifice geometries.

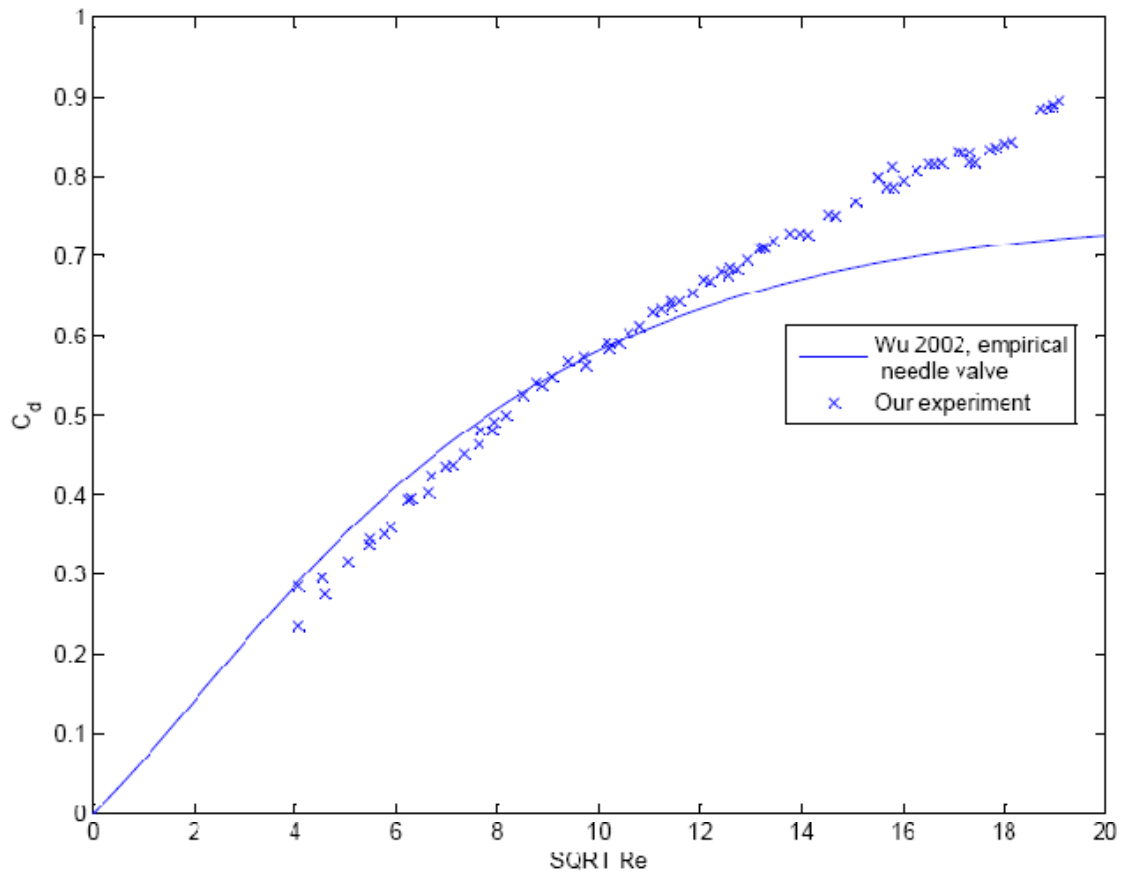


Figure 6.4 Comparison between empirical formula for needle valve (Wu 2002) and this experimental work.

6.3 Simulation results

To simulate a flow through a pipe or any round cross-section it is common to use axisymmetric solver in Fluent, for that purpose a 2D mesh for half of pipe or flow passage should be generated with Gambit.

The orifice was placed between two flowing pipes each of length of 10mm, Fig (6.5) the upper half drawn, the center line defined as axisymmetric axis, and inlet at the left define

to be uniformly distributed pressure, and the outlet at the right define to be uniformly distributed pressure also, the surface is filled with fluid.

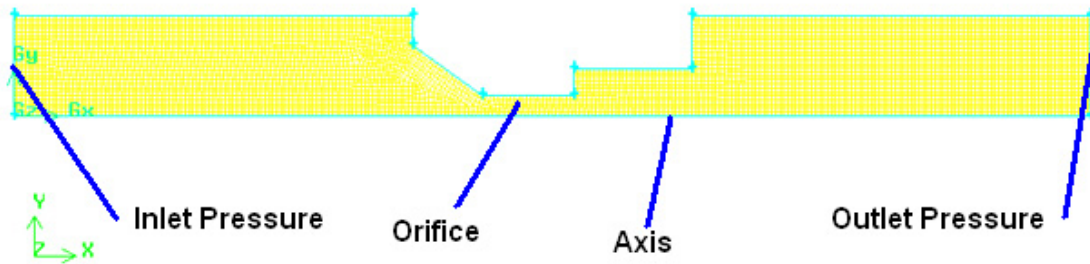


Figure 6.5 This study orifice 1st generated mesh

Then the case is saved and mesh generated in a form that Fluent can handle, in the Fluent interface; read the case by fluent, grid scale: grid was created in mm scale , define model solver axisymmetric , define model viscous laminar, (because the predicted velocity 10m/s , Re about 100) , create material hydraulic oil, density 886kg/m^3 , dynamic viscosity 0.06 Pa.s, define boundary condition P1 and P2, define the fluid as hydraulic oil (previously created) , solve initialize compute from P2 , initial guess for axial velocity 5m/s, radial velocity 0.1 m/s , check plot when solving for monitor residuals and set the criteria of continuity, x-velocity and y-velocity as residual 0.001 , then finally iterate, the velocity vector field and pressure contours are illustrated in Fig (6.6) and Fig (6.7), the key parameter of the results by simulation was the mass flow rate, for that the software was asked to report the flux, the results (P1,P2,mass flow rate) were entered in a table, each run the pressure outlet was change, while fixing the inlet pressure, refer to appendix C1 for data.

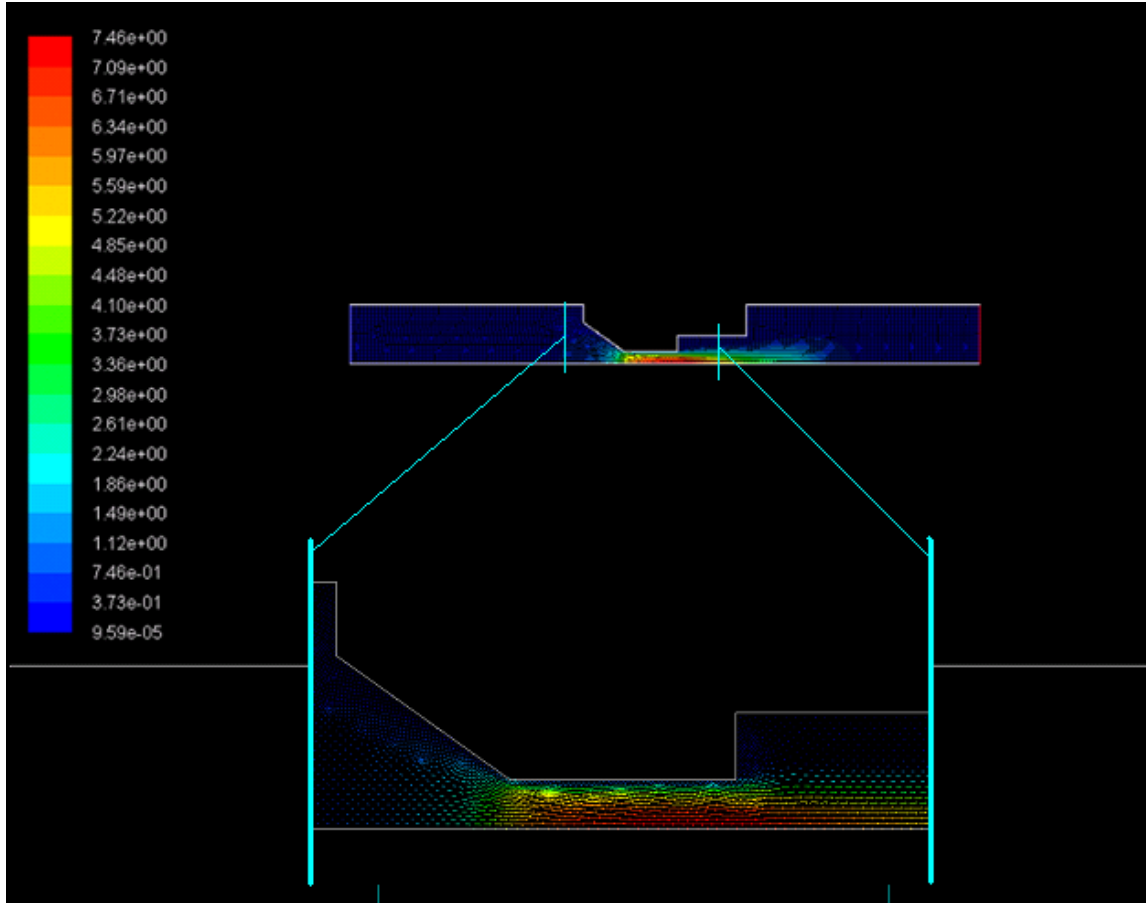


Figure 6.6 Velocity vector field in orifice by simulation

The velocity vector field, Fig (6.6), shows that the velocity is highest at the center line and this is common sense, due to friction at pipe wall. The velocity also shows high values in the middle of the outlet passage after the orifice directly, this is the motivations layers of the flow that drag the rest of the fluid, and “transfer momentum” form a layer to another.

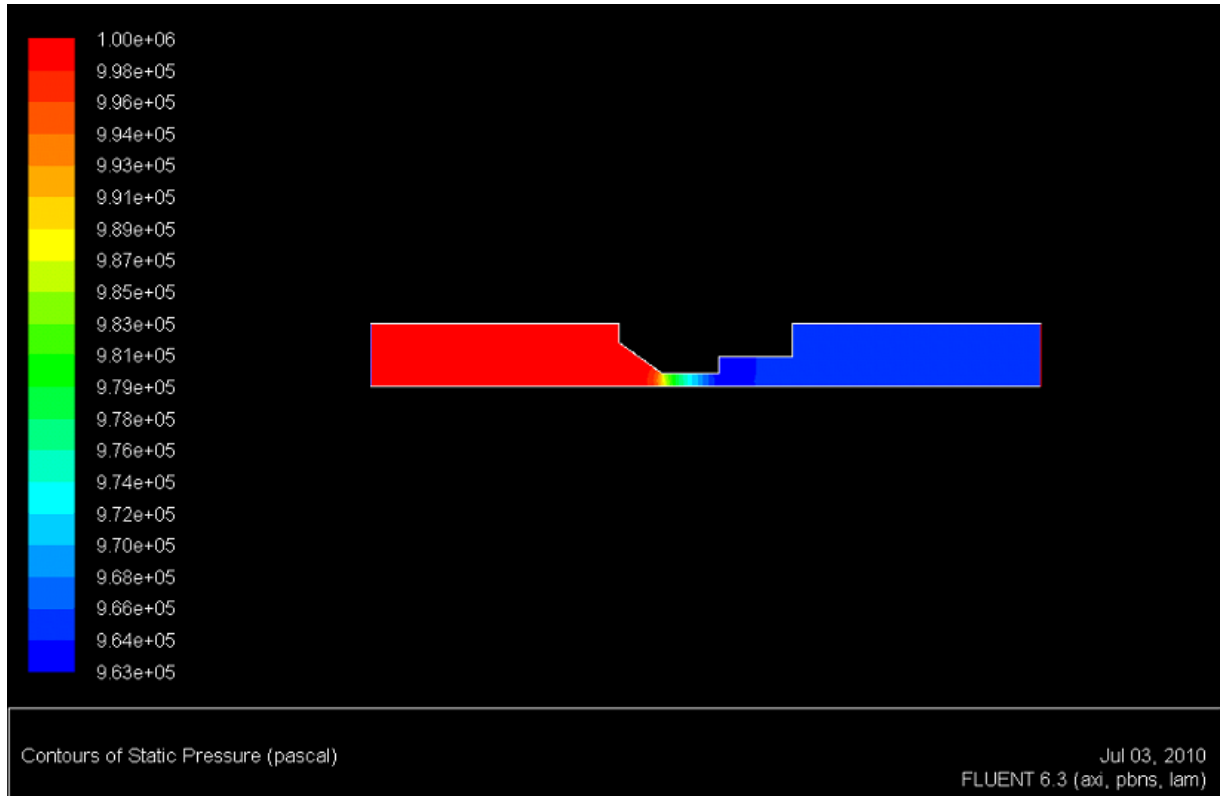


Figure 6.7 Pressure contours in orifice by simulation

At the inlet of the orifice there is a noticeable pressure gradient, the colors changed widely. At the orifice itself the pressure changes dramatically also, this may be caused by the pressure loss in small pipes due to restriction effect, the pressure field in Fig (6.7) is acceptable to be near the real case from a logical point of view.

The resultant of the simulation after applying the pressures at the inlet and the outlet of the orifice would be the mass flow rate. The results were entered to excel sheet manually, and C_d and Re were calculated and plotted in Fig (6.8).

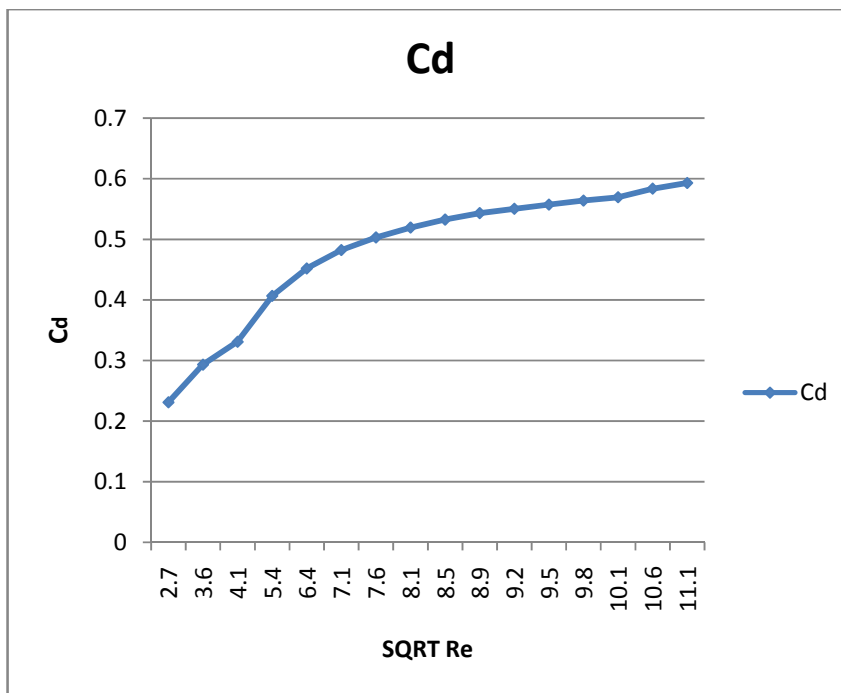


Figure 6.8 Simulation result for C_d v. SQRT Re, first trial

Simulation work definitions

- **Mesh refinement, residual minimizing and pressure near experimental**

The results was good, comparing with experimental work, but to make sure that our results is near the true value –knowing that there is no true value in numerical solution- the solve was repeated with refinement of mesh in the critical positions, which are the neighborhood of converge surface at the inlet and the sharp edge outlet, and with residual criteria of continuity 0.0005, x-velocity and y-velocity as 0.0001, and the pressure inlet and outlet were changed both to values near practical values of experimental work, to guarantee testing the orifice in same conditions and to extend range similar to experimental to make the comparison reasonable as much as possible.

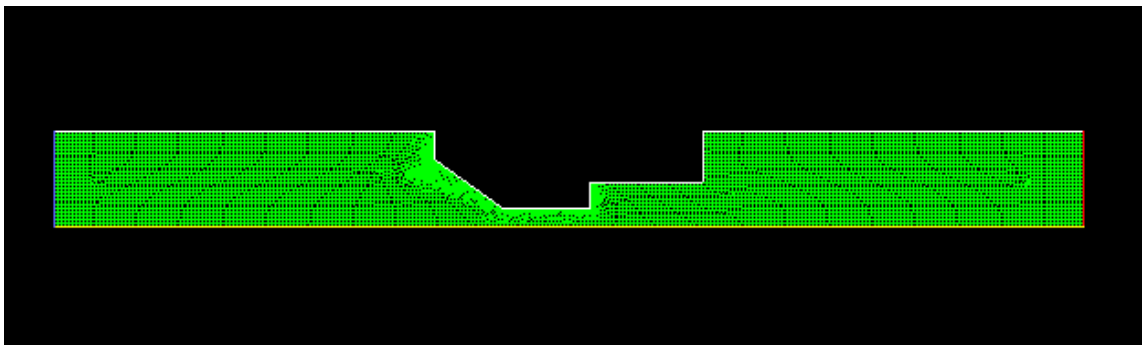


Figure 6.9 Refinement for mesh grid, see crowded cells at orifice edge.

The residual was selected after more than one trial so that Fluent should give answer in reasonable number of iteration for each run, for such simple problem. Knowing that in this experimental work the pressure changed smoothly and gradually, and for accurate simulation same pressure ranges were used, increasing pressure smoothly also, the

software procedure is to try to use the last answer as a guess value for the next run even if one or more of the boundary conditions was/were changed, that means the convergence should occurred in few number of iterations.

Sometimes the residuals may not fall below the convergence criterion set in the case setup. However, monitoring the representative flow variables through iterations may show that the residuals have stagnated and do not change with further iterations. This could also be considered as convergence, see Fig (6.10).

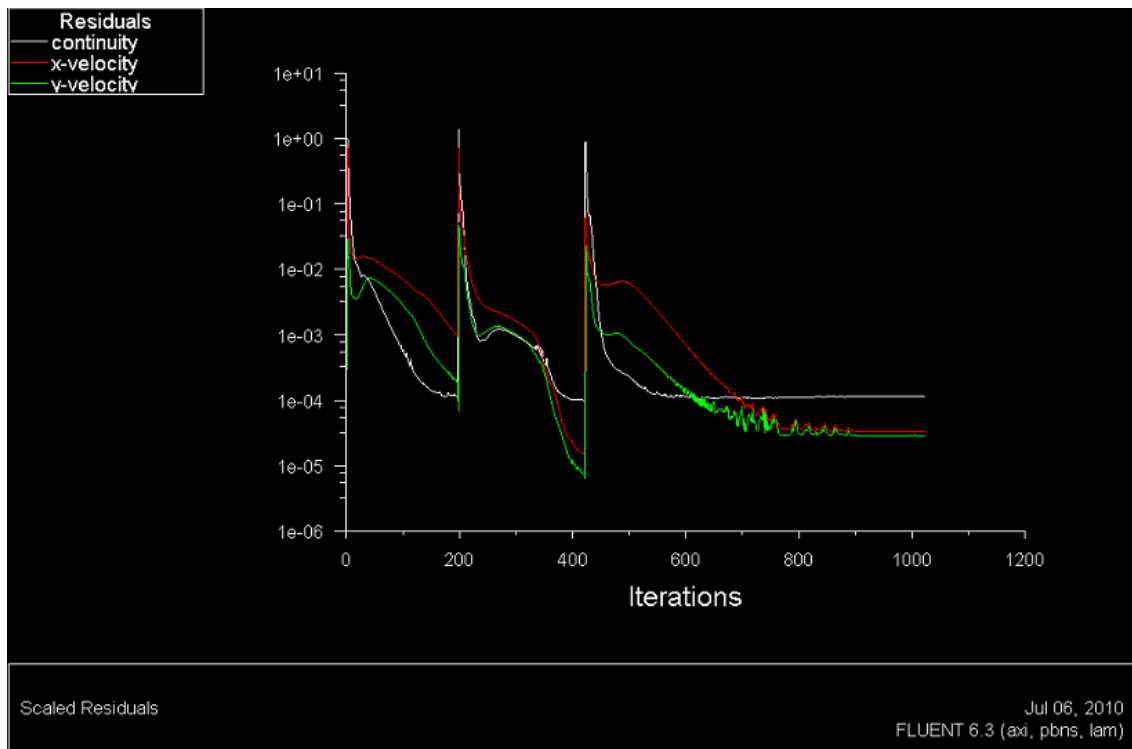


Figure 6.10 Example of run when residual does not change with iterations

The comparison between the two trials of two simulations is shown in Fig (6.12), but the main differences are illustrated in table (6.5).

Table 6.5 Differences between two trials of simulation

	First trial	Second trial
Mesh	Normal	Fine in critical region
Residual criteria of continuity	0.001	0.0005
Residual criteria of x-velocity	0.001	0.0001
Residual criteria of y-velocity	0.001	0.0001
Inlet Pressures	Fixed at 10 bar	Variable from 4.066 to 32 bar
Outlet Pressures	Variable from 9.63 to 8.4 bar	Variable from 3.917 to 17 bar

The number of iterations increased as the input value increased more widely and rapidly, in the first runs in the second trial simulation the pressures were increased so smoothly, the number of iteration for each run was low, but to reach high values of square root of Reynolds number and pressures, and to achieve reasonable comparison with experimental, pressure rapidly increased, specially that the desired relation relates the flow rate –which represents the velocity and Reynolds number- with the square root of pressure difference, therefore increasing pressure smoothly in high range will cause large number of runs with no valuable data, on the other hand maintaining acceptable accuracy with reasonable number was a key object. Fig (6.11) shows how number of iterations increase when pressures were increased roughly.

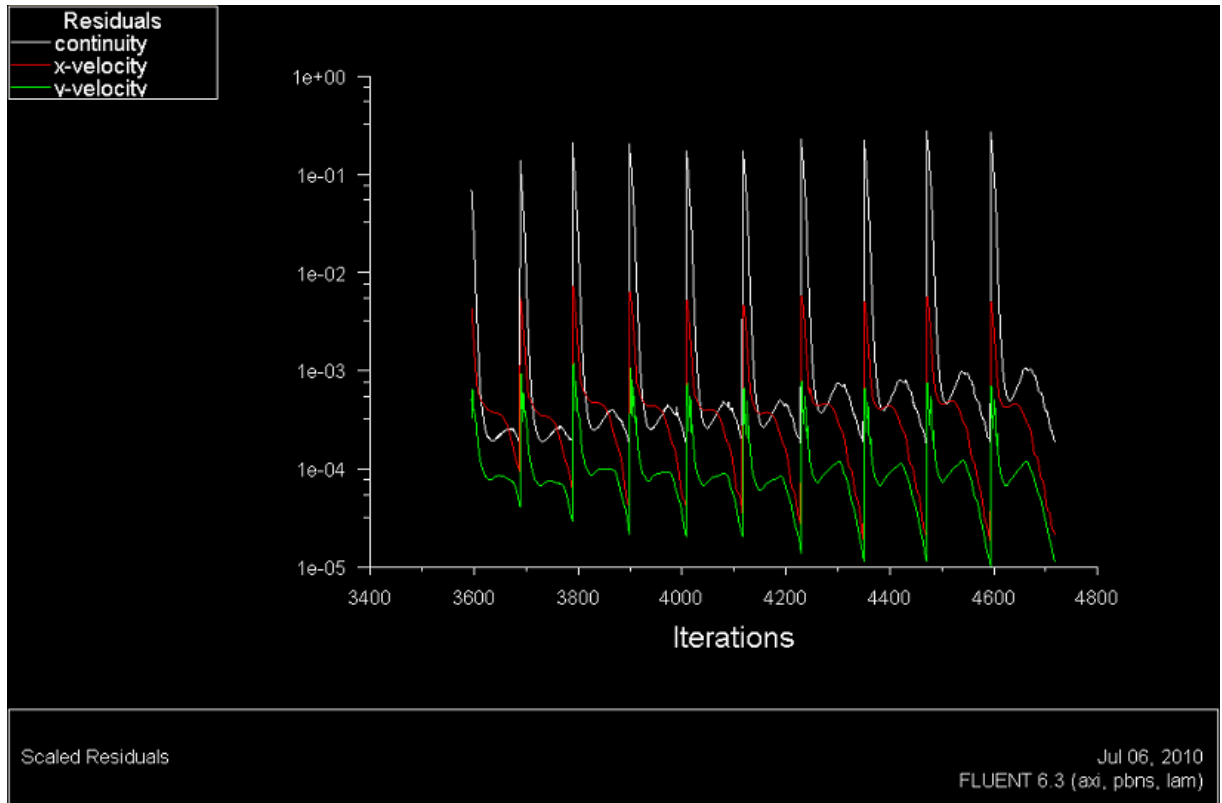


Figure 6.11 Number of iterations change with different run conditions

After carrying out the definition of the simulation case, as shown in table (6.6), the second case is compared with the first case in Fig (6.12), it is expected that the definition is more accurate, as a common sense, even both cases results were close to each other, but the idea from this comparison is that if there was a noticeable difference this could mean that the definition was not optional and it was must, and more modifications from this type could result “better” results. But as in our case the definitions added a little bit enhancement, and the shape of the relation is identical but the curve shifted a little bit. Considering that the residual were decreased by one-fifth or by one-tenth, and that the cell size decreased in the critical area, no more noticeable enhancement was expected for more definition of the case.

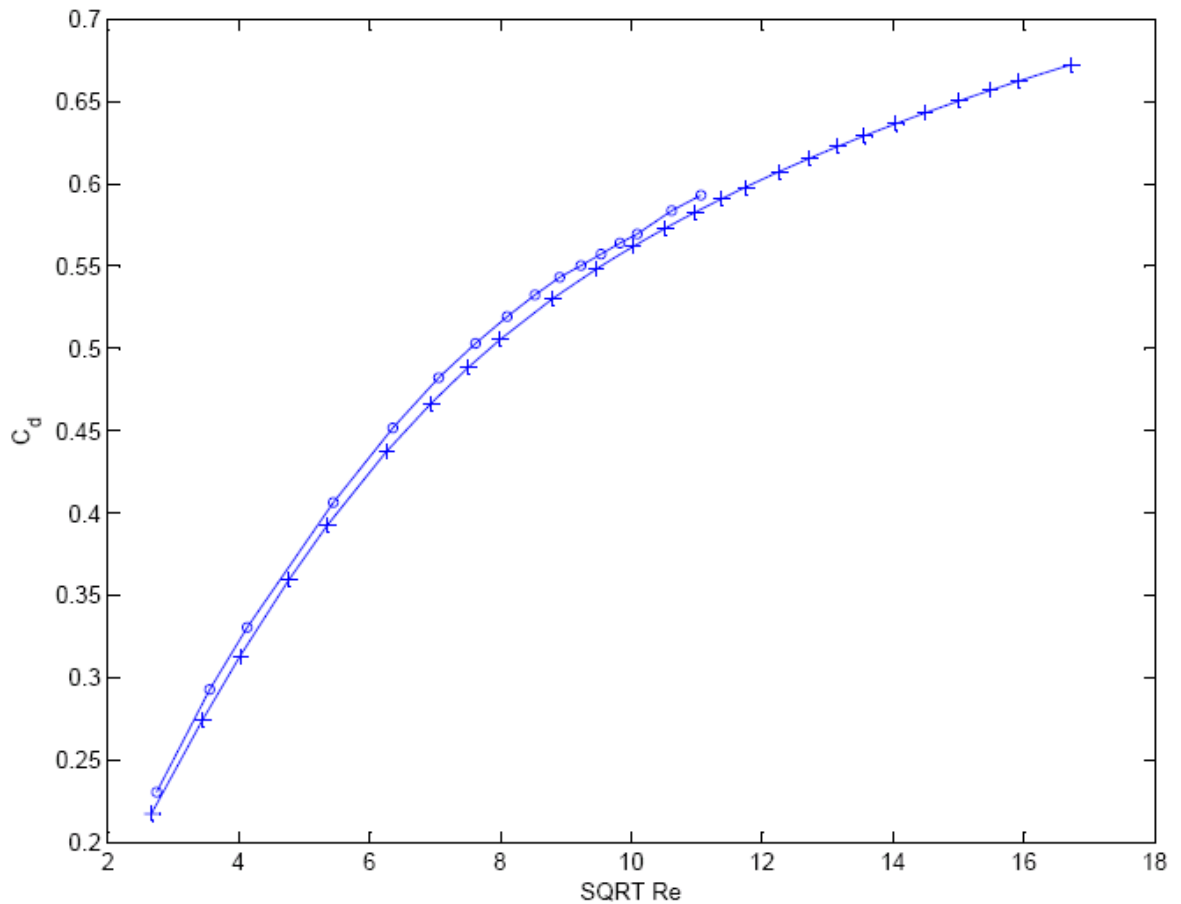


Figure 6.12 Comparison between C_d vs. SQRT Re for two simulations, x-marker for fine mesh, o-marker for coarse mesh

- **Simulation with modification of cross-sections**

Due to the fact that the orifice exists in a practical passage, which is imperfect, and has its physical geometry, the inlet and outlet diameters are not identical. The inlet and outlet diameters are modified and mesh generated to perform the simulation again, mesh is shown in Fig (6.13). SIMPLEC code was used, with second order pressure discretization, and second order momentum discretization. The result curve of the C_d vs. square root of Reynolds number became a little bit higher; Fig (6.14) shows the results.

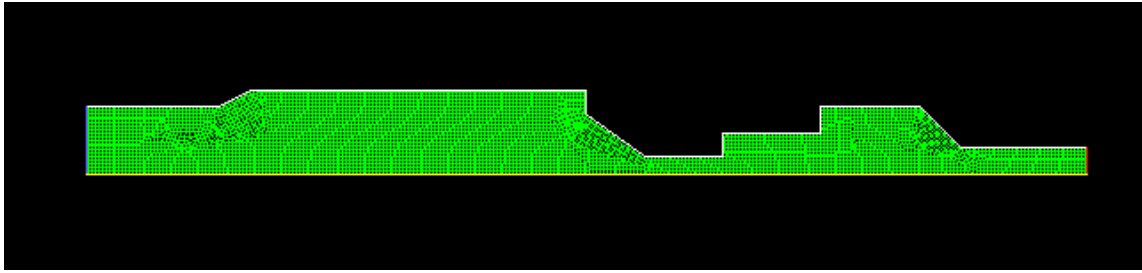


Figure 6.13 Mesh with modification of cross sections

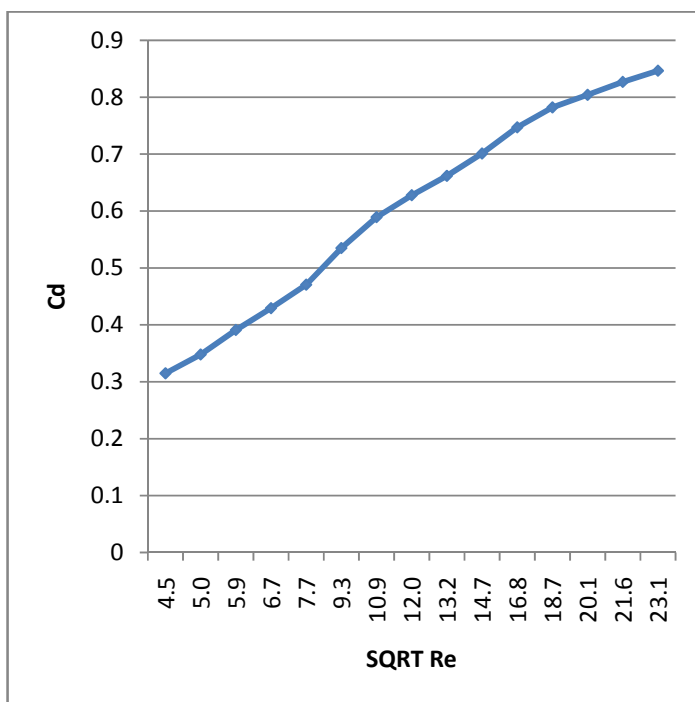


Figure 6.14 Simulation results with modification of cross section

6.4 Experimental and Simulation results comparison

To show the validation of using the numerical simulation in such small opening practical orifice, a comparison should be carried out. To perform a comparison between experimental work and numerical simulation, both results were plotted on one chart, see Fig (6.15) that shows the experimental result of set no. 1 and simulation set no.1, and Fig

(6.16) shows the experimental result of set no. 4 and simulation set no.2, but Fig (6.17) illustrates Comparison between Experimental result of set no. 4 and numerical simulation after modification of cross section, for full results see appendix B for experimental, and appendices C1 and C2 for simulation set no.1 and 2, respectively.

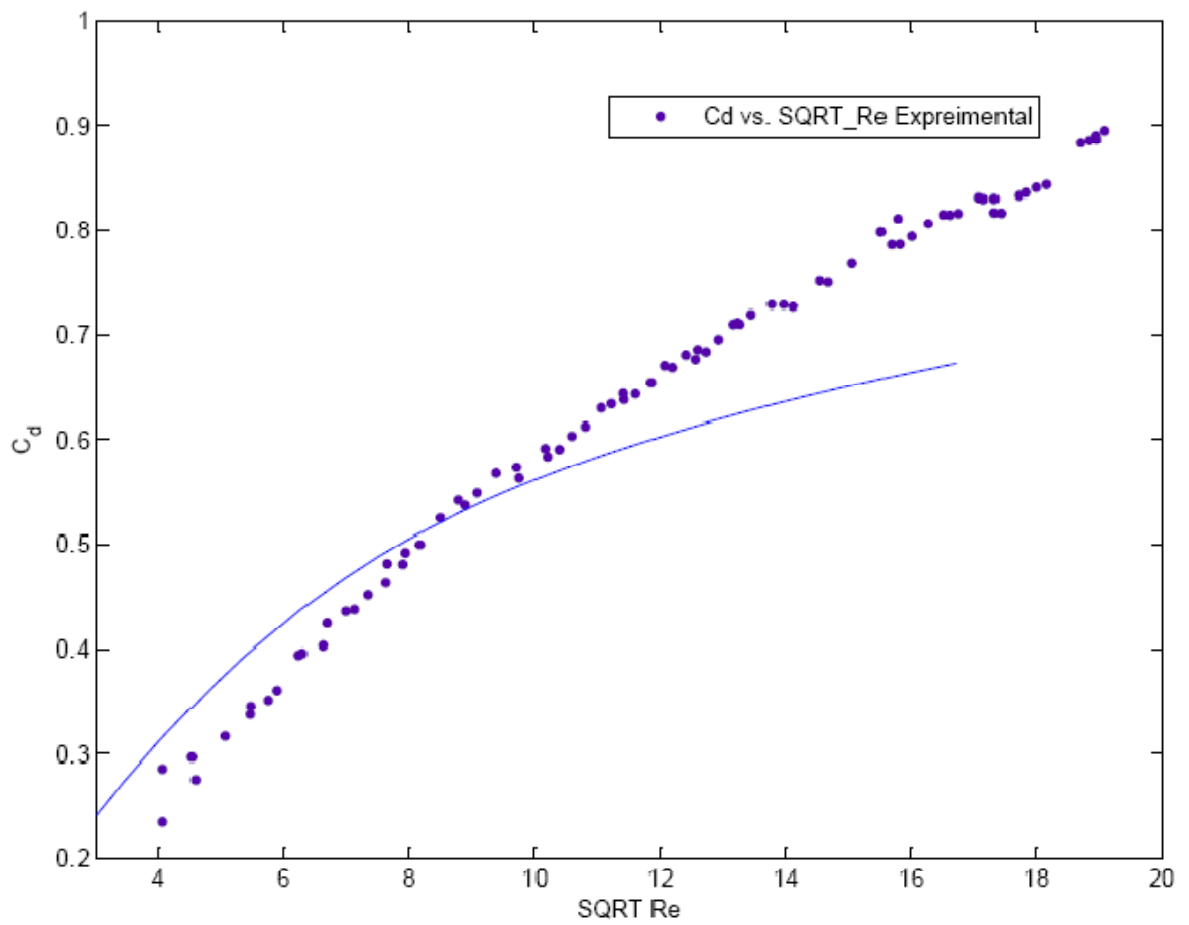


Figure 6.15 Comparison between Experimental result of set no. 1 and numerical simulation with fixed inlet pressure

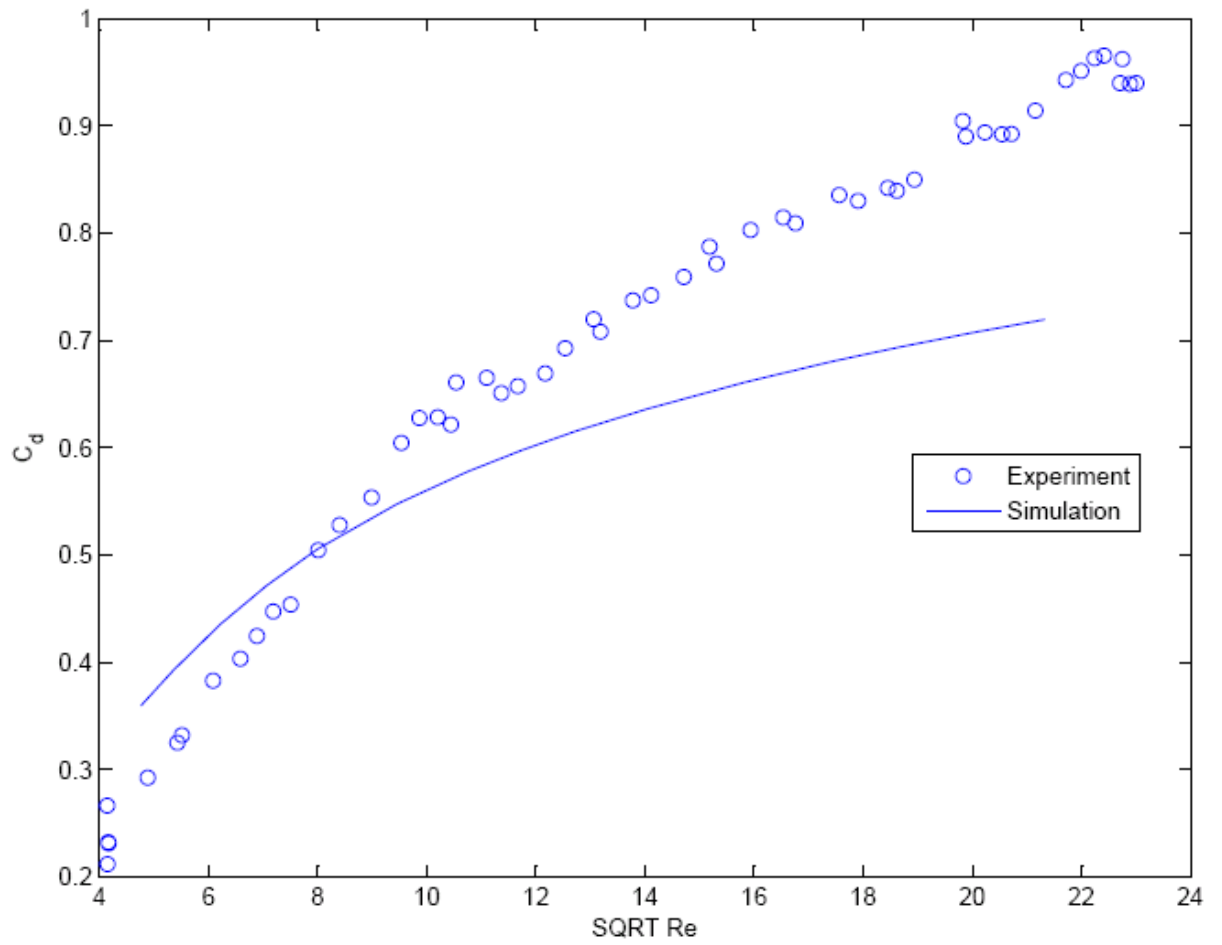


Figure 6.16 Comparison between Experimental result of set no. 4 and numerical simulation with refined mesh and variable inlet and outlet pressures

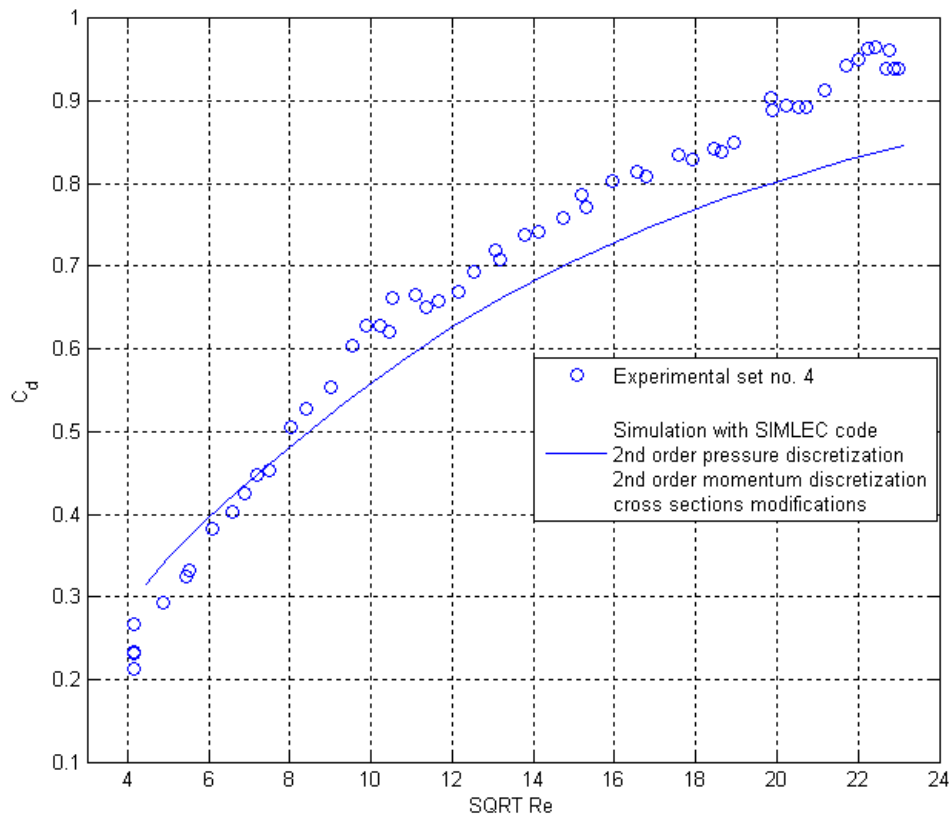


Figure 6.17 Comparison between Experimental result of set no. 4 and numerical simulation after modification of cross section

The simulation showed the phenomena of changing C_d with \sqrt{Re} in small opening orifice in the same shape of experimental relation, but with some shifting up in low range of \sqrt{Re} and shifting down in high range of \sqrt{Re} , naturally two curves (experimental and simulation) intersects at $\sqrt{Re}=8$, and look to have sharing region from $\sqrt{Re}=5$ to $\sqrt{Re}=18$, the maximum absolute tolerance between experimental and simulation occurred at the highest reported point $\sqrt{Re}=23.1$ and simulation $C_d=0.85$, and experimental $C_d=0.94$, that is error of about 10% maximum, but in the low range of \sqrt{Re} the maximum tolerance were reported at $\sqrt{Re}=4.46$ and simulation $C_d=0.31$ while experimental $C_d=0.26$ that is error of about 20% if absolute error was divided by experimental C_d considering that it is the “true”

reference value, in both cases –high and low range-, but when considering the reference is the larger value, the second relative error –at low Reynolds number- would be 17%, both of these errors (20% and 17%) could be ignored, and very low range of Re points could be excluded from experimental work, due to the huge uncertainty in experimental work in the low Re range, because it is almost at the minimum of measuring range of sensors and devices, this will be discussed later.

6.5 The final shape of the flow equation

Knowing that the flow equation in an orifice is:

$$Q = C_d A \sqrt{\frac{2 \Delta P}{\rho}} \dots \dots \dots (6.1)$$

And the resultant Cd formula in this study was

$$C_d = C_{dm} (1 + a e^{-\delta \sqrt{Re}}) \dots \dots \dots (6.2)$$

The flow equation became

$$Q = C_{dm} (1 + a e^{-\delta \sqrt{Re}}) A \sqrt{\frac{2 \Delta P}{\rho}} \dots \dots \dots (6.3)$$

The pressure sensitivity, which represents the sensitivity of the change of the flow rate with the change of the pressure difference, could be then found as

$$K_c = \frac{\partial Q}{\partial \Delta P} = \frac{C_{dm} (1 + a e^{-\delta \sqrt{Re}}) A}{\sqrt{2 \Delta P \rho}}$$

6.6 Uncertainty Analysis

Uncertainty analysis quantifies the variation between the actually measured value of a physical quantity and the true value of the same physical quantity. The result of any physical measurement comprises two parts: an estimate of true value of the measured and the uncertainty of this estimate. Uncertainty analysis provides the experimenter a rational way of evaluating the significance of the scatter on repeated trials. This can be a powerful tool in locating the source of trouble in misbehaving experiment, so it will be used to check the reliability of our data.

To find the value of uncertainty for any function:

Let the variable X_1, X_2, X_3, \dots Provide the result “R” through a functional relationship,

$$R=f(X_1, X_2, X_3, \dots)$$

Then, by differential calculus, a small changes or errors in the measured variable are related to change or error in R as:

$$dR = \frac{dR}{dX_1} dX_1 + \frac{dR}{dX_2} dX_2 + \frac{dR}{dX_3} dX_3 + \dots$$

The error dX_1, dX_2, dX_3, \dots are random in nature, having even changes of positive and negative value. Then through squaring each side, one can be canceling off the sum of product terms. Thus

$$(dR)^2 = \left(\frac{dR}{dX_1} dX_1\right)^2 + \left(\frac{dR}{dX_2} dX_2\right)^2 + \left(\frac{dR}{dX_3} dX_3\right)^2 + \dots$$

Or

$$(W_R)^2 = \left(\frac{dR}{dX_1} W_1\right)^2 + \left(\frac{dR}{dX_2} W_2\right)^2 + \left(\frac{dR}{dX_3} W_3\right)^2 + \dots$$

$$\therefore W_R = \pm \sqrt{\left(\frac{dR}{dX_1} W_1\right)^2 + \left(\frac{dR}{dX_2} W_2\right)^2 + \left(\frac{dR}{dX_3} W_3\right)^2 + \dots}$$

Where, W_{X1} , W_{X2} , $W_{X3} \dots$ are the uncertain or error in the independent variable and W_R is the error in the result. Thus from a knowledge of errors in the measured variables, the probable error in the result “R” can be worked out.

To find the value of uncertainty percentage;

$$\text{Percentage Analysis} = \frac{W_R}{|R|} \times 100\%$$

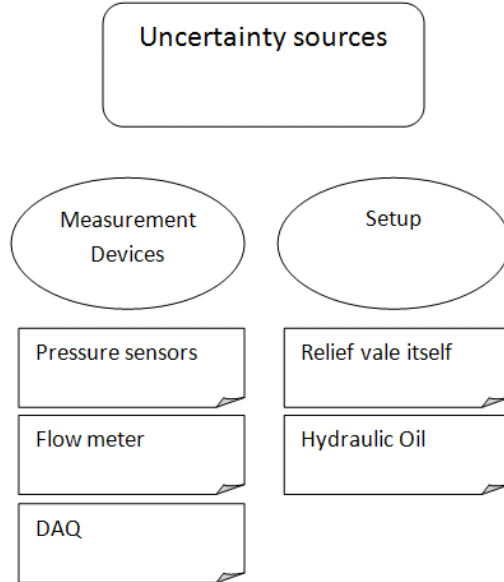


Figure 6.18 Sources of uncertainty in results

6.6.1 Measuring devices uncertainty

Pressure Measurement

The specifications of the pressure sensor stated that pressure is linear with output voltage, so a range of 0-5volt represents the range 0-40bar, simply the conversion factor is inserted in software as 8bar/volt. But the manufacturer specifications also stated a non-linearity of $\pm 0.25\%$ of full scale, so one can expect or doubt a range of error of reading $\pm 0.25\% * 40\text{bar} = \pm 0.1\text{bar}$, for the minimum reading of pressure in this experiment, which is 1.3732bar, the maximum relative error is expected as $0.1/1.3732 = 7.3\%$ which is a little bit large value in such level of technology.

But this is not the end of the story; another source of uncertainty in pressure measurement is the resolution of the DAQ card. The maximum range of the card is 10volt, and the resolution is 12bit, so DAQ discretizes the reading in step of 2.44mV, an error have to be expected or doubted, which could be called as uncertainty, of about $\pm 1.22\text{mV}$, noticing that this is a fixed absolute doubt of error, it is simply noticed that it affects the small readings also more than the large values. Referring to the minimum reading of pressure 1.3732bar, which was read as 0.17167volt, the largest relative expected error –may called uncertainty- is about 0.7%. On the other hand the absolute accuracy of the DAQ is 14.7mV as specification, Appendix H3, which is much larger than the step 1.22mV, so let the combined uncertainty of the measured voltage 15mV, because DAQ systems is not our study.

Knowing that it is independent uncertainties, the combination of them should be derived as follows;

The pressure reading $P = \text{constant of linearity (8bar/volt)} * \text{measured voltage} = C_0 * V_m$

Ideal Uncertainty of pressure is $W_P = \sqrt{\left(\frac{\partial P}{\partial V_m} W_{V_m}\right)^2 + \left(\frac{\partial P}{\partial C_0} W_{C_0}\right)^2}$

$$W_P = \sqrt{(C_0 * W_{V_m})^2 + (V_m * W_{C_0})^2}$$

$$W_P = \sqrt{(8 * 1.22 * 10^{-3})^2 + (0.17167 * (8 * 0.25\%))^2} = 12\%$$

While the Maximum uncertainty is

$$W_P = \sqrt{(8 * 1.22 * 10^{-3})^1 + (0.17167 * (8 * 0.25\%))^1} = 35\%$$

For this reason the low range results were too much scattered to show a physical phenomena, but at higher ranges of results the points tend to condense together.

Flow measurement

As discussed for the pressure, the measuring device has its uncertainty and it equals 1% of indicated reading, and in this case it is relative already, and the DAQ analogue input is same for both pressure and flow, and discussed previously, but in this case the electronic operation amplifier exists, the curve fitting by Matlab showed a root mean square error of about 0.004 for a confidence level 95%, refer to appendix D3,

If the flow simply calculated from the measured voltage as $flow = C_0 * C_1 * V_m$

Where C_0 is the constant of converting measured voltage V_m to current reading, and C_1 is the constant of converting current reading to flow, due to the linear relationships.

Then combined uncertainty is

$$W_{flow} = \sqrt{\left(\frac{\partial flow}{\partial C_0} W_{C_0}\right)^2 + \left(\frac{\partial flow}{\partial C_1} W_{C_1}\right)^2 + \left(\frac{\partial flow}{\partial V_m} W_{V_m}\right)^2}$$

And considering that; $C_0 = 2$ with uncertainty of 0.004, $C_1=7/20$ with uncertainty of 1%, V_m for minimum considered reading 0.15volt with uncertainty of 15mV, the combined uncertainty result a value of about 1.1%.

But to be “scientifically honest”, it was not sure that the specifications from the manufacturer of the flow meter are true, but there was no method to check if the accuracy is 1% of the reading, so one has to “trust” the manufacturer.

6.6.2 Setup uncertainty

The setup uncertainties mainly have no way to be measured -at our technology level- and most of them to be “evaluated” by our limit of experience and sense. The first source is the by-pass flow due to leakage inside the valve, which causes that some of the counted flow by the flow meter did not pass through the orifice of study, instead it by-pass it. This could be expected to be less than 2-3%.

Second is the doubt error of measuring the diameter of the orifice. Such small internal diameter usually measured by “Go/No Go pin gauge”, special for hole shapes, it is a set of needles each has a certain diameter, graded with a step of 0.05mm -in this case- the orifice of this study let the 1mm needle to enter freely –and a little bit loosely- and did not let the

1.05mm to do so. The diameter was considered to be 1.02mm, and knowing that the talking is about traditional manual way of measurement, with such step of about 0.05mm, it is accepted to have a doubt of about ± 0.02 mm. But knowing that it was used to calculate the area, which is related to the square of the diameter, then one would get a really considerable error.

Third is the uncertainty of the oil viscosity. The ISO 51 519 and DIN 51 524 standard allows a wide range of viscosity to be considered in the class, this makes the user doubt in the value of the kinematic viscosity labeled of some product, e.g. the VG 68 hydraulic oil manufacturer could supply oil with viscosity of 61.2 or 74.8 instead of 68 mm²/s. This could cause a serious error in calculation.

The viscosity is affected by two variables; temperature and pressure. The temperature of the oil is observed and recorded in each experiment, but the accuracy in reading the temperature affects the viscosity widely, Appendix F shows how the viscosity is sensitive to the temperature in semi-log scale. Knowing that the temperature was read on an ordinary thermometer, the level of confidence one could judge the viscosity is poor, but the uncertainty is not measurable due to lack in sources.

The viscosity is also sensitive to high pressures, in this study the pressure was lower than the effective pressure range and pressure effect could be neglected on the density up to 150bar so is on the dynamic viscosity, Fig (6.19) shows the variation in dynamic viscosity (in 10⁻³ Pa.s) with temperature and pressure (in bars).

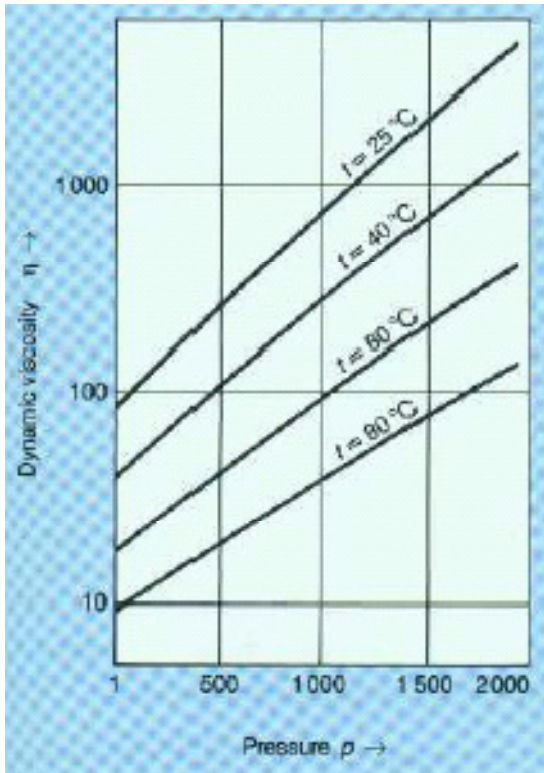


Figure 6.19 Temperature-pressure relation of viscosity

Chapter Seven: Conclusions and Recommendations

7.1 Conclusion

The flow rate through an orifice in pilot operated relief valve usually is small due to small orifice openings. A problem occurs in using the classical orifice flow equation in this case. The discharge coefficient is not a constant due to viscous laminar flow conditions in such small opening orifice. In addition, it is difficult to determine the actual coefficient of discharge. This paper provides an empirical flow equation. In practice, C_d must also be measured (for example, Wu (2002), which requires measurement of other parameters. It is thus possible to differentiate the flow equations with respect to the pressure drop in order to obtain pressure sensitivity of the pilot valve. A comparison between experimental and empirical models showed that CFD approach is valid for such flow conditions.

Briefly the following could be concluded from all this work:

- Coefficient of discharge is not constant at low Reynolds number (less than 700) in small opening orifices (in order of millimeter) in laminar viscous flow.
- The relation between the coefficient of discharge and the square root of Reynolds number is exponential.
- The value of the maximum discharge coefficient varies widely from a shape to another.
- The numerical simulation is valid for rough estimation of flow rate in orifices, using the ordinary option of Fluent without any code modifications.
- The outlet pressure range does not affect the coefficient of discharge independently; the real effect is for the pressure difference.

- The viscosity range does not affect the coefficient of discharge independently; the real effect is for the Reynolds number.

7.2 Recommendations

For further work, next researchers are recommended to:

- Repeat the experimental work with higher accuracy instruments.
- Repeat the reverse engineering of the orifice and the whole valve by slicing it, and make the experiment on identical one, to compare the experiment and the simulation in the same conditions.
- Repeat the experimental work with higher flow rate hydraulic unit, and higher flow rate flow meter, to cover wider range of Reynolds number.
- Repeat the experimental investigation with highly controlled hydraulic unit with thermal conditioning supportive system, to accurately control the temperature of the hydraulic oil.
- To measure the hydraulic oil that will be used in the experiment, with high technology device, and not to depend on the labeled specifications of the manufacturer.
- Calibrate every instrument before using it in testing with the highest possible level of standard (as much as short the chain from the standard to the measuring device as much as it is considered to be accurate).

REFERENCES

- Bulut, H. , Ergut ,M , Asil, V, Bokor , R. ,(2004), “Numerical solution of a viscous incompressible flow problem through an orifice by Adomian decomposition method” , **Applied Mathematics and Computation**, 153 , 733–741 .
- Cruz-Maya, J. , Sanchez-Silva, F. , Quinto-Diez, P. , (2006) , “A new correlation to determine the discharge coefficient of a critical Venturi nozzle with turbulent boundary layer”, **Flow Measurement and Instrumentation** , 17 , 258-266 .
- Engineering Mannesmann Rexroth, “**Basic principle and components of fluid technology**”, the hydraulic trainer volume 1, (1991), Schleunungdruck.
- Fluent Inc., “**FLUENT 6.2 Tutorial Guide**”, (2005).
- Holman, J. , “**Experimental methods for engineers**” ,(2001), McGraw Hill.
- Malek, Mohammad A., “**Pressure Relief Devices**”, (2005), McGraw-Hill.
- Reader-Harris, M. , Sattary J. and Spearman, E. , (1995) , “The orifice plate discharge coefficient equation - further work”, **Flow Measurement and Instrumentation** , 6 (2) , 101-114 .
- Rexroth Bosch Group GMB, “**Hydraulic component catalogue**”, (2004) CD version, Article RE 25 802/01.99.
- Royal Scientific Society, “**Guide to the calculation of uncertainty in calibration and measurement**”, (2002).
- Wu, D., Burton, R. and Schoenau, G. (2002), “An empirical discharge coefficient model for orifice flow”, **International Journal of Fluid Power**, vol. 3(3).
- Wu, D. , Burton, R. , Schoenau, G. and Bitner, D. ,(2003), “Modeling of orifice flow rate at very small openings” , “An empirical discharge coefficient model for orifice flow”, **International Journal of Fluid Power**, vol. 4(1).
- Wu, D. , Burton, R. , Schoenau, G. and Bitner, D., (2007) , “Analysis of a pressure-compensated flow control valve”, **Journal of Dynamic Systems, Measurement, and Control**, 129 , 203-211 .

Appendices

Appendix A

Matlab M-file for averaging experimental reading data

```

1 function
[SQRT_Re,Cd,P1,P2,VolFlowrate,data]=coefficientofdischarge(V1,V2,V3,kin_visc)
2 % this program is used to take the average of each 30 reading due to the
3 % fact that the DAQ card takes 30 reading for each analogue input in a
4 % period of 3 seconds every single run, then each reading vector V1 , V2
5 % and V3 scaled to manufacturer specifications to represent the volumetric
6 % flow rate , upstream pressure and downstream pressure, respectively, and
7 % simple calculation to get square root of Reynolds number and Coefficient
8 % of discharge,
9 % note : V1 V2 and V3 should be column vector first, as copy paste from
10 % excel sheet, one column in each time , not a matrix for all , ENJOY!
11 clc
12 V1=transpose(V1);
13 V2=transpose(V2);
14 V3=transpose(V3);
15
16 d=0.00102; % define orifice diameter %
17
18 [lines,originalsizelength]=size(V1);
19 readinglegth=originalsizelength/30;
20
21 for i=1:1:readinglegth
22
23 sum=0;
24 for j=1:1:30
25
26 sum=sum+V1(30*(i-1)+j);
27 end
28
29 VolFlowrate(i)=sum/30;
30
31 end
32
33 for i=1:1:readinglegth
34
35 sum=0;
36 for j=1:1:30
37
38 sum=sum+V2(30*(i-1)+j);
39 end
40
41 P1(i)=sum/30;
42
43 end
44

```



```

45 for i=1:1:readinglength
46
47 sum=0;
48 for j=1:1:30
49
50 sum=sum+V3(30*(i-1)+j);
51 end
52
53 P2(i)=sum/30;
54
55 end
56 %scaling from voltage to reading in lit/min and bar %
57 VolFlowrate=(VolFlowrate-0.006586)/(0.4969*20/7); % converting voltage
reading to
58 %current in mA
59 %according curve fit of electronic
60 %operational amplifier to
61 %flow in lit/min %
62
63 P1=P1*8; % manufacturer specs 0-5volt represents 0-40bar %
64 P2=P2*8;
65 delta_P=(P1-P2)*100000; % pressure difference across orifice in Pascal%
66 VolFlowrate=VolFlowrate/60000; % converting from lit/min to m^3/sec
67 MassFlowrate=VolFlowrate*886; %then multiply by density
68 velocity=VolFlowrate/((pi/4)*d^2); % simple continuity incompressible
69 Re=velocity*d/kin_visc; % Reynolds number calculation using kinematic
70 % viscosity in unit of m^2/s
71 SQRT_Re=sqrt(Re);
72 for k=1:1:readinglength
73 Cd(k)=VolFlowrate(k)/(((pi/4)*d^2)*sqrt(2*delta_P(k)/886));
74 end
75
76 cftool(SQRT_Re,Cd) % curve fitting tool open for data set SQRT_Re and Cd %
77
78 SQRT_Re=transpose(SQRT_Re);
79 Cd=transpose(Cd);
80 P1=transpose(P1);
81 P2=transpose(P2);
82 VolFlowrate=transpose(VolFlowrate*60000);
83 data=[P1 P2 VolFlowrate SQRT_Re Cd];
84
85 end
86
87

```

Appendix B

Experimental results

Set 1

Spring load	Temperature °C	Kin Viscosity [m ² /s]
medium	27.5	0.000133

Run no.	P1 [bar]	P2 [bar]	Vol Flow		
			[lit/min]	SQRT RE	Cd
1	3.2304	2.979733	0.10550057	4.062384	0.286066
2	3.538667	3.168	0.10550057	4.062384	0.235247
3	3.829333	3.4712	0.130857785	4.52432	0.29685
4	4.0488	3.613333	0.13416831	4.581192	0.276015
5	4.365333	3.874933	0.163376065	5.055309	0.316719
6	4.624	4.058667	0.191245522	5.469519	0.345302
7	4.802667	4.216	0.190517676	5.459101	0.337676
8	5.093333	4.426667	0.21117911	5.7475	0.351121
9	5.331467	4.634667	0.221744617	5.889522	0.360628
10	5.517333	4.7864	0.248275776	6.231903	0.394236
11	5.7424	4.989333	0.252995036	6.290853	0.395782
12	6.082933	5.251467	0.285278527	6.680179	0.424724
13	6.269333	5.381333	0.279831421	6.616096	0.403135
14	6.432	5.490667	0.311645334	6.982064	0.436063
15	6.717333	5.706667	0.324112632	7.120353	0.437676
16	6.972267	5.901333	0.344281009	7.338547	0.45164
17	7.181333	6.069333	0.373840947	7.647103	0.481277
18	7.474667	6.290667	0.371516536	7.623293	0.463514
19	7.68	6.410667	0.398986852	7.900104	0.480763
20	7.834667	6.597067	0.402954786	7.93929	0.49173
21	8.089867	6.749333	0.426175421	8.164841	0.499701
22	8.400267	6.982133	0.460360703	8.485993	0.524808
23	8.746667	7.226667	0.491916348	8.772011	0.541664
24	9.032	7.4048	0.504383645	8.882476	0.536786
25	9.376	7.677333	0.526782518	9.077562	0.548703
26	9.6896	7.877867	0.562846113	9.383144	0.567679
27	10.05333	8.013333	0.603135909	9.713173	0.573272
28	10.31733	8.165333	0.608207352	9.753924	0.562848
29	10.744	8.450667	0.659649628	10.15805	0.591344
30	11.03467	8.642667	0.664627155	10.1963	0.583389
31	11.35387	8.840533	0.689632186	10.38633	0.590545

32	11.54667	8.946667	0.716445093	10.58632	0.603193
33	11.89333	9.152	0.746592004	10.80675	0.612157
34	12.1784	9.330667	0.782373851	11.06269	0.629398
35	12.47733	9.496	0.805571007	11.22549	0.633372
36	12.74133	9.6512	0.832759576	11.41336	0.643119
37	12.97067	9.810667	0.834426578	11.42477	0.637243
38	13.24	9.928	0.861709063	11.61004	0.6428
39	13.61067	10.12667	0.898500503	11.8553	0.653491
40	13.784	10.22667	0.930783994	12.06641	0.669957
41	14.09067	10.37067	0.949402764	12.18649	0.668251
42	14.408	10.55333	0.983775877	12.40514	0.680242
43	14.768	10.72533	1.014768028	12.59902	0.685162
44	14.92	10.816	1.008804387	12.56195	0.676026
45	15.208	10.964	1.036603408	12.73385	0.683102
46	15.4368	11.07547	1.069145167	12.93218	0.695004
47	15.68533	11.184	1.108707117	13.16928	0.709425
48	15.8448	11.26933	1.119906554	13.23562	0.710762
49	15.97333	11.33067	1.126128463	13.27234	0.70952
50	16.22107	11.44187	1.157284967	13.45469	0.718659
51	16.85067	11.73333	1.213141276	13.77556	0.728031
52	17.352	11.9448	1.246810022	13.96541	0.727905
53	17.7976	12.128	1.273834239	14.11595	0.726268
54	18.3376	12.36053	1.352418126	14.54484	0.750978
55	18.7312	12.512	1.377070973	14.67681	0.749634
56	19.33867	12.7608	1.450606896	15.06359	0.767834
57	19.7656	12.9088	1.54015543	15.52158	0.79848
58	20.1816	13.0696	1.594016033	15.79065	0.811441
59	20.6112	13.22827	1.573800698	15.6902	0.786313
60	20.96533	13.34373	1.599674448	15.81865	0.786627
61	21.32533	13.47733	1.638907694	16.01145	0.79421
62	21.7336	13.6168	1.692862212	16.27288	0.806658
63	22.28693	13.83973	1.745407996	16.5235	0.815269
64	22.58427	13.91467	1.767619038	16.6283	0.814985
65	22.97653	14.0488	1.796474609	16.76348	0.816227
66	23.49707	14.19627	1.866981754	17.08927	0.831075
67	23.77387	14.26773	1.884215268	17.16796	0.829639
68	24.25707	14.38133	1.921030187	17.33487	0.82987
69	24.7616	14.57493	1.921006708	17.33477	0.817096
70	25.11493	14.68187	1.943264708	17.4349	0.816745
71	25.48187	14.78533	2.007103844	17.71897	0.833122
72	25.8888	14.98267	2.033094989	17.83333	0.835762

73	26.17333	14.98213	2.071295163	18.00008	0.840551
74	26.584	15.0648	2.108415308	18.16066	0.843345
75	27.02187	15.1792	2.239286711	18.7158	0.883375
76	27.39467	15.25573	2.272744147	18.8551	0.885565
77	27.57413	15.28267	2.298946602	18.96348	0.8902
78	27.69813	15.26427	2.301787549	18.97519	0.886181
79	27.78693	15.26693	2.332920574	19.10308	0.895072

Set 2

Spring load	Temperature °C	Kin Viscosity [m ² /s]
low	28.5	0.000125

Run no.	P1 [bar]	P2 [bar]	Vol Flow [lit/min]	SQRT RE	Cd
1	1.850667	1.373333	0.216415	6.001612	0.425243
2	2.106667	1.498667	0.250389	6.455529	0.435937
3	2.325333	1.546667	0.275652	6.773374	0.424078
4	2.661333	1.746667	0.330828	7.420364	0.469603
5	2.848267	1.810667	0.372221	7.870906	0.496074
6	2.917333	1.866667	0.399903	8.158333	0.529642
7	3.042667	1.922667	0.414459	8.305492	0.531659
8	3.130667	1.997333	0.42857	8.445694	0.546517
9	3.3088	2.040533	0.460619	8.755788	0.555261
10	3.477333	2.12	0.492409	9.052896	0.573777
11	3.713867	2.208	0.52967	9.38917	0.585967
12	4.013333	2.36	0.565945	9.705358	0.597523
13	4.221333	2.453333	0.601046	10.0018	0.613659
14	4.36	2.499467	0.630888	10.24709	0.627905
15	4.602667	2.577333	0.665378	10.52346	0.634718
16	4.765333	2.672	0.690877	10.7232	0.648249
17	5.029333	2.744	0.713768	10.89941	0.640978
18	5.242933	2.824	0.741544	11.10946	0.64727
19	5.466667	2.913333	0.783877	11.42216	0.665969
20	5.710133	3.034667	0.838535	11.81368	0.695956
21	5.994667	3.090667	0.865043	11.99895	0.689128
22	6.156267	3.085333	0.889978	12.17065	0.689452
23	6.402667	3.16	0.929352	12.43696	0.700631
24	6.610667	3.258667	0.952032	12.58781	0.705928
25	6.821333	3.328	0.980137	12.77226	0.711913
26	7.194667	3.477067	1.010284	12.96719	0.711332

27	7.3568	3.522667	1.037824	13.14275	0.719533
28	7.568	3.626667	1.069591	13.34238	0.731403
29	7.861067	3.722667	1.093915	13.49324	0.730008
30	7.952	3.786667	1.172124	13.96725	0.779667
31	8.216	3.849333	1.176608	13.99395	0.764394
32	8.471733	3.970667	1.201684	14.14228	0.768941
33	8.696	4.026667	1.232206	14.32076	0.774134
34	8.877333	4.058667	1.265898	14.51522	0.782881
35	9.205333	4.146667	1.244204	14.39031	0.75099
36	9.568	4.280533	1.384373	15.17927	0.817315
37	9.922667	4.376	1.367938	15.0889	0.788516
38	10.33867	4.488	1.414966	15.34608	0.794152
39	10.70667	4.616	1.48181	15.70437	0.815118
40	11.096	4.696533	1.594955	16.29291	0.855928
41	11.60533	4.789067	1.595683	16.29662	0.829724
42	11.98667	4.898667	1.566217	16.14546	0.798639
43	12.1904	4.944	1.691407	16.77831	0.852996
44	12.63733	5.061333	1.745408	17.04405	0.86087
45	12.9448	5.104	1.747357	17.05356	0.847153
46	13.44987	5.2248	1.805162	17.33335	0.85449
47	13.8016	5.296	1.863225	17.6099	0.867308
48	14.21867	5.36	1.892856	17.74938	0.863363
49	14.67387	5.469333	2.010907	18.29449	0.899812
50	15.18933	5.536267	1.926783	17.90774	0.8419
51	15.46187	5.588533	1.945542	17.9947	0.840561
52	16.072	5.698133	2.012833	18.30325	0.848394
53	16.384	5.752	2.039246	18.42295	0.849029
54	16.61813	5.789333	2.097826	18.68569	0.865446
55	16.848	5.802667	2.098272	18.68768	0.857103
56	17.17867	5.861333	2.215643	19.20323	0.894104
57	17.61333	5.949867	2.272979	19.45011	0.903529
58	17.79013	5.938933	2.305169	19.58735	0.909038
59	18.15733	5.992	2.360555	19.82127	0.918782
60	18.52267	6.06	2.400094	19.98658	0.92296
61	18.85067	6.097867	2.425404	20.09169	0.922023
62	19.22933	6.187467	2.477433	20.30604	0.931306
63	19.82747	6.354933	2.530801	20.52359	0.936038

Set 3

Spring load	Temperature °C	Kin Viscosity [m ² /s]
high	29.5	0.000120

Run no.	P1 [bar]	P2 [bar]	Vol Flow		
			[lit/min]	SQRT RE	Cd
1	7.653333	7.404533	0.077279	3.660322	0.210328
2	7.814667	7.586667	0.077537	3.666433	0.220446
3	7.901333	7.714667	0.077068	3.655314	0.242158
4	8.013333	7.864	0.077749	3.671426	0.273133
5	8.245333	8.021333	0.104538	4.257216	0.299854
6	8.447733	8.117333	0.108623	4.339604	0.256545
7	8.634667	8.282933	0.131562	4.775889	0.301151
8	8.827467	8.472	0.134943	4.836866	0.307264
9	9.026667	8.653333	0.1603	5.271764	0.356161
10	9.221333	8.779733	0.162484	5.307547	0.331937
11	9.458667	9.016	0.181784	5.613917	0.370917
12	9.6984	9.222933	0.191903	5.768057	0.377817
13	9.933333	9.368	0.229352	6.305794	0.414105
14	10.32533	9.648	0.26079	6.724101	0.43018
15	10.66133	9.928	0.275323	6.908923	0.436469
16	10.97467	10.184	0.317914	7.424098	0.485371
17	11.18933	10.33067	0.309955	7.330573	0.454095
18	11.41333	10.504	0.341158	7.690715	0.485685
19	11.7736	10.73333	0.378678	8.102584	0.504031
20	11.98667	10.91467	0.403518	8.364121	0.529086
21	12.6072	11.33867	0.481867	9.140132	0.580814
22	12.93893	11.60533	0.4941	9.255419	0.580848
23	13.21867	11.78667	0.534225	9.623897	0.606057
24	13.52267	11.96747	0.544157	9.712942	0.592368
25	13.88	12.19733	0.602455	10.22	0.630501
26	14.11227	12.3672	0.605085	10.24228	0.621828
27	14.43467	12.59467	0.631123	10.46034	0.631634
28	14.79467	12.84613	0.662725	10.71903	0.644525
29	15.06347	13.05867	0.684396	10.89288	0.656194
30	15.3496	13.24533	0.694962	10.97663	0.650386
31	15.71733	13.496	0.719075	11.16544	0.654979
32	16.1896	13.83707	0.780519	11.6327	0.690838
33	16.66933	14.1472	0.806299	11.82325	0.689243
34	17.06	14.4	0.833464	12.02077	0.693755

35	17.58933	14.7464	0.858117	12.19725	0.690913
36	18.00533	14.992	0.926511	12.67401	0.724582
37	18.568	15.33333	0.952972	12.85372	0.719326
38	19.1376	15.66667	1.014345	13.26116	0.739134
39	19.65067	15.93387	1.037496	13.41164	0.73057
40	20.408	16.35467	1.185248	14.33486	0.799215
41	21.12827	16.73067	1.219128	14.53829	0.789227
42	21.876	17.112	1.269749	14.83705	0.789755
43	22.536	17.42107	1.391346	15.53125	0.835171
44	22.87467	17.536	1.363594	15.37557	0.801178
45	23.5704	17.83733	1.416633	15.67175	0.803201
46	24.01867	18.056	1.471926	15.97466	0.818325
47	24.36133	18.1848	1.447766	15.84302	0.790836
48	24.88	18.41867	1.540414	16.34208	0.822691
49	25.38933	18.62347	1.609747	16.70581	0.840149
50	25.832	18.77867	1.656024	16.94424	0.846505
51	26.112	18.89067	1.716975	17.25324	0.867393
52	26.43707	19.02667	1.756631	17.45135	0.876032
53	26.89333	19.1816	1.772902	17.53198	0.866701
54	27.23707	19.28	1.797508	17.65323	0.865077
55	27.53707	19.4	1.836154	17.84199	0.873847
56	27.92613	19.48613	1.895485	18.12796	0.885747
57	28.51173	19.66933	1.893842	18.1201	0.864607
58	28.85547	19.77333	2.042651	18.81853	0.920154
59	29.12	19.84267	1.929835	18.29148	0.86014
60	29.89627	20.0856	1.993956	18.59287	0.864225
61	30.31253	20.22187	2.048544	18.84566	0.875479
62	30.656	20.2912	2.067515	18.93272	0.871824
63	31.09893	20.4096	2.120296	19.17286	0.880403
64	31.19787	20.40667	2.306882	19.99869	0.953347

Set 4

Spring load	Temperature °C	Kin Viscosity [m ² /s]
medium	34	0.000092

Run no.	P1 [bar]	P2 [bar]	Vol Flow		
			[lit/min]	SQRT RE	Cd
1	4.0664	3.917067	0.075894	4.142745	0.266617
2	4.272	4.072	0.076598	4.161925	0.232521
3	4.512	4.309067	0.076809	4.167662	0.231472
4	4.698667	4.461333	0.076105	4.148509	0.212077
5	4.9144	4.674667	0.105548	4.885505	0.292647
6	5.176	4.88	0.130341	5.429082	0.325234
7	5.328533	5.026667	0.134427	5.513508	0.332153
8	5.602667	5.266133	0.163681	6.08394	0.383041
9	5.869333	5.453333	0.191668	6.583554	0.403426
10	6.1864	5.736	0.209911	6.889747	0.424617
11	6.413333	5.933333	0.228389	7.186595	0.447523
12	6.685333	6.129867	0.249168	7.506397	0.453862
13	6.914133	6.330667	0.283964	8.013401	0.504679
14	7.197333	6.552533	0.312397	8.405018	0.528146
15	7.565333	6.797333	0.357429	8.99043	0.553694
16	7.909333	7.093333	0.40225	9.537481	0.604522
17	8.173333	7.306667	0.430449	9.866113	0.627705
18	8.492533	7.504	0.460384	10.20342	0.628616
19	8.722667	7.704	0.491329	10.54076	0.660872
20	8.941867	7.832	0.482431	10.44487	0.62167
21	9.274133	8.037333	0.544932	11.10086	0.665201
22	9.650933	8.229333	0.571721	11.37045	0.650962
23	10.0456	8.498667	0.602385	11.67138	0.657504
24	10.4976	8.730933	0.655306	12.17328	0.66931
25	10.808	8.952	0.69522	12.53853	0.692777
26	11.2776	9.254133	0.754246	13.05996	0.719823
27	11.57067	9.397333	0.769014	13.1872	0.70816
28	12.0808	9.6904	0.839733	13.78022	0.737337
29	12.60907	10.01093	0.881103	14.11558	0.742089
30	13.31787	10.38667	0.95748	14.71466	0.759219
31	13.73973	10.64747	1.019863	15.18645	0.787343
32	14.2072	10.87733	1.03705	15.31388	0.771519
33	14.83733	11.22933	1.123522	15.93956	0.802988
34	15.75253	11.69333	1.209103	16.53549	0.814711

35	16.3072	11.9616	1.24249	16.76223	0.809149
36	17.45093	12.53867	1.364134	17.56362	0.835558
37	18.35653	12.97573	1.418347	17.90922	0.830079
38	19.256	13.35893	1.506228	18.45571	0.842041
39	19.69067	13.544	1.532994	18.61897	0.839423
40	20.208	13.7824	1.586785	18.94281	0.849809
41	20.80773	13.99493	1.738998	19.83056	0.904475
42	21.3336	14.2184	1.748719	19.88591	0.889993
43	22.05067	14.4856	1.810867	20.23619	0.893801
44	22.86667	14.79147	1.867264	20.54888	0.89205
45	23.23173	14.8856	1.898866	20.72204	0.892302
46	23.69867	15.05253	1.980056	21.16042	0.91417
47	24.21413	15.19173	2.085876	21.71849	0.942731
48	24.67547	15.34427	2.140135	21.99916	0.951115
49	24.95467	15.44	2.188173	22.24469	0.963042
50	25.31467	15.5488	2.222523	22.4186	0.965498
51	26.28347	15.84853	2.289414	22.75347	0.962144
52	26.8024	15.94907	2.280633	22.70979	0.939797
53	27.2928	16.0672	2.317589	22.89305	0.939057
54	27.58213	16.14373	2.341467	23.01068	0.939866

Set 5

Spring load	Temperature °C	Kin Viscosity [m ² /s]
medium	40	0.000068

Run no.	P1 [bar]	P2 [bar]	Vol Flow		
			[lit/min]	SQRT RE	Cd
1	2.117333	1.954667	0.076128	4.826123	0.256247
2	2.309333	2.112	0.075894	4.818675	0.231935
3	2.530667	2.328	0.077068	4.855801	0.232403
4	2.757333	2.510667	0.107966	5.747356	0.295115
5	2.968	2.712	0.107215	5.727324	0.28767
6	3.050667	2.826667	0.110196	5.806421	0.316085
7	3.2056	3.0128	0.132994	6.378837	0.411188
8	3.36	3.122667	0.164409	7.092313	0.458149
9	3.472	3.165333	0.156544	6.920583	0.383763
10	3.618933	3.301333	0.1634	7.070503	0.393614
11	3.784	3.4184	0.194063	7.705419	0.435712
12	3.994667	3.578667	0.193875	7.701689	0.408071
13	4.208	3.797333	0.226675	8.327735	0.480197
14	4.381333	3.965333	0.246773	8.689081	0.519412
15	4.645333	4.122667	0.245904	8.673773	0.461758
16	4.902133	4.352533	0.28711	9.37236	0.525757
17	5.154667	4.528	0.314228	9.804994	0.538874
18	5.466667	4.763467	0.364849	10.56528	0.590655
19	5.674933	4.906667	0.372949	10.68192	0.577635
20	5.917333	5.093333	0.401851	11.08811	0.600983
21	6.135733	5.26	0.433477	11.51617	0.628841
22	6.405333	5.429333	0.461558	11.88333	0.634252
23	6.632	5.565333	0.489803	12.24153	0.643825
24	6.872267	5.730667	0.516076	12.56556	0.655718
25	7.098667	5.917333	0.552022	12.99581	0.689495
26	7.394667	6.0888	0.576933	13.2858	0.685388
27	7.690667	6.272	0.602901	13.58151	0.687173
28	7.885333	6.410667	0.643355	14.02976	0.719224
29	8.133067	6.618667	0.675803	14.37921	0.745522
30	8.443733	6.752	0.701583	14.6509	0.732274
31	8.728	6.952	0.746099	15.10856	0.760038
32	9.021333	7.08	0.778875	15.43686	0.758889
33	9.36	7.290667	0.826068	15.89765	0.779581
34	9.650667	7.4248	0.863846	16.2571	0.786044

35	9.938667	7.605333	0.896646	16.56286	0.79688
36	10.26133	7.744	0.921956	16.795	0.78886
37	10.648	7.9568	0.985161	17.36115	0.815257
38	10.87467	7.981333	1.024981	17.70854	0.818045
39	11.3304	8.24	1.069075	18.08543	0.825584
40	11.81333	8.453333	1.119484	18.50691	0.829103
41	11.968	8.546667	1.128547	18.58167	0.82829
42	12.29333	8.696267	1.179684	18.99799	0.844407
43	12.63173	8.853867	1.221969	19.33548	0.853488
44	12.89333	8.981333	1.241058	19.48592	0.85183
45	13.17867	9.088	1.277215	19.76774	0.857289
46	13.33147	9.1664	1.259911	19.63337	0.838087
47	13.64267	9.328	1.315721	20.0635	0.859905
48	13.90667	9.392	1.358922	20.39023	0.868244
49	14.32533	9.595467	1.397098	20.67466	0.872093
50	14.6432	9.703733	1.422667	20.86299	0.869008
51	14.98933	9.888	1.47641	21.2534	0.887413
52	15.24533	9.9736	1.451546	21.07368	0.858251
53	15.55467	10.08453	1.477396	21.2605	0.857548
54	15.82427	10.19387	1.561451	21.85692	0.893345
55	16.16293	10.328	1.598524	22.11487	0.898383
56	16.40267	10.39467	1.602328	22.14117	0.887456
57	16.6152	10.5072	1.656	22.50894	0.909644
58	17.1328	10.67733	1.682884	22.69091	0.899188
59	17.60533	10.832	1.741205	23.08075	0.908258
60	18.17067	11.01947	1.806289	23.50815	0.916976
61	18.44267	11.12987	1.837187	23.70836	0.922299
62	19.01627	11.29333	1.896424	24.08755	0.926413
63	19.33067	11.39067	1.89356	24.06935	0.912282
64	19.98267	11.58293	2.050563	25.04733	0.960508
65	20.072	11.60773	1.951412	24.43427	0.910573
66	20.2376	11.63733	1.952868	24.44338	0.904018
67	20.544	11.73867	1.991303	24.68275	0.911013
68	20.7376	11.77867	2.012833	24.81583	0.912935
69	21.06133	11.8536	2.039528	24.97985	0.91246
70	21.44747	11.96453	2.097333	25.33137	0.924606
71	21.7528	12.01947	2.135322	25.55975	0.929165
72	22.05067	12.084	2.218273	26.05148	0.953895
73	22.28053	12.136	2.254548	26.26362	0.960957
74	22.55467	12.20027	2.278708	26.40397	0.961361
75	22.95733	12.29173	2.305638	26.55953	0.958427

76	23.29067	12.36	2.367388	26.91284	0.97209
77	23.4424	12.38213	2.369055	26.92232	0.967058
78	23.70693	12.44533	2.393614	27.0615	0.96831
79	23.86347	12.49787	2.417492	27.19615	0.973485
80	23.89413	12.4816	2.411786	27.16404	0.969188

Appendix C

Appendix C1

Simulation data and results, first mesh, residual criteria of continuity, x-velocity and y-velocity as 0.001,

P1	P2	Delta P	vol flow		Mass flow	Velocity		SQRT		Cd
			rate	rate [kg/s]		d [m]	[m/s]	Re	Re	
[bar]	[bar]	[Pa]	[m ³ /s]							
10	9.96	4000	5.45E-07	0.0004826	0.001	0.69388	7.5422	2.7463	0.23092	
10	9.93	7000	9.15E-07	0.00081039	0.001	1.16517	12.665	3.55878	0.29312	
10	9.9	10000	1.23E-06	0.0010931	0.001	1.57165	17.083	4.13318	0.33079	
10	9.8	20000	2.14E-06	0.0019	0.001	2.73181	29.694	5.44918	0.40657	
10	9.7	30000	2.92E-06	0.002586	0.001	3.71813	40.415	6.35724	0.45182	
10	9.6	40000	3.6E-06	0.0031876	0.001	4.58311	49.816	7.05808	0.48232	
10	9.5	50000	4.2E-06	0.0037175	0.001	5.345	58.098	7.62219	0.50311	
10	9.4	60000	4.74E-06	0.0042039	0.001	6.04434	65.699	8.10551	0.51937	
10	9.3	70000	5.26E-06	0.004656	0.001	6.69437	72.765	8.53023	0.53255	
10	9.2	80000	5.73E-06	0.0050777	0.001	7.30069	79.355	8.90816	0.54328	
10	9.1	90000	6.16E-06	0.005456	0.001	7.8446	85.267	9.23404	0.55037	
10	9	100000	6.57E-06	0.005824	0.001	8.37371	91.019	9.54037	0.55734	
10	8.9	110000	6.98E-06	0.006181	0.001	8.887	96.598	9.82842	0.56398	
10	8.8	120000	7.36E-06	0.006519	0.001	9.37298	101.88	10.0936	0.56949	
10	8.6	140000	8.14E-06	0.007216	0.001	10.3751	112.77	10.6195	0.58362	
10	8.4	160000	8.85E-06	0.0078385	0.001	11.2701	122.5	11.068	0.59302	

Appendix C2

Simulation data and results, refined mesh, residual criteria of continuity 0.0005, x-velocity and y-velocity as 0.0001,

P1	P2	Delta P	vol flow		d [m]	Velocity		SQRT	
			rate	Mass flow		[m/s]	Re	Re	Cd
[bar]	[bar]	[Pa]	[m ³ /s]	rate [kg/s]					
4.066	3.917	14900	1.6374E-06	0.0014507	0.001	2.086	22.672	4.761	0.3597
4.272	4.072	20000	2.0716E-06	0.0018354	0.001	2.639	28.684	5.356	0.3927
5.176	4.88	29600	2.7959E-06	0.0024772	0.001	3.562	38.714	6.222	0.4357
5.87	5.45	42000	3.605E-06	0.003194	0.001	4.592	49.916	7.065	0.4716
6.9	6.3	60000	4.6184E-06	0.0040919	0.001	5.883	63.949	7.997	0.5055
8.5	7.5	100000	6.4602E-06	0.0057237	0.001	8.23	89.451	9.458	0.5477
10	8.5	150000	8.3475E-06	0.0073959	0.001	10.63	115.58	10.75	0.5779
11.25	9.25	200000	9.9722E-06	0.0088354	0.001	12.7	138.08	11.75	0.5979
12.6	10	260000	1.1704E-05	0.01037	0.001	14.91	162.06	12.73	0.6154
14.8	11.2	360000	1.4238E-05	0.012615	0.001	18.14	197.15	14.04	0.6363
18.4	13	540000	1.8121E-05	0.016055	0.001	23.08	250.91	15.84	0.6612
22	14.5	750000	2.1983E-05	0.019477	0.001	28	304.39	17.45	0.6806
24.7	15.3	940000	2.5078E-05	0.022219	0.001	31.95	347.24	18.63	0.6935
28	16	1200000	2.8896E-05	0.025602	0.001	36.81	400.11	20	0.7073
32	17	1500000	3.2868E-05	0.029121	0.001	41.87	455.11	21.33	0.7195

Appendix C3

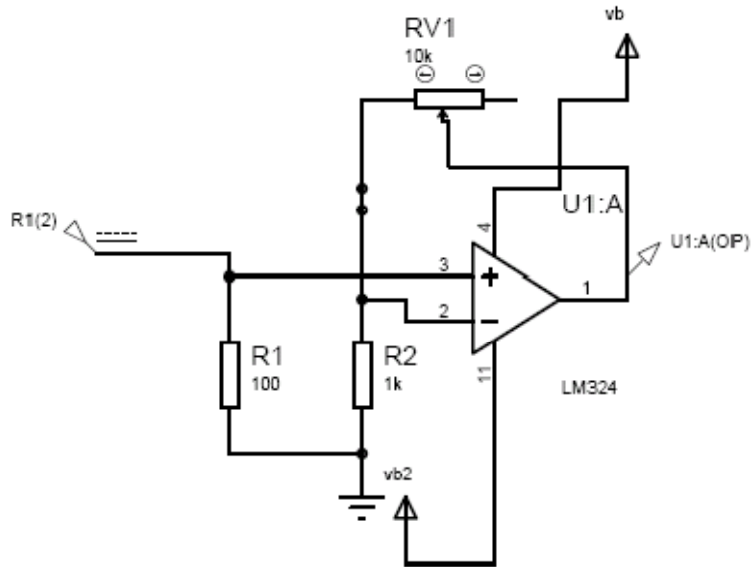
Simulation data and results, modified cross section, SIMPLEC code, second order pressure discretization second order momentum discretization, residual criteria of continuity 0.0001, x-velocity and y-velocity as 0.00001,

P1 [bar]	P2 [bar]	Delta P [Pa]	vol flow rate [m ³ /s]	Mass flow rate [kg/s]	d [m]	Velocity [m/s]	Re	SQRT Re	Cd
4.07	3.917	14900	1.4334E-06	0.00127	0.001	1.83	19.8	4.46	0.315
4.27	4.072	20000	1.8352E-06	0.001626	0.001	2.34	25.4	5.04	0.348
5.18	4.88	29600	2.509E-06	0.002223	0.001	3.2	34.7	5.89	0.391
5.87	5.45	42000	3.2822E-06	0.002908	0.001	4.18	45.4	6.74	0.429
6.9	6.3	60000	4.2991E-06	0.003809	0.001	5.48	59.5	7.72	0.471
8.5	7.5	100000	6.3093E-06	0.00559	0.001	8.04	87.4	9.35	0.535
10	8.5	150000	8.5124E-06	0.007542	0.001	10.8	118	10.9	0.589
11.3	9.25	200000	1.0471E-05	0.009277	0.001	13.3	145	12	0.628
12.6	10	260000	1.2585E-05	0.01115	0.001	16	174	13.2	0.662
14.8	11.2	360000	1.5688E-05	0.0139	0.001	20	217	14.7	0.701
18.4	13	540000	2.0474E-05	0.01814	0.001	26.1	283	16.8	0.747
22	14.5	750000	2.526E-05	0.02238	0.001	32.2	350	18.7	0.782
24.7	15.3	940000	2.9074E-05	0.02576	0.001	37	403	20.1	0.804
28	16	1200000	3.3781E-05	0.02993	0.001	43	468	21.6	0.827
32	17	1500000	3.8668E-05	0.03426	0.001	49.3	535	23.1	0.847

Appendix D

Appendix D1

Experimental setup electronic circuit for flow meter, signal conditioner (operational amplifier and simple filter), current to voltage convertor



Appendix D2

Experimental setup electronic circuit for flow meter, readings of current to voltage convertor.

Due to unnecessary full range, we chosen to calibrate the lower half range, the reason is that the flow meter full range is 7lit/min. represented by 20mA, but the hydraulic source range 3lit/min. max, so linearization for smaller range for a good number of reading is better, (in our opinion).

mA	Volt
5.00E-05	0.0071
0.159	0.0865
0.274	0.1434
0.29	0.1513
0.3	0.1557
0.3033	0.1583
0.43	0.2209
0.585	0.297
0.67	0.3397
0.68	0.3451
0.7	0.3551
0.8	0.403
0.853	0.431
0.95	0.479
1	0.502
1.1	0.553
1.32	0.662
1.439	0.722
1.5	0.752
1.533	0.769
1.55	0.777
1.606	0.805
1.757	0.881
1.929	0.966
2.05	1.025
2.1	1.05
2.11	1.055
2.4	1.199
2.606	1.303
2.8	1.392
2.908	1.453
3	1.498
3.005	1.501

3.126	1.562
3.25	1.622
3.325	1.661
3.405	1.669
3.42	1.706
3.985	1.984
4.012	2.002
4.673	2.33
4.83	2.403
4.976	2.482
5	2.487
5.03	2.509
5.06	2.523
5.265	2.626
5.57	2.778
5.59	2.784
5.83	2.903
5.844	2.914
5.88	2.926
6.2	3.089
6.288	3.134
6.3	3.139
6.59	3.283
6.9	3.437
7	3.484
7.431	3.701
8.15	4.06
8.2	4.08
8.3	4.13
8.404	4.18
8.555	4.26
9.07	4.51
9.08	4.52
9.862	4.91
9.94	4.94
10.1	5.02

Appendix D3

Experimental setup electronic circuit for flow meter, fitting of readings of current to voltage convertor.

fittedmodel1 =

Linear model Poly1:

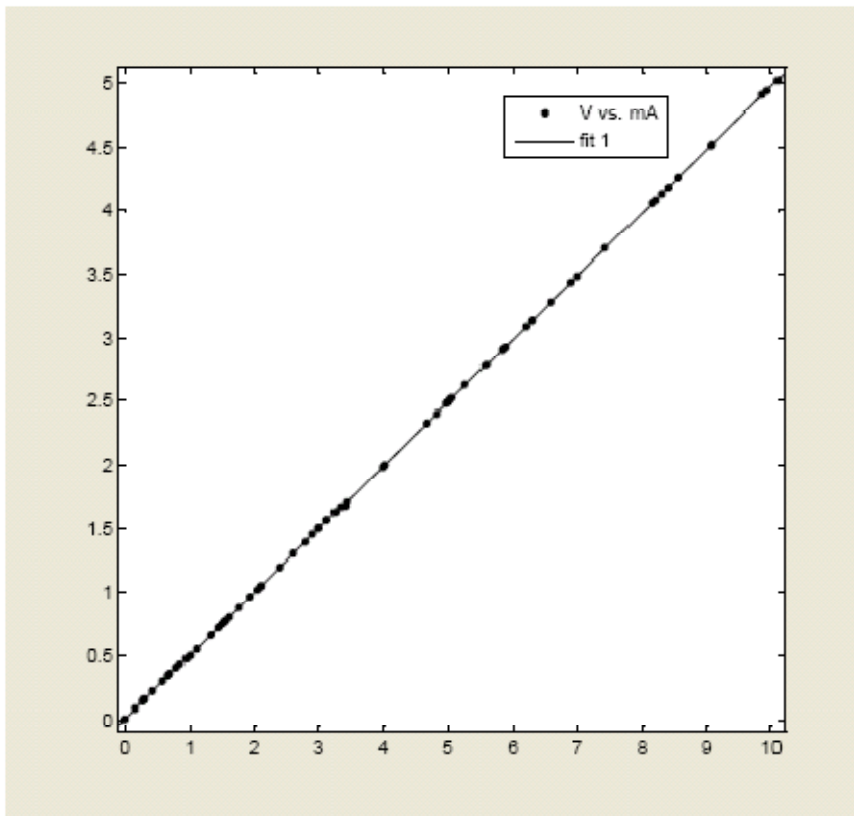
$$\text{fittedmodel1}(x) = p1*x + p2$$

Coefficients (with 95% confidence bounds):

$$p1 = 0.4969 \text{ (0.4965, 0.4972)}$$

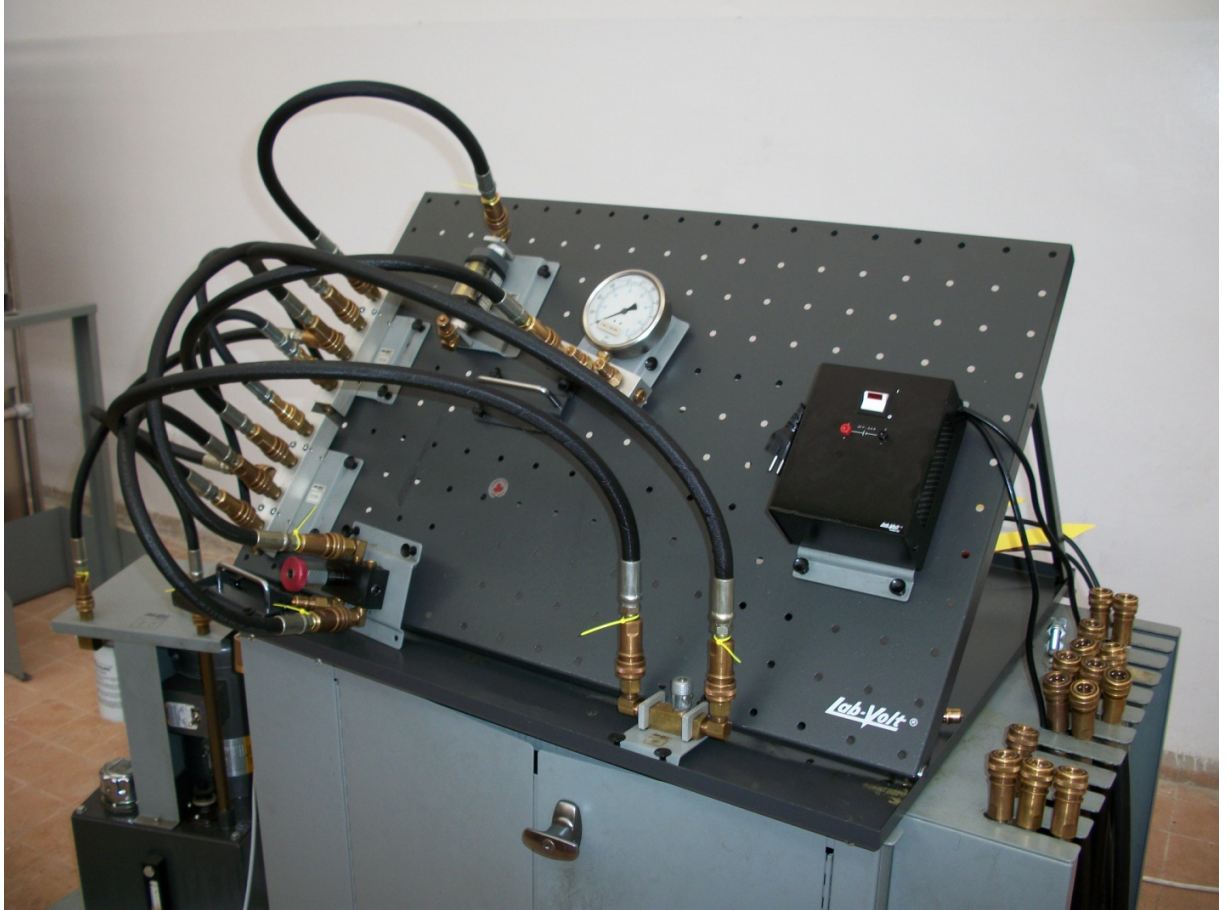
$$p2 = 0.006586 \text{ (0.004901, 0.008271)}$$

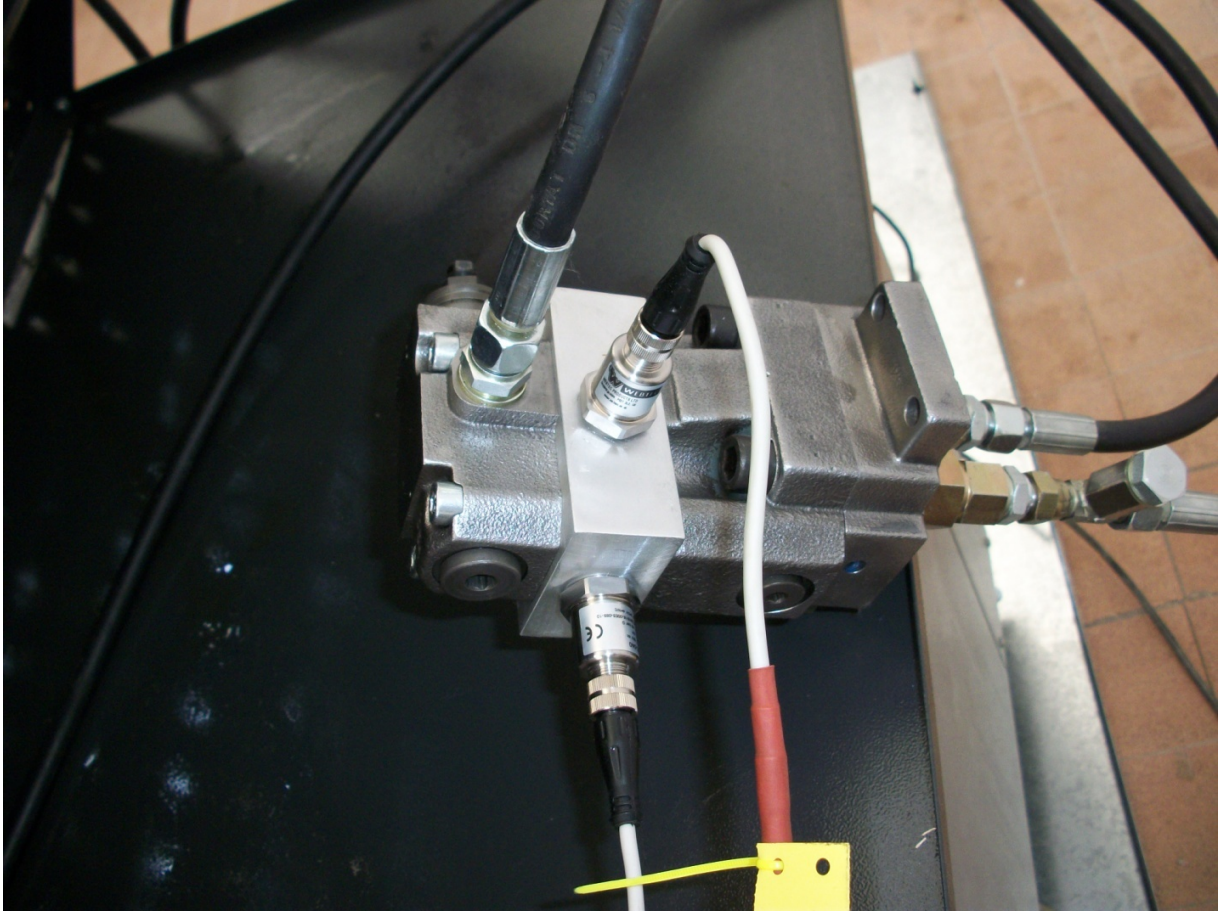
RMSE= 0.00419

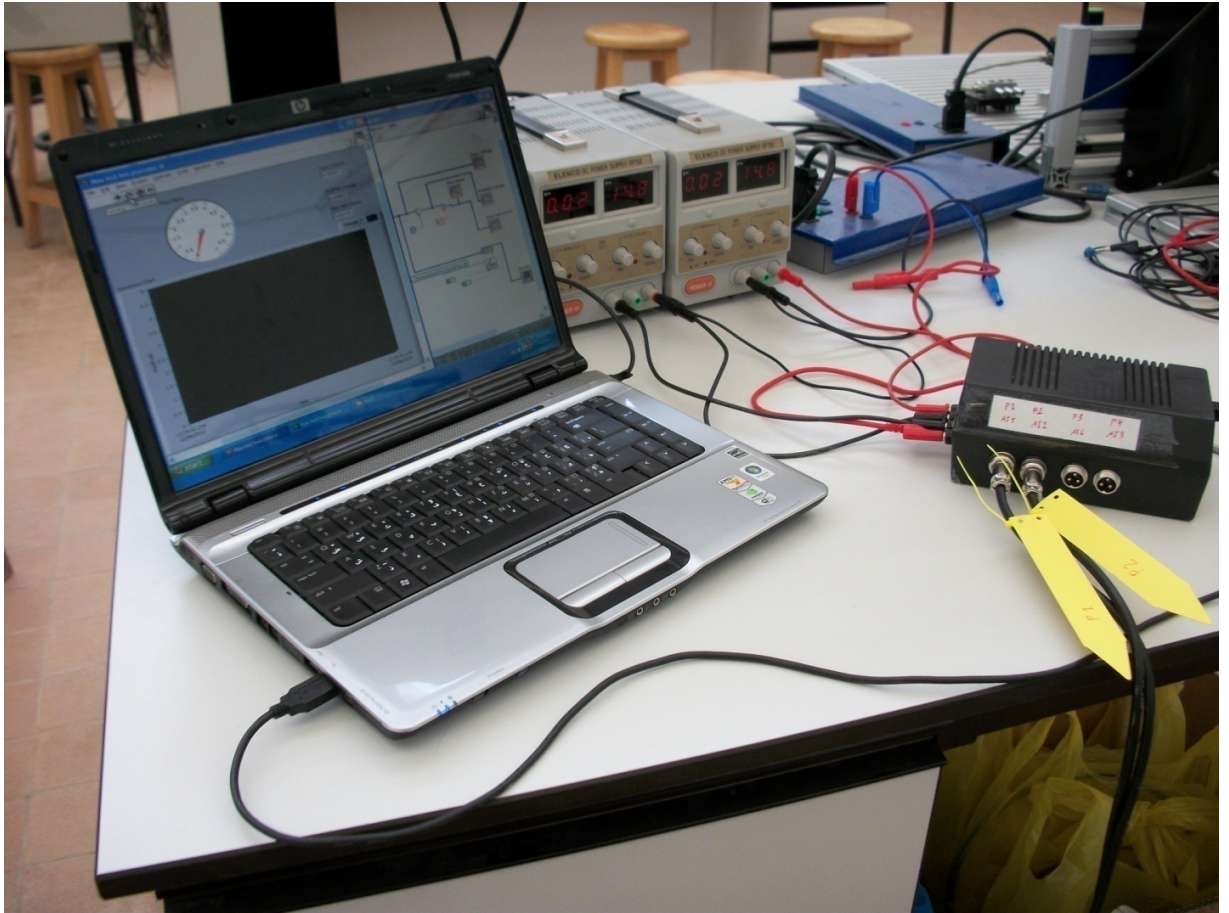


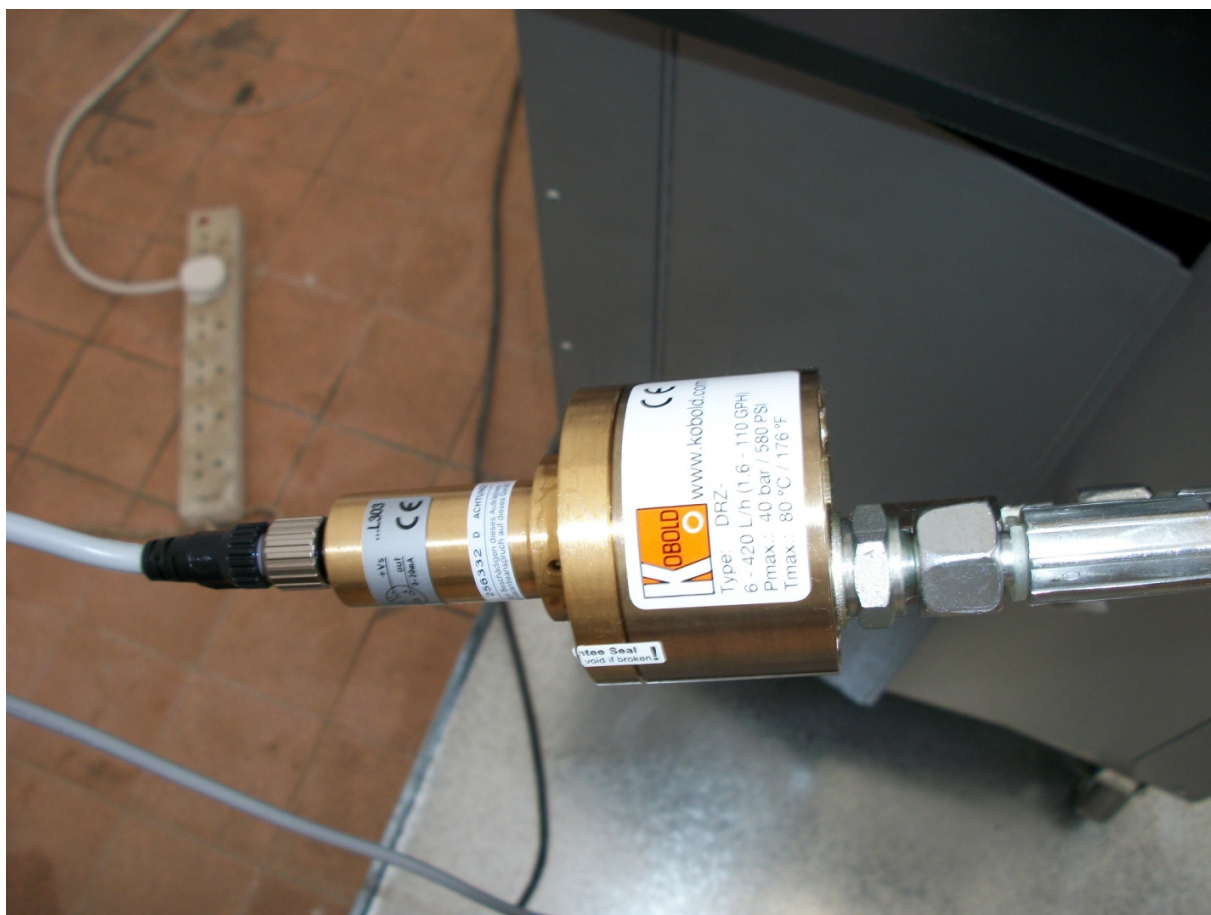
Appendix E

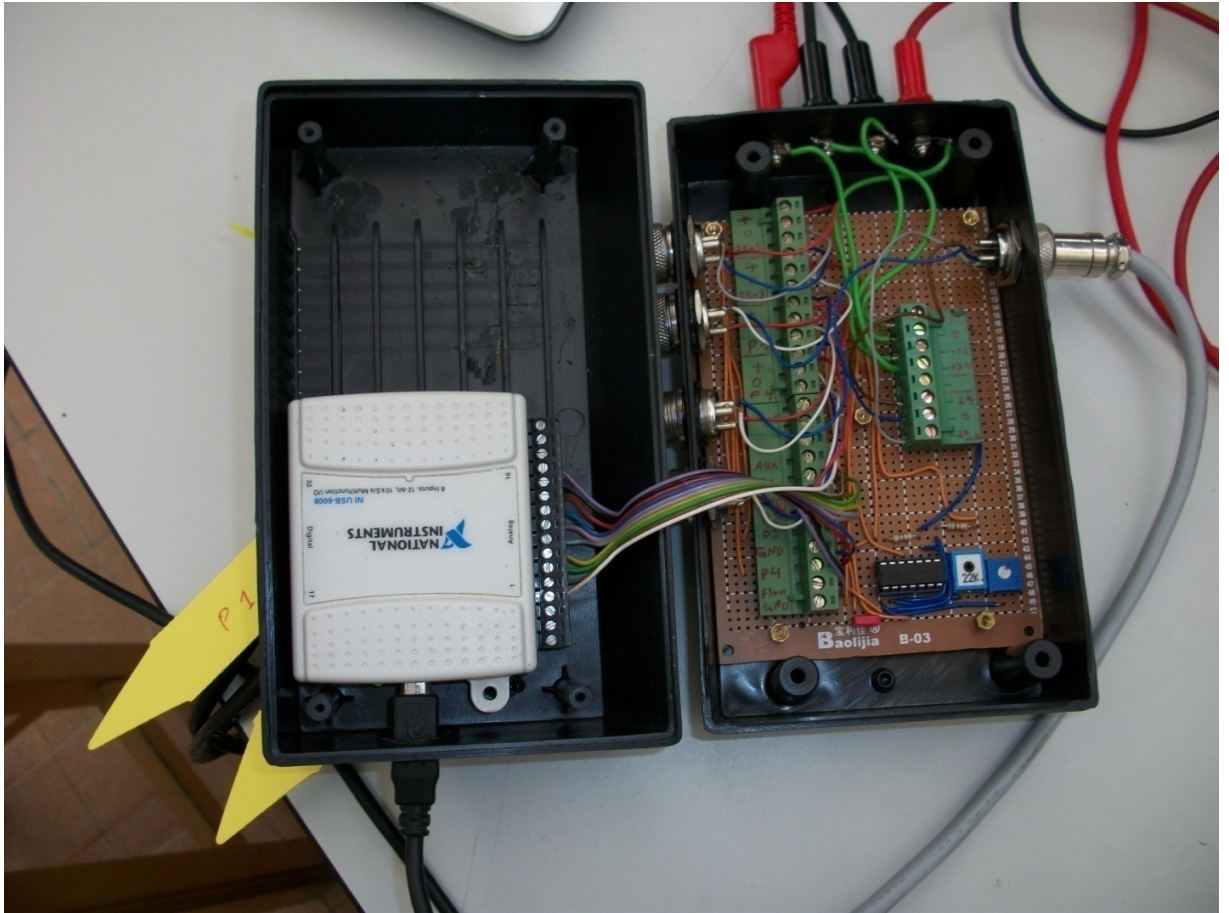
Experimental setup photos











Appendix F

Hydraulic oil specification

Shell Tellus oil, Grade 68

Shell Tellus Oils High performance hydraulic oil



Shell Tellus Oils are premium quality, solvent refined, high viscosity index mineral oil based fluids generally acknowledged to be the 'standard-setter' in the field of industrial hydraulic and fluid power lubrication.

Applications

- Industrial hydraulic systems
- Mobile hydraulic fluid power transmission systems
- Marine hydraulic systems

Performance Features and Benefits

- **Thermal stability**
Thermally stable in modern hydraulic systems working in extreme conditions of load and temperature. Tellus Oils are highly resistant to degradation and sludge formation therefore improving system reliability and cleanliness.
- **Oxidation resistant**
Resist oxidation in the presence of air, water and copper. Turbine Oil Stability Test (TOST) results show outstanding performance for Tellus Oils; low acidity, low sludge formation, low copper loss; therefore extending oil drain interval life and minimising maintenance costs.
- **Hydrolytic stability**
Tellus Oils have good chemical stability in the presence of moisture, which ensures long oil life and reduces the risk of corrosion and rusting.
- **Outstanding anti-wear performance**
Proven anti-wear additives are incorporated to be effective throughout the range of operating conditions, including low and severe duty high load conditions. Outstanding performance in a range of piston and vane pump tests; including the tough Denison T6C (dry and wet versions) and the demanding Vickers 35VQ25. Tellus Oils help system components last longer.
- **Superior filterability**
Tellus Oils are suitable for ultra-fine filtration, an essential requirement in today's hydraulic systems. Unaffected by the usual products of contamination, such as water and calcium, which are known to cause blockage of fine filters. Customers can use finer filters, therefore achieving all the benefits of having in use cleaner fluids.

• Low friction

Tellus Oils possess high lubrication properties and excellent low friction characteristics in hydraulic systems operating at low or high speed. Prevents stick-slip problems in critical applications enabling very fine control of machinery.

• Excellent air release and anti-foam properties

Careful use of additives to ensure quick air release without excessive foaming. Quick air release helps minimise cavitation and slow oxidation, maintaining system and fluid performance.

• Good water separation

Good water separation properties (demulsibility). Resists the formation of water-in-oil emulsions and prevents consequent hydraulic system and pump damage.

• All round versatility

Tellus Oils are suitable for a wide range of other industrial applications.

Specifications and Approvals

Tellus Oils have the following approvals:

CINCINNATI P-68 (ISO 32)
CINCINNATI P-70 (ISO 46)
CINCINNATI P-69 (ISO 68)
DENISON HF-0
DENISON HF-1
DENISON HF-2
Eaton (Vickers) M-2950 S
Eaton (Vickers) I-286 S

Tellus Oils meet the requirements of:

ISO 11158 HM
GMLS/2
AFNOR NF-E 48-603
Bosch Rexroth Ref 17421-001 and RD 220-1/04.03
Swedish Standard SS 15 54 34 AM

Compatibility

Tellus Oils are compatible with most pumps. However, please consult your Shell

SIPC

Tellus Page 1 of 3

03/08/2006

Representative before using in pumps containing silver plated components

Guidance on Health and Safety are available on the appropriate Material Safety Data Sheet which can be obtained from your Shell representative.

Seal & Paint Compatibility

Tellus Oils are compatible with all seal materials and paints normally specified for use with mineral oils.

Health & Safety

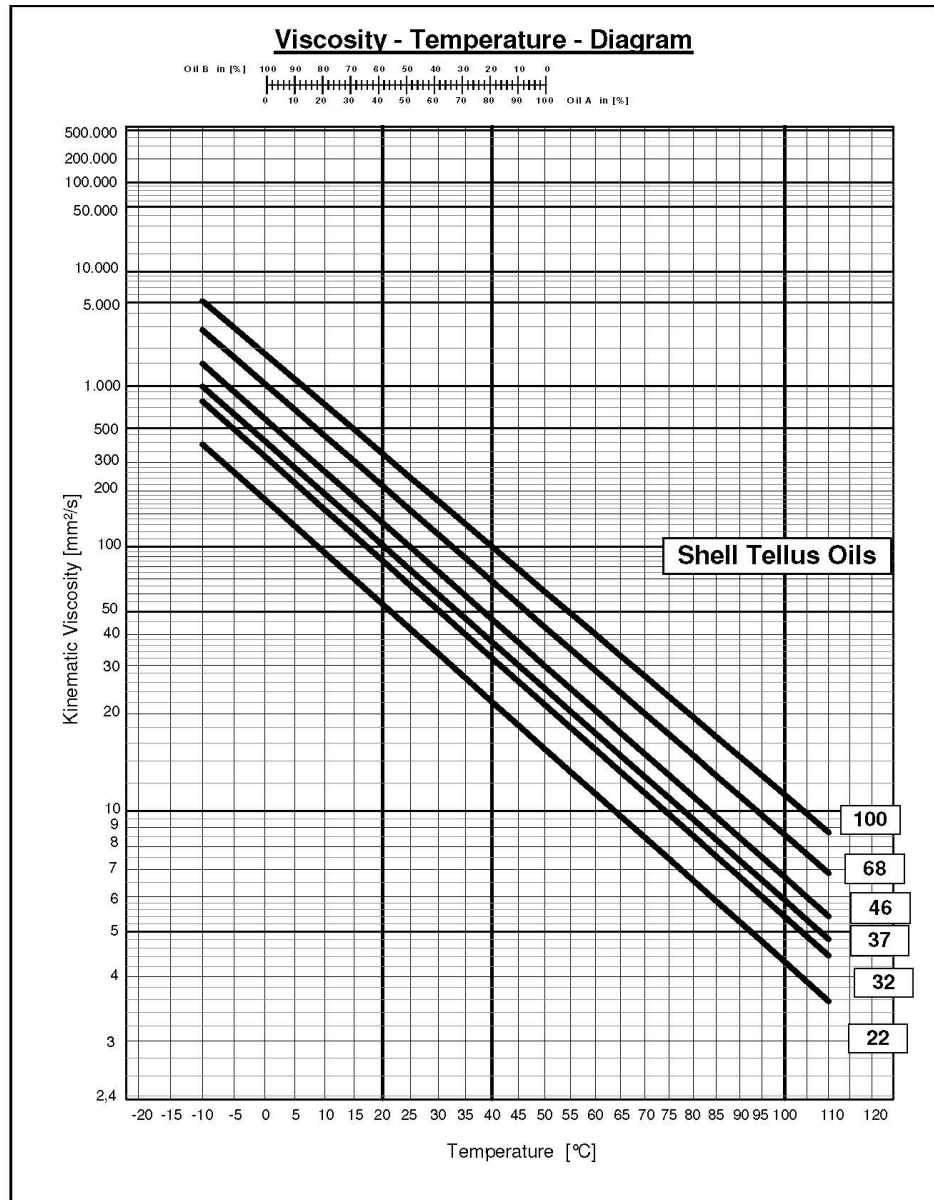
Protect the environment

Take used oil to an authorised collection point. Do not discharge into drains, soil or water.

Typical Physical Characteristics

Shell Tellus Oil	22	32	37	46	68	100
ISO Oil Type	HM	HM	HM	HM	HM	HM
Kinematic Viscosity						
@ 0°C cSt	180	338	440	580	1040	1790
40°C cSt	22	32	37	46	68	100
100°C cSt (IP 71)	4.3	5.4	5.9	6.7	8.6	11.1
Viscosity Index (IP 226)	100	99	99	98	97	96
Density @ 15°C/kg/l (IP 365)	0.866	0.875	0.875	0.879	0.886	0.891
Flash Point °C (Pensky-Martens Closed Cup) (IP 34)	204	209	212	218	223	234
Pour Point °C (IP 15)	-30	-30	-30	-30	-24	-24

These characteristics are typical of current production. Whilst future production will conform to Shell's specification, variations in these characteristics may occur.

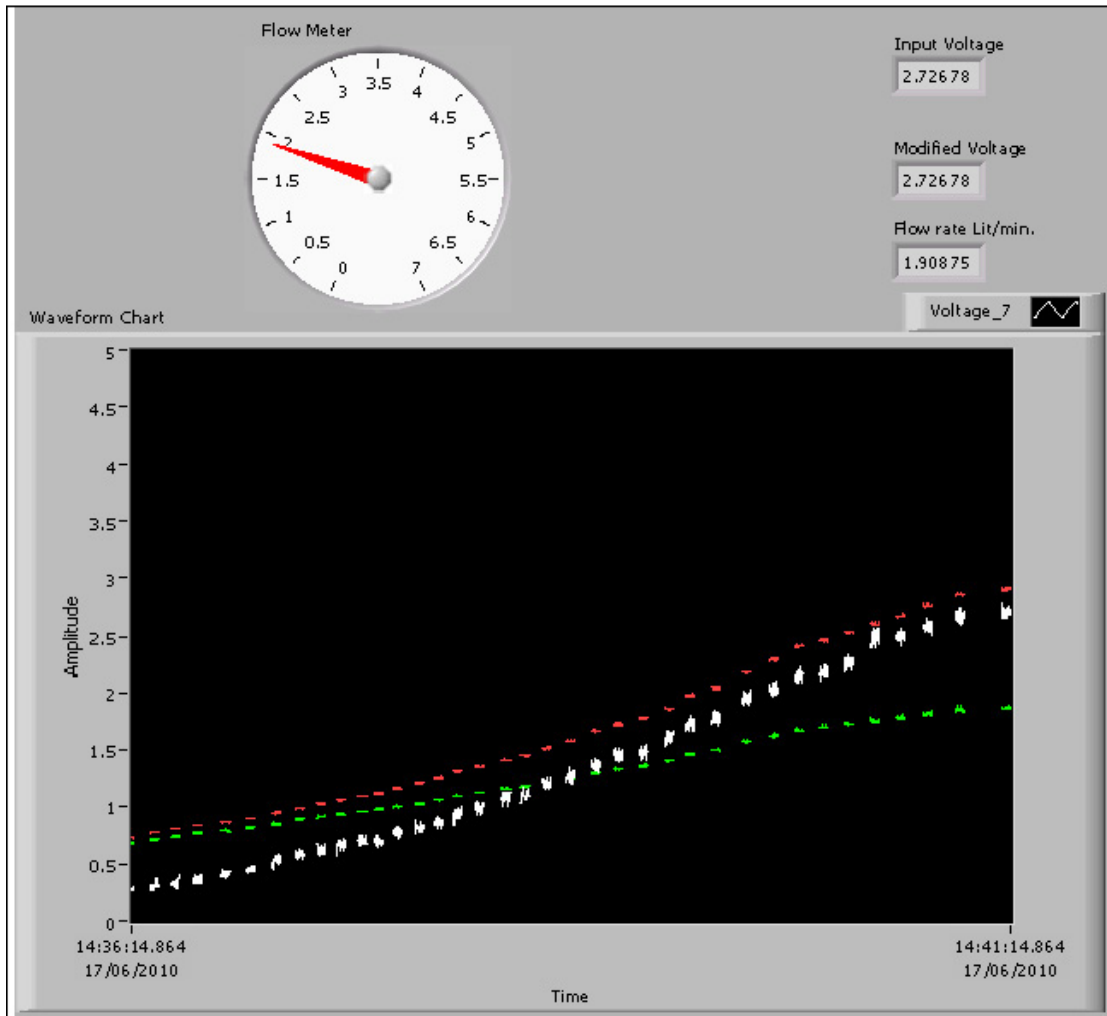


Appendix G

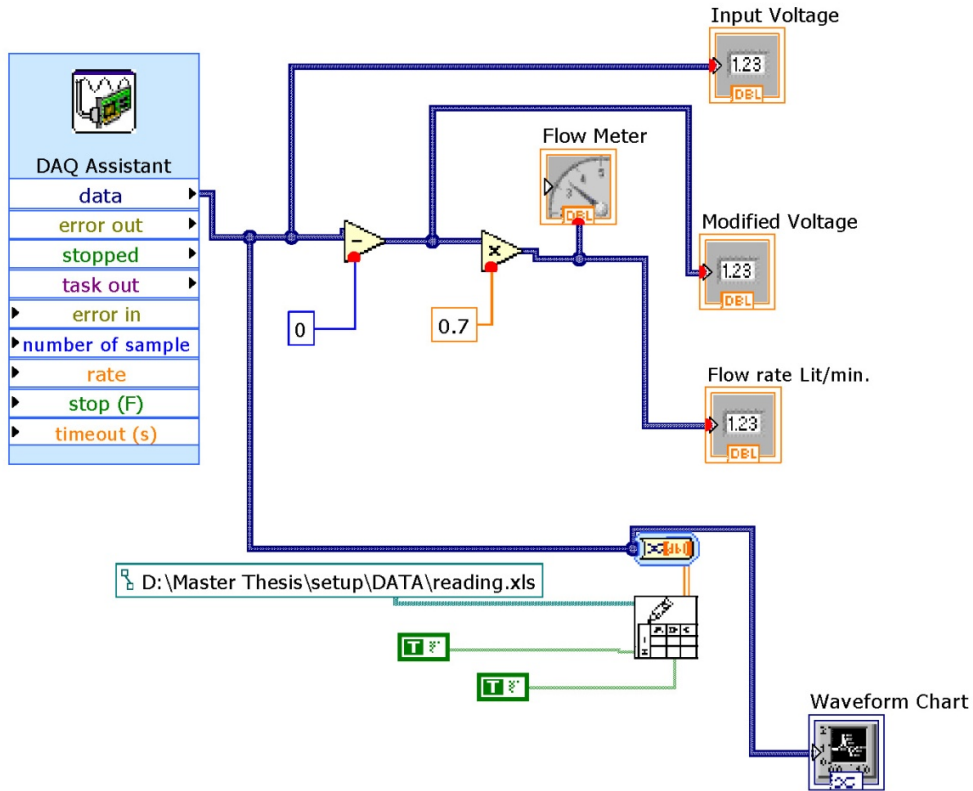
LabVIEW front panel and control panel

flow test two pressure.vi
D:\Master Thesis\setup\DATA\flow test two pressure.vi
Last modified on 6/9/2010 at 2:39 PM
Printed on 6/17/2010 at 2:41 PM

flow test two pressure.vi



flow test two pressure.vi
 D:\Master Thesis\setup\DATA\flow test two pressure.vi
 Last modified on 6/9/2010 at 2:39 PM
 Printed on 6/17/2010 at 2:41 PM



Convert from Dynamic Data

Convert from Dynamic Data

Converts the dynamic data type to numeric, Boolean, waveform, and array data types for use with other VIs and functions.



DAQ Assistant

DAQ Assistant

Creates, edits, and runs tasks using NI-DAQmx. Refer to the DAQ Quick Start Guide for information on devices supported by NI-DAQmx.

When you place this Express VI on the block diagram, the DAQ Assistant launches to create a new task. After you create a task, you can double-click the DAQ Assistant Express VI in order to edit that task. For continuous measurement or generation, place a loop around the DAQ Assistant Express VI.

For continuous single-point input or output, the DAQ Assistant Express VI might not provide satisfactory performance. Refer to examples\DAQmx\Analog In\Measure Voltage.llb\Cont Acq&Graph Voltage-Single Point Optimization.vi for techniques to create higher-performance, single-point I/O applications.

Appendix H

Measurement devices and instruments

Appendix H1

Pressure Transducers

MPT Series Pressure Transducers

Up to
600 bar, 10000 psi

The MPT pressure sensors are designed for continuous monitoring of oil, gas, water, hydraulic and other pressure media in mobile equipment, industrial hydraulics, compressors and process control equipment.

Economical price and rugged design allows the MPT transducers to be designed into O.E.M. machinery to give control and condition monitoring information. The compact construction makes it ideal for installing where space is at a premium.

Combined with one of the wide range of Webtec digital readouts both continuous and peak pressures can be measured.

The MPT series utilises thin film techniques along with fully automated production methods to produce a standard of performance previously only associated with high price pressure transducers.



Manufacturers of hydraulic components and test equipment
for the Mobile, Industrial and Agricultural industries



WEBTEC
WEBTEC PRODUCTS LIMITED

Nuffield Road,
St. Ives, Cambs.,
PE27 3LZ, UK
Tel: +44(0)1480 397400
Fax: +44(0)1480 466555
www.webtec.co.uk
E-mail: sales@webtec.co.uk

Features:

- **ACCURATE**
± 0.25% Full Scale)
- **ECONOMICALLY**
priced
- **RUGGED** design
- **OUTPUT OPTIONS:**
4 - 20mA or 0 - 5V
- **STAINLESS**
Steel wetted parts
- **CONNECTOR:**
Male 4 pin M12 x1.0
- **TWO** thread forms
available





Certificate No.8242

MPT-BU-ENG-1918.pdf 11/09
(Version 4)

Specification

Model number	Outputs available	Pressure range (Gauge)	Pressure Connection
MPT016BB**	5V, mA	16 Bar	1/4" BSPP
MPT040BB**	5V, mA	40 Bar	1/4" BSPP
MPT100BB**	5V, mA	100 Bar	1/4" BSPP
MPT250BB**	5V, mA	250 Bar	1/4" BSPP
MPT400BB**	5V, mA	400 Bar	1/4" BSPP
MPT600BB**	5V, mA	600 Bar	1/4" BSPP
MPT200PU**	5V, mA	200 psi	7/16" -20UN #4 SAE ORB Male
MPT600PU**	5V, mA	600 psi	7/16" -20UN #4 SAE ORB Male
MPT1K5PU**	5V, mA	1500 psi	7/16" -20UN #4 SAE ORB Male
MPT4K0PU**	5V, mA	4000 psi	7/16" -20UN #4 SAE ORB Male
MPT6K0PU**	5V, mA	6000 psi	7/16" -20UN #4 SAE ORB Male
MPT7K5PU**	5V, mA	7500 psi	7/16" -20UN #4 SAE ORB Male
MPT10K0PU**	5V, mA	10000 psi	7/16" -20UN #4 SAE ORB Male

Replace ** with mA or 5V to give complete model number

Functional specification

Operating temperature: Ambient - 5 to 40°C (41 to 104°F)
Fluid temperature: -20 to 100°C (-4 to 212°F) Compensated range
Temperature effects: ±2% Full scale typical
Accuracy: ± 0.25% Full scale
Proof pressure: Minimum 2 times full scale
Weight: 53g (0.1 lbs)

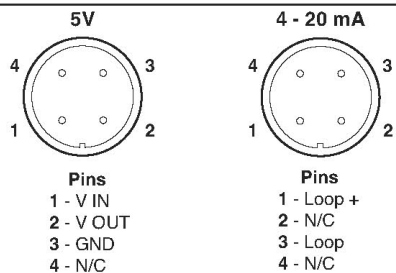
Electrical specification

Supply voltage (VS): 10 - 30 VDC all models
Current output: 4- 20 mA, 2 wire loop, max loop resistance = (VS-7.5) x 50 ohms
Voltage output: 0 - 5 VDC, current consumption = 8mA
Connection type: M12 x 1 4 pin

Construction material

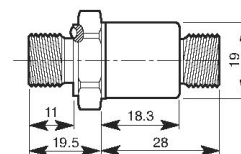
Body: 17-4PH stainless steel (wetted parts)

Connection Details



Connecting cable (5m) FT9879-05
Extension cable (5m) FT10229-5
Connector (M12x1 4 pin) FT9880

Dimensions



Accessories

For Panel meters (readouts) see DP 130 bulletin
 For temperature transducers TP bulletin
 For flow meters see CT, CTR or flowhub bulletin

Calibration is included when complete systems (sensors, cable panel meter) is purchased in one order.

For help and advice, please contact Webtec sales office.



APPROVED

Webtec Products Limited reserve the right to make improvements and changes to the specification without notice

Appendix H2

Positive displacement piston type flow meter

DRZ-1110 G1 L303

DRZ SERIES PISTON TYPE POSITIVE DISPLACEMENT FLOWMETER



Flow
Pressure
Level
Temperature
measurement
monitoring
control



- Flow Range 1.6 to 110 GPH
- Accurate Measurements for Lubricating Media
- Economical Brass Construction
- Accuracy $\pm 1\%$ Reading

S4



USA
KOBOLD Instruments Inc.
1801 Parkway View Drive
USA- Pittsburgh, PA 15205
☎ +1 412-788-2830
Fax +1 412-788-4890
E-mail: info@koboldusa.com



CANADA
KOBOLD Instruments Canada Inc.
9A Aviation
Pointe-Claire, QC H9R 4Z2
☎ +1 514-428-8090
Fax +1 514-428-8899
E-mail: kobold@kobold.ca

Visit KOBOLD Online at
www.kobold.com

Model:
DRZ



DRZ - Piston Type Positive Displacement Flowmeter

Features

- Flow Range 1.6 to 110 GPH
- Accurate Measurements of Lubricating Media
- Economical Brass Construction
- Accuracy $\pm 1\%$ Reading

The KOBOLD DRZ series rotary piston positive displacement flowmeter combines economy with high performance. The DRZ series is designed to measure any clean liquid with lubricating properties and viscosity ranging from 5 to 100 centistoke. The unique design uses a single piston rotating on a camshaft to meter very precise volume of liquid with each rotation of the piston. Piston rotation is detected by a Hall effect sensor. The signal is processed by electronics into a blind pulse output (PNP or NPN based on model ordered) or a full featured controller with flowrate indication, analog output and switches.

An economical brass body is rugged and provides a pressure rating to 580 PSIG. The DRZ has a low pressure drop of 20 PSI maximum.

Use the DRZ with lubricating media such as:

- Lubricating oil
- Diesel fuel
- Glycol mixtures
- Waxes/pastes
- Paint
- Latex polymers
- Sugar solutions
- Detergents

Specifications

Area of Application:	Low and medium viscosity liquids which have some lubricating properties
Measuring Range:	1.6-110 GPH
Max. Throughput:	160 GPH
Accuracy:	$\pm 1.0\%$ of reading
Repeatability:	$\pm 0.2\%$ of reading
Viscosity Range:	5-100 cSt
Process Temp. Range:	-4°F to +176°F



Ambient Temp. Range:	-4°F to +140°F	Output Type F3X0 = PNP pulse with frequency divider
Max. Pressure:	580 PSIG	Power Requirement: 24 VDC $\pm 20\%$ @ 10 mA Max.
Max. Differential Pressure:	20 PSI	Output: PNP Open Collector
Wetted Materials:	Brass, aluminum, Acetal, Viton	Max. Output Load: 25 mA
Req. Filtration:	150 mesh or better	Elec. Protection: NEMA 4X/IP65
Electrical Specifications		Elec. Connection: Micro-DC, 4 pin male
Output Type 0000 = OEM NPN Pulse		Output Type L303, L343 = (0)4-20 mA
Power Requirement: 5-24 VDC		Power Requirement: 24 VDC $\pm 20\%$ @ 10 mA Max.
Output: @10 mA Max. NPN Open Collector		Output: 3-wire 0-20 mA or 4-20 mA depending on model code
Max. Output Load: 15 mA		Max. Output Load: 500 ohms
K-factor: 1633 pulses/gal.		Elec. Protection: NEMA 4X/IP65
Elec. Protection: NEMA 4X/IP65		Elec. Connection: Micro-DC, 4 pin male
Elec. Connection: DIN 43650 Plug		Output Type C30M, C30R, C34N, C34P compact electronics
Note: May be combined with AUF-4000 to provide LED display with 2-wire 4-20 mA output		Housing Material: 303 stainless steel
AUF-4000 pulse to 4-20 mA converter with display		Power Supply: 24 VDC $\pm 20\%$
Power Requirement: 14-30 VDC		Display: 3 digit LED
Input: Pulse		Output Types: Analog output +1 switch or 2 switches based on model code
Output: 4-20 mA, 2-wire		4-20 mA, 3-wire
Max. Output Load: 250 ohms		Rloop < 500 ohms
Elec. Protection: NEMA 4X/IP65		PNP or NPN open collector, 300 mA max.
Elec. Connection: DIN 43650 Plug		Switch:
Output Type F300 = PNP Pulse		Elec. Protection: NEMA 4X/IP65
Power Requirement: 24 VDC $\pm 20\%$ @ 10 mA Max.		Elec. Connection: Micro-DC, 5 pin male
Output: PNP Open Collector		
Max. Output Load: 25 mA		
K-factor: 1633 pulses/gal.		
Elec. Protection: NEMA 4X/IP65		
Elec. Connection: Micro-DC, 4 pin male		

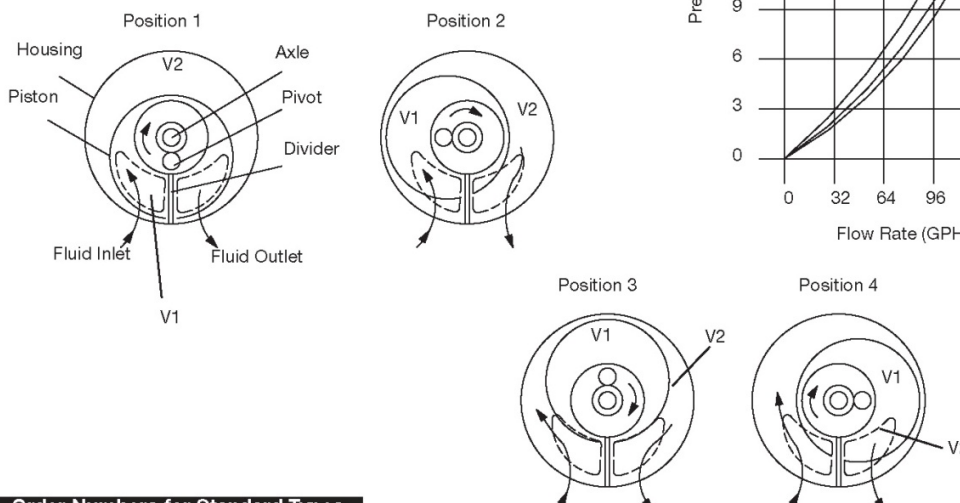
DRZ - Piston Type Positive Displacement Flowmeter



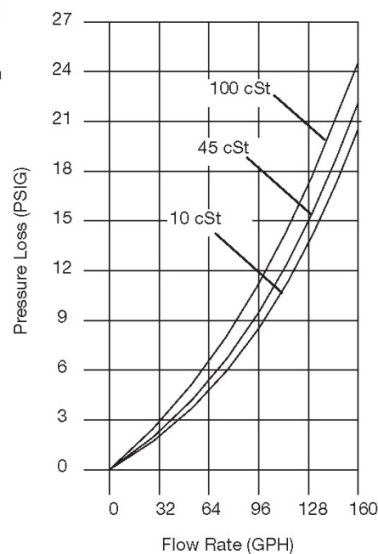
DRZ Principle of Operation

1. Liquid enters the meter through the inlet port. Liquid momentum causes the internal piston to rotate about its cammed axle.
 2. As the piston rotates, a known volume fills the meter cavity V2.
 3. The liquid volume is sealed inside the meter cavity by the piston and a partition which separates the inlet port from the outlet port.
 4. When the piston rotates past the outlet port, the known liquid volume V2 exits the meter. The piston rotation is detected by a Hall effect sensor and an output pulse is generated.
- Each pulse correlates to a precisely measured volume for liquid flow. Unlike other piston type meters, the DRZ piston rotates in an orbital fashion which minimizes flow pulsations.

Operating Principle



DRZ dp vs. Flowrate



S4

Order Numbers for Standard Types

Measuring Range	Fittings	Output Type
6-420 LPH = DRZ-1110...	...N1... = 1/8" NPT ...N2... = 1/4" NPT ...G1... = 1/8" BSP ...G2... = 1/4" BSP	...0000 = OEM NPN pulse ...F300 = PNP pulse ...F320 = PNP pulse, 1:2 Freq. divider ...F340 = PNP pulse, 1:4 Freq. divider ...F390 = PNP pulse, custom Freq. divider ...L303 = 0-20 mA, 3-wire micro-DC plug ...L343 = 4-20 mA, 3-wire, micro-DC plug ...C30M = LED display w/ 2 NPN switches, micro-DC plug ...C30P = LED display w/ 2 PNP switches, micro-DC plug ...C34N = LED display w/ 4-20 mA + 1 NPN switch micro-DC plug ...C34P = LED display w/ 4-20 mA + 1 PNP switch micro-DC plug

Accessories

- Part Number 807.037** = Mating 4-pin micro-DC plug with 6 feet of cable for output type F300, 320, 340, 390, L303 and L343
- Part Number 807.007** = Mating 5-pin micro-DC plug with 6 feet of cable for output type C30M, 30P, 34N and C34P
- Part Number AUF-4000** = Snap-on display, pulse input to 2-wire 4-20 mA for output type 0000

Example DRZ model number: DRZ-1120N2C34P

Subject to change without prior notice.

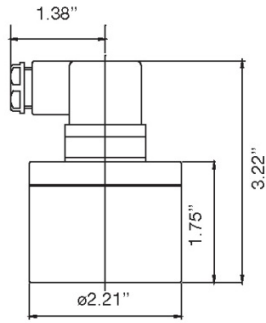
177



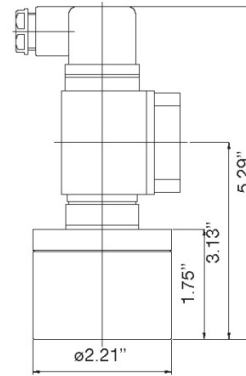


DRZ - Piston Type Positive Displacement Flowmeter

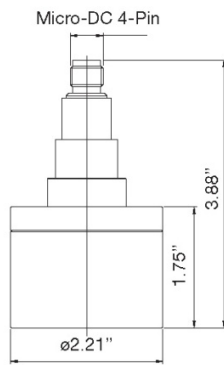
DRZ with Output Type 0000 (OEM Pulse)



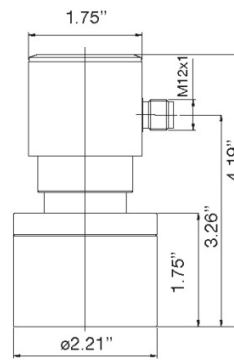
DRZ with Output Type 0000 and AUF-4000



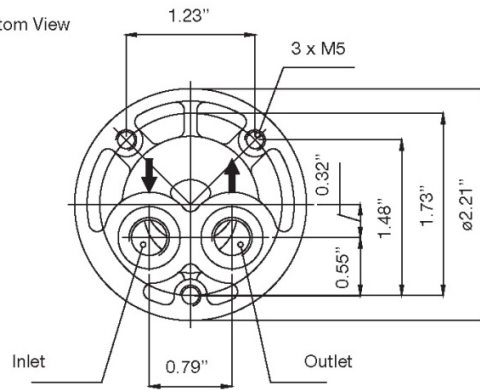
DRZ with Output Type F3xx or L3xx



DRZ with Output Type C3xx



DRZ Bottom View



Appendix H3

National Instrument Data acquisition Card

NI-6008USB

Low-Cost, Bus-Powered Multifunction DAQ for USB – 12- or 14-Bit, up to 48 kS/s, 8 Analog Inputs

NI USB-6008, NI USB-6009

- 8 analog inputs at 12 or 14 bits, up to 48 kS/s
- 2 analog outputs at 12 bits, software-timed
- 12 TTL/CMOS digital I/O lines
- 32-bit, 5 MHz counter
- Digital triggering
- Bus-powered
- 1-year warranty

Operating Systems

- Windows Vista (32- and 64-bit)/XP/2000
- Mac OS X¹
- Linux^{*1}
- Windows Mobile¹
- Windows CE¹

Recommended Software

- LabVIEW
- LabVIEW SignalExpress
- LabWindows/CVI
- Measurement Studio

Other Compatible Software

- C#, Visual Basic .NET
- ANSI C/C++

Measurement Services Software (included)

- NI-DAQmx driver software
- Measurement & Automation Explorer configuration utility
- LabVIEW SignalExpress LE

¹You need to download NI-DAQmx Base for these operating systems.



Product	Bus	Analog Inputs ¹	Input Resolution (bits)	Max Sampling Rate (kS/s)	Input Range (V)	Analog Outputs	Output Resolution (bits)	Output Rate (Hz)	Output Range (V)	Digital I/O Lines	32-Bit Counter	Trigger
USB-6009	USB	8 SE/4 DI	14	48	±1 to ±20	2	12	150	0 to 5	12	1	Digital
USB-6008	USB	8 SE/4 DI	12	10	±1 to ±20	2	12	150	0 to 5	12	1	Digital

¹SE = single ended, DI = differential. *Software-based

Overview and Applications

With recent bandwidth improvements and new innovations from National Instruments, USB has evolved into a core bus of choice for measurement applications. The NI USB-6008 and USB-6009 are low-cost entry points to NI flagship data acquisition (DAQ) devices. With plug-and-play USB connectivity, these modules are simple enough for quick measurements but versatile enough for more complex measurement applications.

The USB-6008 and USB-6009 are ideal for a number of applications where low cost, small form factor, and simplicity are essential.

Examples include:

- Data logging – quick and easy environmental or voltage data logging
- Academic lab use – student ownership of DAQ hardware for completely interactive lab-based courses (Academic pricing available. Visit ni.com/academic for details.)
- OEM applications as I/O for embedded systems

Recommended Software

National Instruments measurement services software, built around NI-DAQmx driver software, includes intuitive application programming interfaces, configuration tools, I/O assistants, and other tools designed to reduce system setup, configuration, and development time. National Instruments recommends using the latest version of NI-DAQmx

driver software for application development in NI LabVIEW, LabVIEW SignalExpress, LabWindows/CVI, and Measurement Studio software.

To obtain the latest version of NI-DAQmx, visit

ni.com/support/daq/versions.

NI measurement services software speeds up your development with features including:

- A guide to create fast and accurate measurements with no programming using the DAQ Assistant.
- Automatic code generation to create your application in LabVIEW.
- LabWindows/CVI, LabVIEW SignalExpress, and C#, Visual Studio .NET, ANSI C/C++, or Visual Basic using Measurement Studio.
- Multithreaded streaming technology for 1,000 times performance improvements.
- Automatic timing, triggering, and synchronization routing to make advanced applications easy.
- More than 3,000 free software downloads available at ni.com/zone to jump-start your project.
- Software configuration of all digital I/O features without hardware switches/jumpers.
- Single programming interface for analog input, analog output, digital I/O, and counters on hundreds of multifunction DAQ hardware devices. M Series devices are compatible with the following versions (or later) of NI application software – LabVIEW, LabWindows/CVI, or Measurement Studio versions 7.x, and LabVIEW SignalExpress 2.x.



Low-Cost, Bus-Powered Multifunction DAQ for USB – 12- or 14-Bit, up to 48 kS/s, 8 Analog Inputs

Every M Series data acquisition device also includes a copy of LabVIEW SignalExpress LE data-logging software, so you can quickly acquire, analyze, and present data without programming. The NI-DAQmx Base driver software is provided for use with Linux, Mac OS X, Windows Mobile, and Windows CE operating systems.

Recommended Accessories

The USB-6008 and USB-6009 have removable screw terminals for easy signal connectivity. For extra flexibility when handling multiple wiring configurations, NI offers the USB-600x Connectivity Kit, which includes two extra sets of screw terminals, extra labels, and a screwdriver.

In addition, the USB-600x Prototyping Kit provides space for adding more circuitry to the inputs of the USB-6008 or USB-6009.

NI USB DAQ for OEMs

Shorten your time to market by integrating world-class National Instruments OEM measurement products into your embedded system design. Board-only versions of NI USB DAQ devices are available for OEM applications, with competitive quantity pricing and available software customization. The NI OEM Elite Program offers free 30-day trial kits for qualified customers. Visit ni.com/oem for more information.

Information for Student Ownership

To supplement simulation, measurement, and automation theory courses with practical experiments, NI has developed the USB-6008 and USB-6009 student kits, which include the LabVIEW Student Edition and a ready-to-run data logger application. These kits are exclusively for students, giving them a powerful, low-cost, hands-on learning tool. Visit ni.com/academic for more details.

Information for OEM Customers

For information on special configurations and pricing, call (800) 813 3693 (U.S. only) or visit ni.com/oem. Go to the Ordering Information section for part numbers.

Ordering Information

NI USB-6008 ¹	779051-01
NI USB-6009 ¹	779026-01
NI USB-6008 OEM	193132-02
NI USB-6009 OEM	193132-01
NI USB-6008 Student Kit ^{1,2}	779320-22
NI USB-6009 Student Kit ^{1,2}	779321-22
NI USB-600x Connectivity Kit	779371-01
NI USB-600x Prototyping Kit	779511-01

¹ Includes NI-DAQmx software, LabVIEW SignalExpress LE, and a USB cable.

² Includes LabVIEW Student Edition.

BUY NOW!

For complete product specifications, pricing, and accessory information, call 800 813 3693 (U.S. only) or go to ni.com/usb.

BUY ONLINE at ni.com or CALL 800 813 3693 (U.S.)

Low-Cost, Bus-Powered Multifunction DAQ for USB – 12- or 14-Bit, up to 48 kS/s, 8 Analog Inputs

Specifications

Typical at 25 °C unless otherwise noted.

Analog Input

Absolute accuracy, single-ended

Range	Typical at 25 °C (mV)	Maximum (0 to 55 °C) (mV)
±10	14.7	138

Absolute accuracy at full scale, differential¹

Range	Typical at 25 °C (mV)	Maximum (0 to 55 °C) (mV)
±20	14.7	138
±10	7.73	84.8
±5	4.28	58.4
±4	3.59	53.1
±2.5	2.96	45.1
±2	2.21	42.5
±1.25	1.70	38.9
±1	1.53	37.5

Number of channels..... 8 single-ended/4 differential
Type of ADC Successive approximation

ADC resolution (bits)

Module	Differential	Single-Ended
USB-6008	12	11
USB-6009	14	13

Maximum sampling rate (system dependent)

Module	Maximum Sampling Rate (kS/s)
USB-6008	10
USB-6009	48

Input range, single-ended..... ±10 V
Input range, differential..... ±20, ±10, ±5, ±4, ±2.5, ±2, ±1.25, ±1 V
Maximum working voltage..... ±10 V
Overvoltage protection ±35 V
FIFO buffer size 512 B
Timing resolution 41.67 ns (24 MHz timebase)
Timing accuracy 100 ppm of actual sample rate
Input impedance 144 kΩ
Trigger source..... Software or external digital trigger
System noise..... 5 m V_{rms} (±10 V range)

Analog Output

Absolute accuracy (no load) 7 mV typical, 36.4 mV maximum at full scale
Number of channels..... 2
Type of DAC Successive approximation
DAC resolution 12 bits
Maximum update rate 150 Hz, software-timed

¹Input voltages may not exceed the working voltage range.

Output range 0 to +5 V
Output impedance..... 50 Ω
Output current drive..... 5 mA
Power-on state 0 V
Slew rate..... 1 V/μs
Short-circuit current 50 mA

Digital I/O

Number of channels..... 12 total
8 (P0.<0..7>)
4 (P1.<0..3>)
Direction control Each channel individually programmable as input or output
Output driver type
USB-6008 Open-drain
USB-6009 Each channel individually programmable as push-pull or open-drain
Compatibility CMOS, TTL, LVTTTL
Internal pull-up resistor 4.7 kΩ to +5 V
Power-on state Input (high impedance)
Absolute maximum voltage range..... -0.5 to +5.8 V

Digital logic levels

Level	Min	Max	Units
Input low voltage	-0.3	0.8	V
Input high voltage	2.0	5.8	V
Input leakage current	–	50	μA
Output low voltage (I _L = 8.5 mA)	–	0.8	V
Output high voltage (push-pull, I _L = 8.5 mA)	2.0	3.5	V
Output high voltage (open-drain, I _L = -0.6 mA, nominal)	2.0	5.0	V
Output high voltage (open-drain, I _L = -8.5 mA, with external pull-up resistor)	2.0	–	V

Counter

Number of counters 1
Resolution 32 bits
Counter measurements..... Edge counting (falling edge)
Pull-up resistor 4.7 kΩ to 5 V
Maximum input frequency..... 5 MHz
Minimum high pulse width..... 100 ns
Minimum low pulse width..... 100 ns
Input high voltage 2.0 V
Input low voltage 0.8 V

Power available at I/O connector

+5 V output (200 mA maximum) +5 V typical
+4.85 V minimum
+2.5 V output (1 mA maximum) +2.5 V typical
+2.5 V output accuracy 0.25% max
Voltage reference temperature drift... 50 ppm/°C max

BUY ONLINE at ni.com or CALL 800 813 3693 (U.S.)

Low-Cost, Bus-Powered Multifunction DAQ for USB – 12- or 14-Bit, up to 48 kS/s, 8 Analog Inputs

Physical Characteristics

If you need to clean the module, wipe it with a dry towel.

Dimensions (without connectors).....	6.35 by 8.51 by 2.31 cm (2.50 by 3.35 by 0.91 in.)
Dimensions (with connectors).....	8.18 by 8.51 by 2.31 cm (3.22 by 3.35 by 0.91 in.)
Weight (without connectors).....	59 g (2.1 oz)
Weight (with connectors).....	84 g (3 oz)
I/O connectors.....	USB series B receptacle (2) 16-position (screw-terminal) plug headers
Screw-terminal wiring.....	16 to 28 AWG
Screw-terminal torque.....	0.22 to 0.25 N•m (2.0 to 2.2 lb•in.)

Power Requirement

USB (4.10 to 5.25 VDC).....	80 mA typical 500 mA maximum
USB suspend.....	300 µA typical 500 µA maximum

Environmental

The USB-6008 and USB-6009 are intended for indoor use only.

Operating environment	
Ambient temperature range.....	0 to 55 °C (tested in accordance with IEC-60068-2-1 and IEC-60068-2-2)
Relative humidity range.....	10 to 90%, noncondensing (tested in accordance with IEC-60068-2-56)
Storage environment	
Ambient temperature range.....	-40 to 85 °C (tested in accordance with IEC-60068-2-1 and IEC-60068-2-2)
Relative humidity range.....	5 to 90%, noncondensing (tested in accordance with IEC-60068-2-56)
Maximum altitude.....	2,000 m (at 25 °C ambient temperature)
Pollution degree.....	2

Safety and Compliance

Safety

This product is designed to meet the requirements of the following standards of safety for electrical equipment for measurement, control, and laboratory use:

- IEC 61010-1, EN 61010-1
- UL 61010-1, CSA 61010-1

Note: For UL and other safety certifications, refer to the product label or visit ni.com/certification, search by model number or product line, and click the appropriate link in the Certification column.

Electromagnetic Compatibility

This product is designed to meet the requirements of the following standards of EMC for electrical equipment for measurement, control, and laboratory use:

- EN 61326 EMC requirements; Minimum Immunity
- EN 55011 Emissions; Group 1, Class A
- CE, C-Tick, ICES, and FCC Part 15 Emissions; Class A

Note: For EMC compliance, operate this device according to product documentation.

CE Compliance

This product meets the essential requirements of applicable European Directives, as amended for CE marking, as follows:

- 2006/95/EC; Low-Voltage Directive (safety)
- 2004/108/EC; Electromagnetic Compatibility Directive (EMC)

Note: Refer to the Declaration of Conformity (DoC) for this product for any additional regulatory compliance information. To obtain the DoC for this product, visit ni.com/certification, search by model number or product line, and click the appropriate link in the Certification column.

Waste Electrical and Electronic Equipment (WEEE)

EU Customers: At the end of their life cycle, all products must be sent to a WEEE recycling center. For more information about WEEE recycling centers and National Instruments WEEE initiatives, visit ni.com/environment/weee.htm.

电子信息技术污染控制管理办法 (中国 RoHS)

中国客户 National Instruments 符合中国电子信息技术污染控制使用有害物质限制令 (RoHS)。关于 National Instruments 中国 RoHS 合规性信息，请联系 s11_0045@ni.com 或 ni.com/cn/rohs。 (For information about China RoHS compliance, go to ni.com/cn/rohs.)

BUY ONLINE at ni.com or CALL 800 813 3693 (U.S.)

NI Services and Support



NI has the services and support to meet your needs around the globe and through the application life cycle – from planning and development through deployment and ongoing maintenance. We offer services and service levels to meet customer requirements in research, design, validation, and manufacturing. Visit ni.com/services.

Training and Certification

NI training is the fastest, most certain route to productivity with our products. NI training can shorten your learning curve, save development time, and reduce maintenance costs over the application life cycle. We schedule instructor-led courses in cities worldwide, or we can hold a course at your facility. We also offer a professional certification program that identifies individuals who have high levels of skill and knowledge on using NI products. Visit ni.com/training.

Professional Services

Our Professional Services Team is comprised of NI applications engineers, NI Consulting Services, and a worldwide National Instruments Alliance Partner program of more than 600 independent consultants and



integrators. Services range from start-up assistance to turnkey system integration. Visit ni.com/alliance.

OEM Support

We offer design-in consulting and product integration assistance if you want to use our products for OEM applications. For information about special pricing and services for OEM customers, visit ni.com/oem.

Local Sales and Technical Support

In offices worldwide, our staff is local to the country, giving you access to engineers who speak your language. NI delivers industry-leading technical support through online knowledge bases, our applications engineers, and access to 14,000 measurement and automation professionals within NI Developer Exchange forums. Find immediate answers to your questions at ni.com/support.

We also offer service programs that provide automatic upgrades to your application development environment and higher levels of technical support. Visit ni.com/ssp.

Hardware Services

NI Factory Installation Services

NI Factory Installation Services (FIS) is the fastest and easiest way to use your PXI or PXI/SCXI combination systems right out of the box. Trained NI technicians install the software and hardware and configure the system to your specifications. NI extends the standard warranty by one year on hardware components (controllers, chassis, modules) purchased with FIS. To use FIS, simply configure your system online with ni.com/pxiadvisor.

Calibration Services

NI recognizes the need to maintain properly calibrated devices for high-accuracy measurements. We provide manual calibration procedures, services to recalibrate your products, and automated calibration software specifically designed for use by metrology laboratories. Visit ni.com/calibration.

Repair and Extended Warranty

NI provides complete repair services for our products. Express repair and advance replacement services are also available. We offer extended warranties to help you meet project life-cycle requirements. Visit ni.com/services.



ni.com • (800) 813 3693

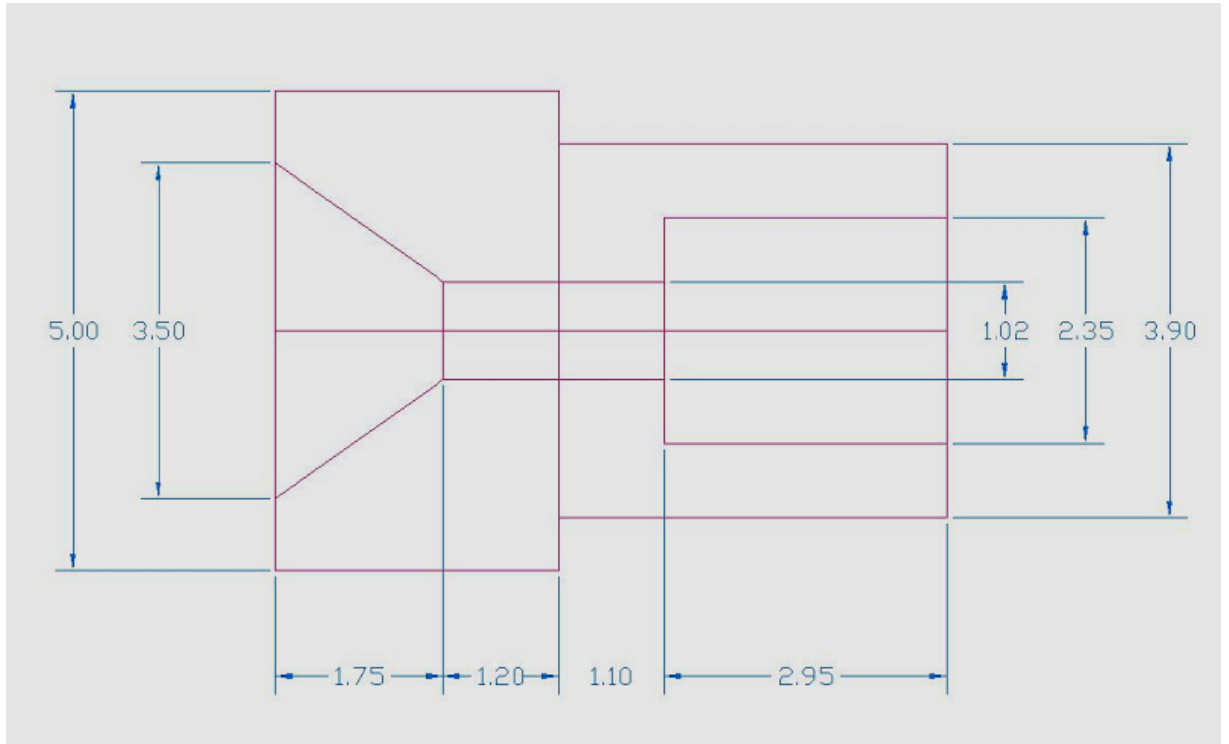
National Instruments • info@ni.com



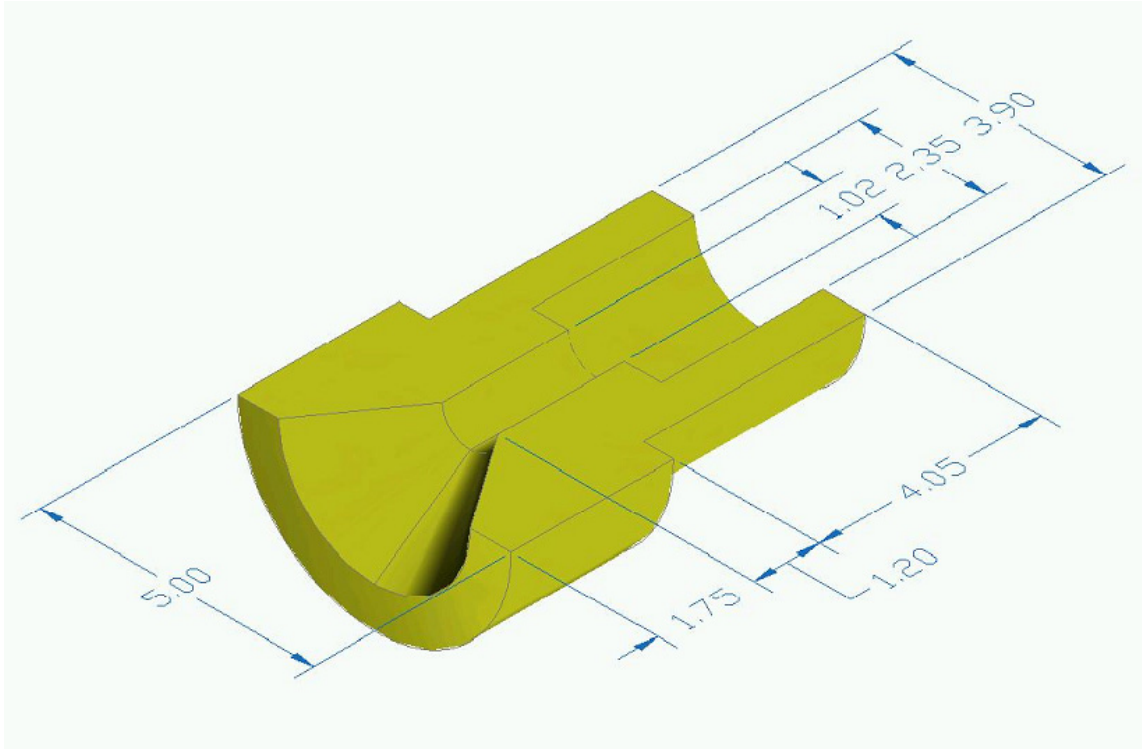
©2008 National Instruments. All rights reserved. CVI, LabVIEW, Measurement Studio, National Instruments, National Instruments Alliance Partner, NI, ni.com, SCXI, and Signal Express are trademarks of National Instruments. The mark LabWindows is used under a license from Microsoft Corporation. Windows is a registered trademark of Microsoft Corporation in the United States and other countries. linux® is the registered trademark of Linus Torvalds in the U.S. and other countries. Other product and company names listed are trademarks or trade names of their respective companies. A National Instruments Alliance Partner is a business entity independent from NI and has no agency, partnership, or joint-venture relationship with NI.

Appendix I

Study orifice geometry



3D isometric view of our study orifice geometry



معامل التصريف في الاختناقات عند عدد رينولد منخفض في صمام الأمان ثنائي المرحلة بالنمذجة الحاسوبية و بالتجربة العملية

إعداد

ماهر خضر مطر

المشرف

الدكتور أحمد سعيد السلايمة

ملخص

تفترض معادلة التدفق داخل الاختناقات أن معدل التدفق الحجمي يتناسب طردياً مع الجذر التربيعي لفرق الضغط قبل و بعد الاختناق, باعتبار ان معامل التناسب هو معامل التصريف, كرقم ثابت لكل نوع اختناق. غير أن الدراسات التفصيلية أثبتت أن معامل التصريف يتغير تبعاً لتغيير عدد رينولدز, في حالة تدفق مائع عالي اللزوجة في اختناقات صغيرة في حدود المليمتر, عند التدفقات الطبقيّة وبالذات عند عدد رينولدز أقل من سبعمائة .

هذه الدراسة تتقصى هذه الظاهرة في صمام الأمان ثنائي المرحلة المستخدم في الأنظمة الهيدروليكية - حيث تستخدم فيه الاختناقات لكسر الضغط جزئياً بين المرحلة الرئيسية والمرحلة الثانوية- بالتجربة العملية و بالنمذجة الحاسوبية للوصول الى علاقة واضحة بين عدد رينولدز و معامل التصريف, و التي تؤدي الى وصف علاقة واضحة بين فرق الضغط على طرفي الاختناق و معدل التدفق الحجمي من خلاله , بأقل خطأ حسابي ممكن, وبطريقة مباشرة دون اللجوء الى الحل الرقمي الذي يعتمد طريقة التجربة و الخطأ , و ذلك لتوفير الوقت.

وجد ان قيم معامل التصريف تراوحت بين 0.21 و 0.97 و كان شكل العلاقة بين معامل التصريف و الجذر التربيعي لعدد رينولدز أسية.